Structure and Dynamics of the Corticothalamic Driver Pathway in the Mouse Whisker System

Anton Sumser

Dissertation der Graduate School of Systemic Neuroscience der Ludwig-Maximilians-Universität

München, 17. Oktober 2016

1. Reviewer, Supervisor: Prof. Dr. Bert Sakmann

2. Reviewer: Prof. Dr. Alexander Borst

3. Reviewer: Prof. Dr. Patrik Krieger

Defense: 6. Oktober 2016

Contents

Summary

To generate a sensory percept of the environment, the brain needs to analyze and integrate spatially and temporally distributed sensory signals. Consequently, sensation on a neuronal basis is a distributed, non-linear and dynamic process. Following sensory receptor activation the signal travels through many brain regions wherein the pathway is split, loops back onto itself and joins together with others. At each step, neurons dynamically transform and filter the signal. To understand how the brain arrives at a sensory percept, it is therefore essential to determine the neuronal connectivity along the processing chain, the stimulus specificity of responses as well as the input-output transformations at each station. An interesting model system for investigating these dynamical processes is the rodent whisker system. Rodents can solve highly complicated tasks with their whiskers alone, distributed receptors at the follicles require spatial integration and rhythmic movements suggest temporal processing components.

The posterior group nucleus of the thalamus (PO) is in a key position of the whisker sensory system. In addition to being part of the ascending paralemniscal pathway it is mainly driven by somatosensory barrel cortex (BC) and projects to many cortical and subcortical areas. Due to its poor excitability by whisker deflections, its function is unclear. The origin of the corticothalamic drive onto PO neurons are 'thick-tufted' layer 5B cortical neurons, which have large synaptic terminals in thalamus. One of those synapses alone has a strong influence on postsynaptic target neurons – a very unusual property for cortical synapses. Here, using quantitative anatomy, in vivo electrophysiology and optogenetics I characterize the organization and input-output computations along the BC L5B to PO pathway.

Using a dual anterograde tract tracing approach and large scale anatomical reconstructions we demonstrate that BC L5B synaptic boutons divide PO in 4 subregions with different projection parameters. The lateral area (POm lateral) receives most boutons with the highest density. Additionally, L5B neurons innervate two inhibitory nuclei in thalamus and midbrain that both inhibit PO. In all 6 regions we report map specific projections, with different map orientations, showing that somatotopic projections are the rule in these cortico-subcortical projections.

Next we investigated the L5B to POm action potential transfer efficacy during spontaneous slow oscillations in anesthesia. Using pharmacology and cell-type specific optogenetics we show that cortical activity is necessary and L5B activation is sufficient to evoke large excitatory postsynaptic potentials (EPSPs) in POm, typical for L5B inputs. Simultaneous cortical local field potential and L5B as well as POm juxtasomal recordings demonstrate that the gain of action potential transmission is high following periods of relative cortical silence, but dynamically decreases during periods of higher

cortical activity. Isolation of individual EPSPs allowed us to determine the frequency dependent adaptation of the L5B to POm synapse in vivo. We determined that approximately half of the recorded POm neurons follow a simple rule of EPSP adaptation, suggesting that the subthreshold activity in these neurons originates from a single active L5B input. Using two independent modeling approaches, we determined that on average POm neurons receive 2-3 functional inputs from BC L5B.

Finally we investigated how whisker deflection signals reach POm. We found that POm neurons fall into two groups. Approximately one third of the recorded neurons were activated at a relatively short latency by large EPSPs and fired action potentials following whisker stimulation. All neurons had long latency sub- and suprathreshold responses, due to Up-state initiation by the whisker stimulation. POm whisker responses were entirely dependent on cortex and were blocked by optogenetic cortical inactivation.

Taken together we quantified the anatomical and physiological properties of the L5B to POm projection. The connection is sparse, parallel, strong and the dominant input for POm spontaneous activity as well as whisker evoked responses. Its gain is dynamically regulated and depends on cortical activity states.

Acknowledgements

First, I thank Bert Sakmann, who was able to motivate me by his constant enthusiasm for neuroscientific research even before I started my PhD. His excitement over every minutely detailed finding was often infectious. To speed up the accumulation of results he delightedly took even the most repetitive tasks science could think of, like pipette pulling or manual computer analyses, onto himself. I hope I can follow his model and also keep this enthusiasm alive for decades. Bert Sakmann's support before and during my PhD was invaluable and by his supervision I learned how to structure research projects and avoid getting side-tracked on fruitless endeavors.

My special thanks go to Alex, who consistently advised and helped me in all small and large day to day problems. Even when I started as a student worker reconstructing dendritic morphologies – a profoundly boring task in itself – Alex managed to spark my fascination with brain functions, by allowing me to participate in his experiments and listening to my completely unfounded theories. In the following years he would always have an ear for my crazy ideas and support me to follow them up. Alex, the track changes function in Word and I became very good friends.

Furthermore I thank Rebecca, who was of great help when I learned to analyze data and even did not shy back from low-level squirrel personalization of my Matlab program. We had the best research discussions during one of the many wonderful meals she prepared. Even though I took up quite some space in his institute, Arthur Konnerth always supported me and my research. By inviting me to institute events and lab retreats, providing access to technical personal and discussing my findings he made me feel a part of his institute, which I am very thankful for. Furthermore I thank Thomas Misgeld for providing access to his confocal microscope for probably thousands of hours. Without the help of student workers, in particular Julia Bechtner, and the workshop (Felix) the presented work would not have been possible. I greatly appreciated the support I received from the Boehringer Ingelheim Fonds both financially and in the form of interesting retreats and courses.

Finally, I want to thank Lena, my family and my friends for suffering my moods sometimes and then always finding ways to pull me up. Only the fun time I had and will have with them gives me the energy to pursue the frustratingly awesome life as a scientist.

Introduction

Each moment of life, our brains excel at the complex tasks of acquiring information about the environment, processing and analyzing those signals, store and retrieve memories, decide on appropriate behavior and finally coordinate the muscular contractions for an appropriate behavioral response. Accordingly, the brain is an equally complex structure and we therefore are still at the beginning of trying to understand how it works. The standard building elements giving rise to brain function are neurons, whose defining characteristics are active electric signal propagation by action potentials and integration of synaptic inputs (Kandel et al. 2013). Their sheer number (humans: >80 billion (Azevedo et al. 2009)), cell-type-specific biophysical differences, connectivity and plasticity make the brain the complex and flexible organ as it is. When trying to understand brain function, we necessarily need to understand the neuronal substrate of perception, cognition and behavior.

It is still not clear how the brain generates a percept of the environment from spatially and temporally distributed receptor activations on a neuronal basis. For example, how can I come to the conclusion that I am holding a cup, from the parallel and serial activation of pressure receptors in my fingertips alone? One hypothesis is that different neurons or groups of neurons are activated by different stimulus features, e.g. spatial or temporal patterns. Based on connectivity and input-output filter functions, feature selectivity could be generated. Any sensed object would then cause specific sensory patterns and thereby activate specific subsets of neurons, whose coincident activity could identify the object. To understand sensory computations, it is therefore important to determine the connectivity and dynamic input-output functions of the microcircuits in the processing cascade.

To comprehend brain function, we need to understand how physical signals from receptors are encoded in the 'language' of neurons and subsequently integrated to create a neuronal percept of the environment. Even though each sensory modality is processed in different ways, there are remarkable parallels – giving hope that processing principles, found out in one modality, will be transferable to others and might also be applicable to other species (Sherman 2016). Following transduction of a physical sensory signal (e.g. mechanical pressure, sound, light, chemicals…) into a neuronal signal at receptors, the information travels through a number of subcortical stations (e.g. olfactory bulb, spinal cord, brainstem, midbrain or thalamus). Subcortical signals are subjected to various signal transformations, for example filtering (Castro-Alamancos 2002) and parallelization into different pathways for different information contents (Brand et al. 2002). When looking at connectivity charts, it becomes evident that feedforward signal flow is insufficient in describing processing steps (Figure 1). Widespread signal divergence, feedback excitation, feedforward and feedback inhibition are the rule and obscure the major signal pathways. Nevertheless, it is thought

that sensory signals enter the cortex at primary sensory cortical areas, from where they mainly continue to higher and often multimodal cortices, association areas then premotor and finally motor areas, where an appropriate motor response is generated (Kandel et al. 2013).

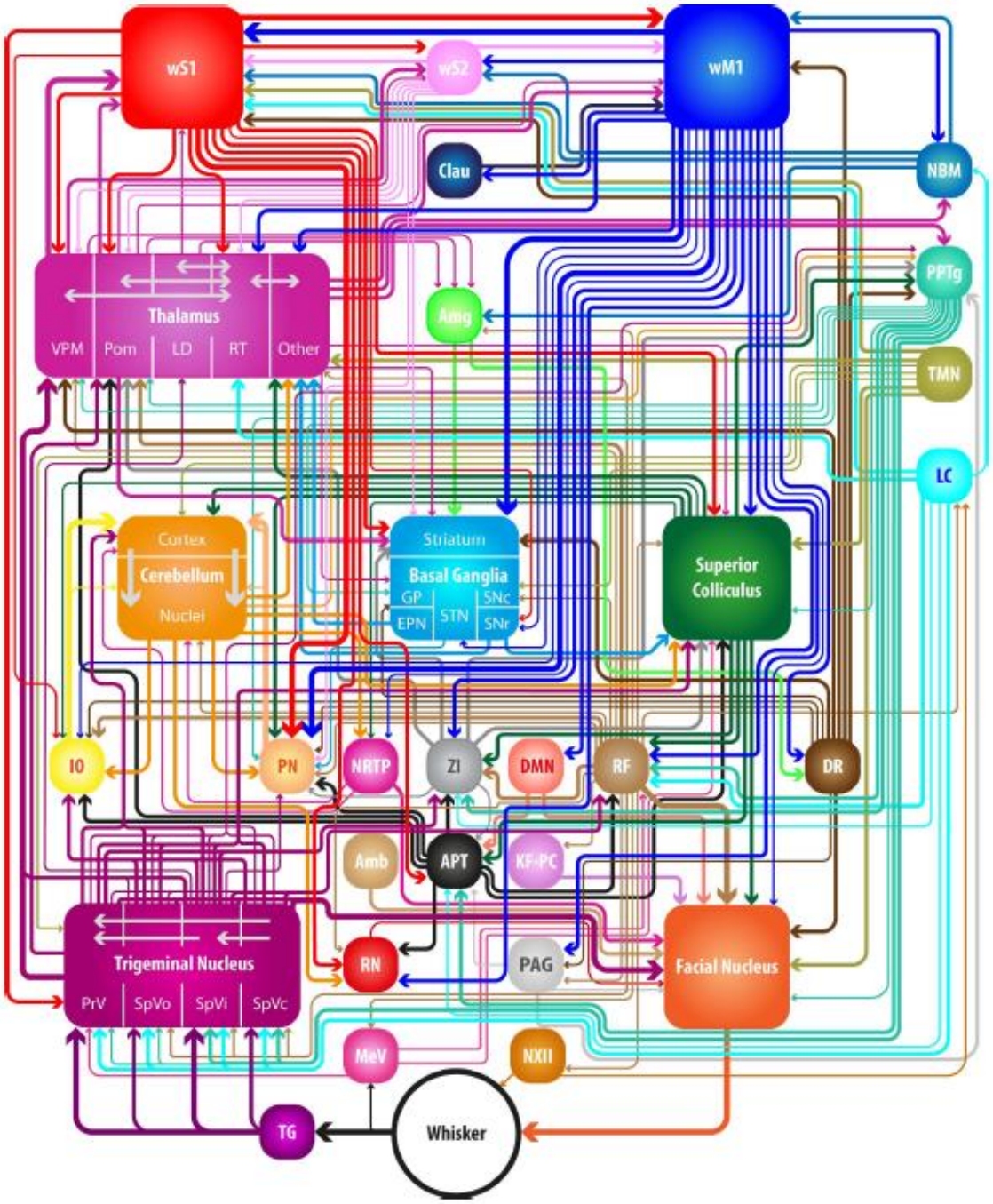

Figure 1: Nonlinear feedforward and feedback pathways

Simplified overview of the signal pathways in the sensorimotor whisker system as an example, illustrating the nonlinear connectivity typical for neuronal signaling. (Bosman et al. 2011).

Aside from this 'conscious' pathway however, there is lower level connectivity between sensory and motor areas (Diamond et al. 2008), further highlighting the fundamentally non-linear structure of signal pathways. Sensory-motor loops (Matthews et al. 2015) conceptually allow for faster reaction times, while motor-sensory connections underline the inherently active nature of sensation: Typically, perception and behavior are viewed as separate steps in the processing chain, however it should be considered that each influences the other and they sometimes even are reciprocally dependent. For example moving my eyes will subsequently change the visual scene I experience and in order to feel the roughness of sandpaper I need to move my finger along it. Therefore, sensory processing cannot be understood without studying motor behavior, reflected by motor areas commonly projecting to sensory areas (Urbain and Deschênes 2007a; Lee et al. 2013).

Neuronal cell physiology in vivo is not possible in humans; therefore investigating neuronal processing principles in animal model systems serves as a starting point. Mice are a common choice for a model organism, because as mammals, their brain structure is reasonably similar to that of humans and their small body size makes them relatively easy to keep and breed. Additionally mice are accessible for genetic modifications. The mouse whisker system is an interesting model for investigating signal transformations along processing pathways, because receptor organization and rhythmic movements demand extensive neuronal integration and processing and signal pathways are reasonably well established (Figure 1). Additionally, neuronal organization in receptor map structures and superb stimulus control make the whisker system an attractive model system for systems neuroscience.

The Mouse Whisker System as a Model for Active Sensing

Mice are nocturnal animals, typically living in enclosed and dark spaces. In this ecological niche, vision is of limited use and whisker somatosensation is the mouse's most important sense to explore its environment. Mice rhythmically sweep their whiskers forward and backward during exploration (Woolsey et al. 1975) (Figure 2). Any obstacles lead to angular displacements (Carvell and Simons 1990), which exert forces (Hires et al. 2013) on the follicles that can be detected by specialized mechanoreceptors. Mice and other animals with rhythmically moving whiskers (like rats or shrews) can discriminate object location differences down to ~1° (Knutsen et al. 2006) on a very fast timescale (e.g. an Etruscan tree shrew needs only 25 ms from whisker contact to a behavioral response (Brecht et al. 2011)).

Signal Flow from Whiskers to Cortex

The cerebral cortex is arguably the 'cognitive' headquarter of the brain, thought to accommodate distinct cortical circuits for decision making, conscious perception and other cognitive functions. But before signals reach the cortex, they are processed throughout all ascending stations. Additionally, cortico-subcortical projections and loops are participating in signal processing. In contrast to the cortex, subcortical structures like the thalamus are located deep in the brain and are thus hardly accessible with cellular imaging techniques, rendering the study of cortico-subcortical interactions a major challenge in neuroscience. This generated a disparity in what we know about intracortical processing and subcortical interactions. Therefore, the long range interactions between the cortex and the thalamus, studied with anatomical and deep brain electrophysiology techniques in combination with optogenetics are the focus of this thesis. To understand processing principles in deep structures I will briefly review the canonical view how signals from whisker receptors travel from the periphery to cortex.

Whiskers and Receptors

Mice have a stereotypical arrangement of ca. 30 whiskers ('macrovibrissae') of 10-30 mm length and 70-90 µm base diameter (Ibrahim and Wright 1975) on both sides of their snouts (Brecht et al. 1997). Each conically shaped whisker grows out of a whisker follicle sinus complex (Rice et al. 1986). Follicles are arranged in five rows (named A-E from dorsal to ventral), each row has 4 to ca. 9 columns of follicles (called arcs and named by numbers from posterior to anterior) (Figure 2a,b). A set of muscles is attached to each follicle, generating whisker movements by changing the angle relative to the skin. By rhythmic contractions of these muscles, whiskers can be swept forward and backward ("whisking") in a mostly horizontal plane (Figure 2c). Individual whiskers move mostly synchronously (Sachdev et al. 2002). In the follicle, around the base of the whiskers, specialized mechanoreceptors, mostly Aβ fibers with slowly-adapting Merkel-cell endings or rapidly-adapting lanceolate endings (Rice et al. 1986), are located and detect changes of pressure, caused by bending the whisker (Figure 2d).

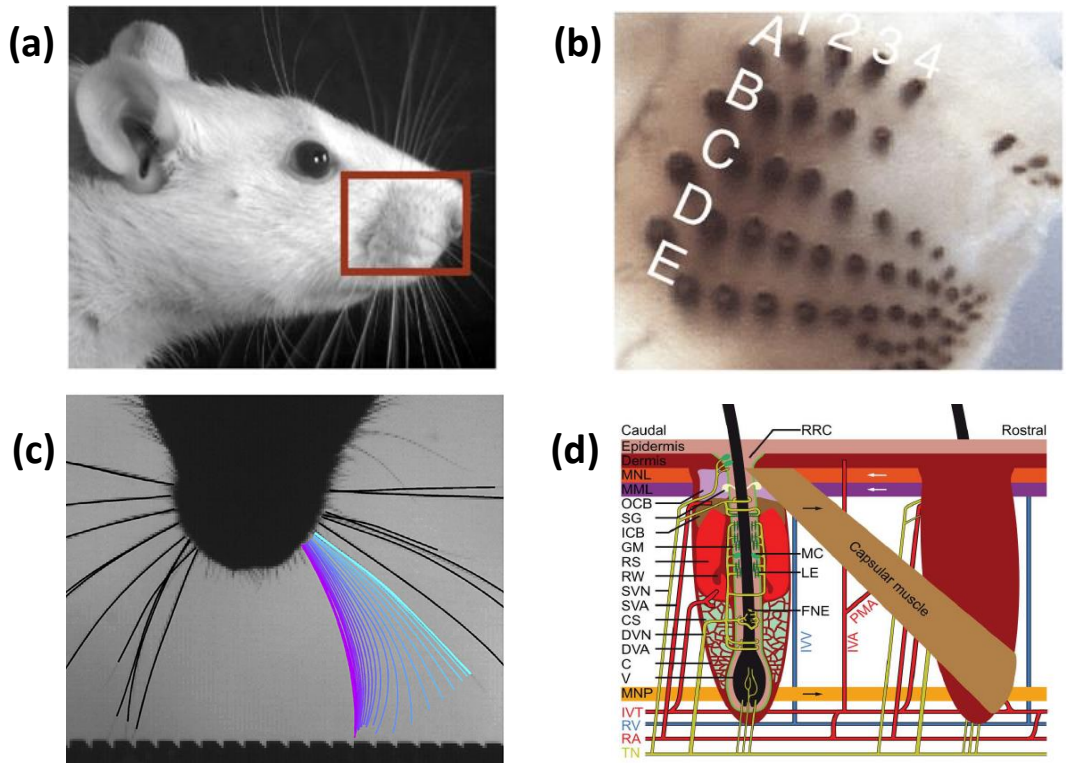

Figure 2: Whiskers

(a,b): The whisker pad with row and arc organization of a rat (Knutsen and Ahissar 2009) (permission granted); (c): illustrated whisking behavior in view from top (Maravall and Diamond 2014) (permission granted); (d): Whisker follicle sinus complex, illustrating muscles and sensory innervation (Bosman et al. 2011).

Trigeminal Ganglia

Activation of mechanoreceptors is translated into action potentials (APs) in nerve endings of trigeminal ganglion neurons. Trigeminal ganglion neurons always innervate a single follicle with 150-200 neurons per follicle in total (Rice et al. 1986). These neurons do not fire APs spontaneously, are mostly slowly adapting, partly rapidly adapting and each neuron has an individual threshold of activation (Gibson and Welker 1983a, 1983b; Lichtenstein et al. 1990; Leiser and Moxon 2007). Thereby ganglion neurons precisely encode receptor information on kinematic parameters (Arabzadeh et al. 2005). As whisking in air causes pressure changes at the follicles due to inertia and air resistance, trigeminal ganglion neurons transmit also self-motion (re-afferent) signals (Leiser and Moxon 2007). Ganglionic axons bundle into the fifth nerve and bifurcate on their way to the brainstem, innervating two trigeminal brainstem nuclei, thereby giving rise to two ascending pathways of whisker signals to cortex (Hayashi 1980) (Figure 3).

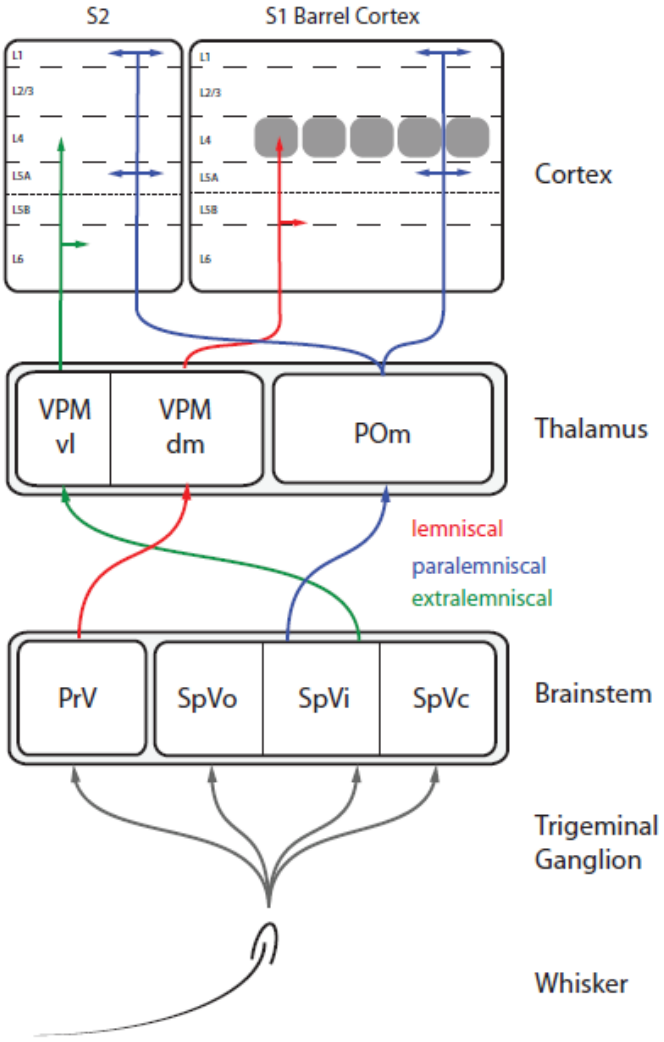

Figure 3: Ascending pathways in the whisker system

At least 3 pathways contain peripheral information and travel to cortex. PrV: principal trigeminal nucleus; SpVo: spinal trigeminal nucleus oralis; SpVi: spinal trigeminal nucleus intermedialis; SpVc: spinal trigeminal nucleus caudalis; VPMvl/dm: ventral posterior medial thalamic nucleus ventrolateral and dorsomedial part; POm: posterior medial nucleus; S1/S2: somatosensory barrel cortex 1 and 2; L1-6: cortical layers; grey rounded rectangles indicate barrels in layer 4.

Brainstem

The somatosensory trigeminal brainstem is subdivided in two nuclei, the rostral trigeminal nucleus principalis (PrV) and the spinal trigeminal nucleus, which is further subdivided into an oral (SpVo), intermediate (SpVi) and caudal (SpVc) part. In each (sub)nucleus, except SpVo, barrelettes can be visualized by histological methods (Ma 1991) (Figure 4). The barrelettes consist of groups of neurons receiving inputs from the same whisker. Together they represent a map of the whisker pad.

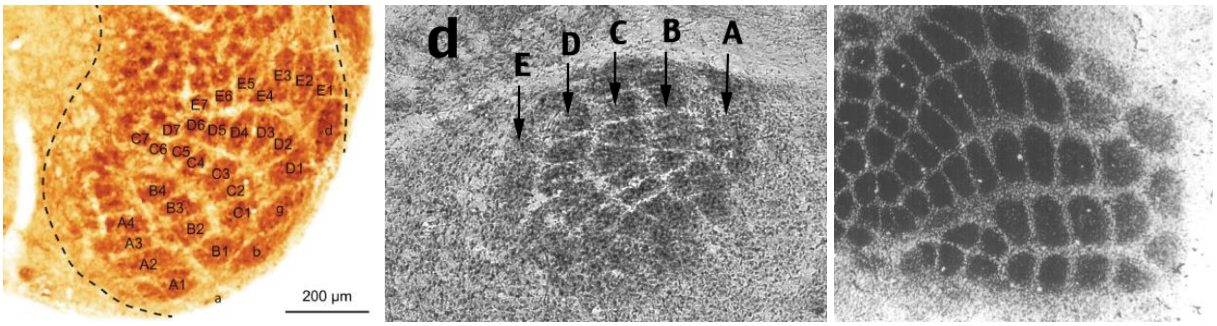

Figure 4: Sensory receptor maps in the brain

Barrelettes (SpVi), barrelloids (VPM) and barrels (BC) (Senft and Woolsey 1991; Haidarliu and Ahissar 2001; Bosman et al. 2011) (permissions granted).

At the level of the brainstem the signal is thought to be split into at least three pathways. The so called lemniscal pathway starts in PrV. Barrelette neurons in PrV have receptive fields (RF) of the same single whisker. Responses to whisker deflections are very reliable and precisely timed (Figure 5). Already at this stage signal modulation, via GABAergic and glycinergic innervation from SpVi (Furuta et al. 2008) takes place. PrV axons cross over to the contralateral hemisphere and terminate mostly in the dorsomedial part of the ventral posterior medial nucleus of the thalamus (VPM) (Figure 3) (Erzurumlu et al. 1980).

The paralemniscal and extralemniscal pathways begin in the intermediate spinal trigeminal nucleus (SpVi). All spinal subnuclei receive ganglionic input, however mostly SpVi takes part in the ascending pathway, while SpVo and SpVc are thought to participate mostly in intra-trigeminal processing and modulation. However, there is a poorly characterized pathway from SpVo to posterior thalamus (Veinante, Jacquin, et al. 2000). SpVi and SpVc also have the morphological feature of barrellettes, however individual barrellettes are innervated by trigeminal ganglion neurons from more than one follicle and in consequence neuronal RFs typically encompass multiple whiskers (Jacquin et al. 1986; Timofeeva 2004). SpVi axons also cross over to the contralateral hemisphere and terminate mostly in the posterior medial nucleus of the thalamus (POm), continuing the paralemniscal pathway (Erzurumlu et al. 1980; Veinante, Jacquin, et al. 2000) (Figure 3). In the caudal part of SpVi begins the extralemniscal pathway, which continues to the ventrolateral part of VPM (Pierret et al. 2000) (Figure 3).

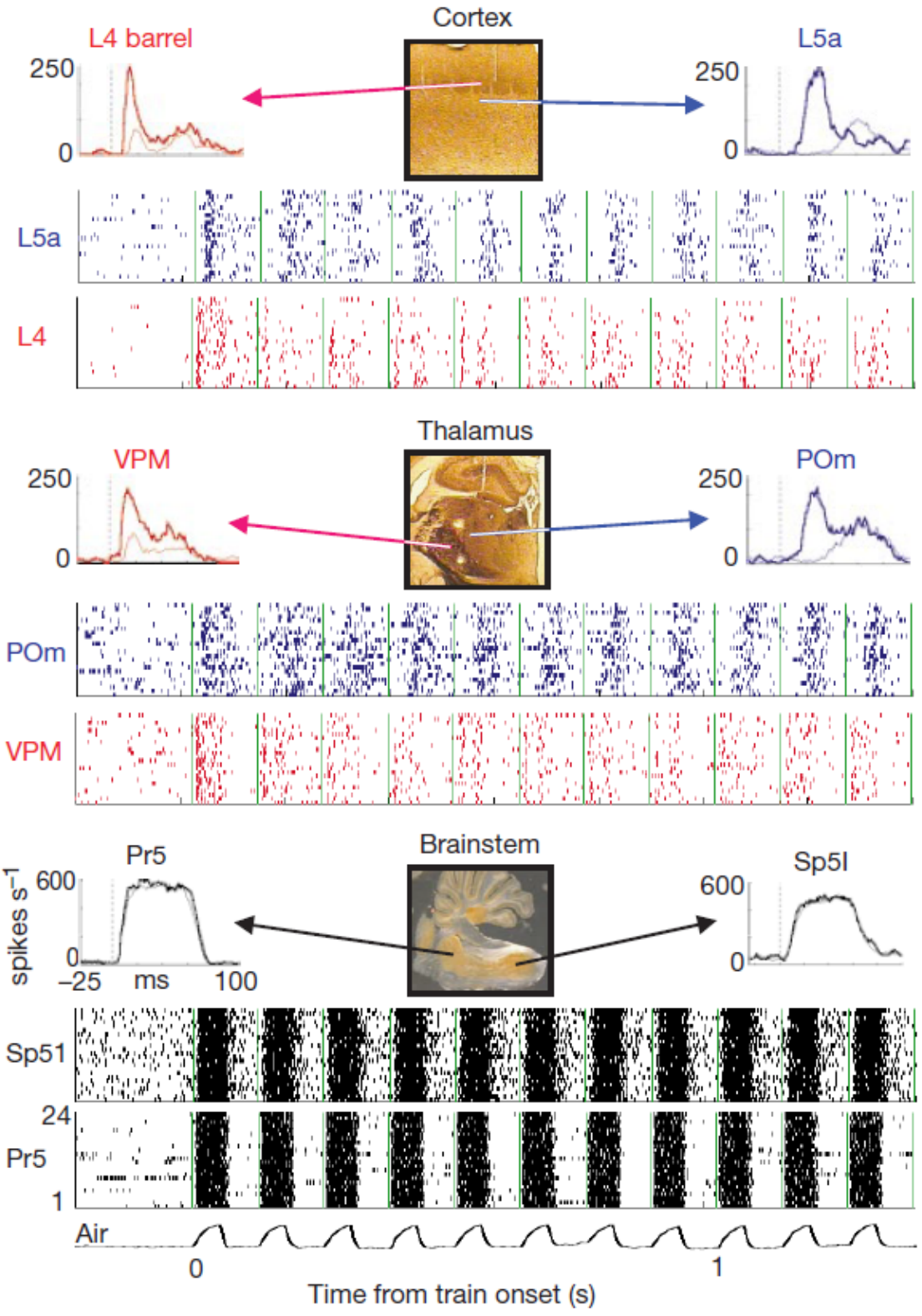

Figure 5: Neuronal responses along the lemniscal and paralemniscal pathways to repetitive whisker stimulations (Ahissar et al. 2000) (permission granted).

Note increasing variability and adaptation at each ascending station. At each level, the lemniscal structure is below the paralemniscal structure. At the bottom the stimulus shape is indicated. Pr5: principal trigeminal nucleus; SpVI: spinal trigeminal nucleus intermedialis; VPM: ventral posterior medial thalamic nucleus; POm: posterior medial nucleus; L4/L5a: cortical layers.

Thalamus

Two thalamic nuclei participate in ascending somatosensory whisker processing: The lemniscal VPM and the paralemniscal POm. In the dorsomedial part of VPM (VPMdm), neuronal clusters ('barrelloids') represent the whisker map (Figure 4), visualized by histochemical methods (Haidarliu and Ahissar 2001). Most VPM neurons respond only to a single whisker (Veinante and Deschênes 1999). Due to adaptive filtering, low spontaneous firing and inhibition from other nuclei, whisker deflection signals are processed further into kinematic components (Petersen et al. 2008) and variability increases (Ito 1988) (Figure 5). Still, neurons respond very reliably and with short latencies (5-10 ms) to whisker deflections (Diamond, Armstrong-James, and Ebner 1992). Neurons in VPMdm send their axons mostly into the barrel structures of layer 4 (L4) in somatosensory barrel cortex (BC) (Chmielowska et al. 1989), continuing the lemniscal pathway. A significant portion of VPMdm axons directly innervate deep layer 5 (L5) and high layer 6 (L6) neurons in barrel cortex (Meyer, Wimmer, Oberlaender, et al. 2010; Constantinople and Bruno 2013). In the ventrolateral direction barrelloid structures fade out (Haidarliu and Ahissar 2001) and the area further differs from VPMdm, as it is mostly innervated by SpVi, consequently has multi-whisker RFs and sends its axons mostly to secondary somatosensory cortex (Pierret et al. 2000).

The organization of POm synaptic inputs and outputs is less clear. For example, barrelloids are not evident based on histological methods, however somatotopic representations can be found by physiological RF mapping (Diamond, Armstrong-James, and Ebner 1992). Interestingly, SpVi innervates only a part of POm (approximately one third of its volume (Groh et al. 2014)). In POm, neurons have multi-whisker RFs and respond to whisker deflections with longer latencies (~25ms) and with far more failures than VPM neurons (Diamond, Armstrong-James, and Ebner 1992) (Figure 5). Additionally, compared to VPM neurons under anesthesia, POm neurons show substantially more spontaneous AP activity, which is synchronized with cortical oscillations (Diamond, Armstrong-James, Budway, et al. 1992; Slézia et al. 2011). It has been shown that POm is under control of zona incerta feedforward or continuous inhibition (Trageser and Keller 2004; Lavallée et al. 2005). This inhibitory control is state dependent and can putatively be relieved by arousal or movement through cholinergic systems or motor cortex (Masri et al. 2006; Trageser et al. 2006; Urbain and Deschênes 2007a). POm axons terminate in L1 and L5A of barrel cortex (Deschênes et al. 1998; Meyer, Wimmer, Hemberger, et al. 2010) (Figure 3). The function of POm in whisker processing is a matter of ongoing debate (see below).

Somatosensory Barrel Cortex

The somatosensory barrel cortex has a six–layered organization, whereas L4 is considered to be the major bottom-up input layer and L2/3, L5 and L6 the output layers. Recently, it has been directly

shown that deep (L5/6) layers function quite independent of upper layers and are equally strongly innervated by VPM (Constantinople and Bruno 2013). Staining for Cytochrome C Oxidase activity reveals the particular barrel-shaped structures in L4 of barrel cortex (Figure 4) giving the cortical area its name (Woolsey and van der Loos 1970). Each barrel in L4 correlates to a single whisker; together they map the same relative positions of whisker follicles on the contralateral snout (Welker 1971). L4 barrel neurons are the target of the lemniscal pathway and consequently have single whisker RFs (Brecht and Sakmann 2002). The cortical region from pia to white matter and with the width of one barrel is called a cortical column (Mountcastle 1997). L4 neurons mostly innervate L2/3 cells in the same and neighboring columns. L2/3 cells fire very sparsely, in turn innervate L5 of barrel cortex and also send collaterals out of barrel cortex to motor cortex and secondary somatosensory cortex (de Kock et al. 2007; Kerr et al. 2007; Chen et al. 2013; Yamashita et al. 2013; Narayanan et al. 2015). POm axons span multiple columns and terminate in L5A, directly below the barrels, and in L1, which is nearly empty of somata, but where L2/3 and L5 neurons have their extensive apical dendrites (Deschênes et al. 1998; Meyer, Wimmer, Hemberger, et al. 2010). L1 is also the major target for cortico-cortical innervations from motor cortex, secondary somatosensory cortex and others, therefore it is often considered as a 'contextual input' layer (Cauller 1995; Manita et al. 2015). Barrel cortex L5 neurons fall into two categories, defined by characteristic apical dendrite architectures and soma depth in respect to the pia (Manns et al. 2004; de Kock et al. 2007; Groh et al. 2010): slender-tufted L5A have cortico-cortical and cortico-striatal projections. Their activity correlates with whisker movement parameters (de Kock and Sakmann 2009). Thick-tufted L5B neurons project subcortically, respond reliably to whisker deflections and have wide RFs (de Kock et al. 2007; Oberlaender et al. 2011; Ramaswamy and Markram 2015). L5B characteristics will be described in more detail below. Finally L6 neurons extensively project intracortically as well as either to thalamus (Both VPM and POm) or other cortical areas (Zhang and Deschênes 1997; Zliang and Deschênes 1998). A subset of cortico-cortical L6 neurons reliably responds to whisker deflections and send weak but dense projections to their respective targets (McCormick and von Krosigk 1992; Bourassa et al. 1995; de Kock et al. 2007; Mease et al. 2014). In addition to the aforementioned well-studied excitatory pathways, each layer has its individual inhibitory and disinhibitory microcircuits, which will not be covered here. Barrel cortex, in parallel to other cortical areas exhibits spontaneous oscillation patterns in various frequency ranges. Under deep anesthesia, those oscillations result in phases of elevated spontaneous activity, in turn with phases of very low spontaneous activity, respectively named up- and down states. Up- and down states oscillations are very slow, with frequencies below 1 Hz (Steriade et al. 1993; Stroh et al. 2013).

Barrel Cortex Layer 5B neurons

Although they are only one of many cortico-efferent cell types, L5B ('thick-tufted') neurons are nevertheless often seen as the main cortical output neurons (Feldmeyer 2012). L5B neurons have extensive apical dendritic arbors in L1 (Oberlaender et al. 2011), and can thereby sample inputs throughout most of the cortical column. In anesthesia, Layer 5B neurons have the broadest receptive fields to whisker deflection stimuli and highest spontaneous activities (3-6 Hz) in barrel cortex (de Kock et al. 2007). Spiking is strongly locked to cortical up- and down state oscillations (Stroh et al. 2013). L5B axons only sparsely innervate the cortical column and target mainly subcortical structures in thalamus, midbrain and brainstem (Wise and Jones 1977a, 1977b; Bourassa et al. 1995; Veinante, Lavallee, et al. 2000) (Figure 6). In thalamus, L5B projects prominently to the posterior group (PO), including POm. Here multiple areas of L5B innervation are evident (Deschênes et al. 1998; Veinante, Lavallee, et al. 2000; Alloway et al. 2003; Aronoff et al. 2010). Another L5B target area in thalamus is the GABAergic zona incerta (ZI) (Mitrofanis and Mikuletic 1999), which additionally gets inputs from SpVi (Veinante, Jacquin, et al. 2000) and interestingly has strong inhibitory control over POm and was therefore suggested to gate paralemniscal signals in POm (Urbain and Deschênes 2007a, 2007b; Furuta et al. 2008). In the midbrain, L5B boutons were reported in the GABAergic anterior pretectum (APT) (Foster et al. 1989; Cadusseau and Roger 1991; Aronoff et al. 2010; Bosman et al. 2011), which is associated with somatosensory and nociceptive processing and inhibits POm (Foster et al. 1989; Bokor et al. 2005; Murray et al. 2010). The main midbrain target however is the

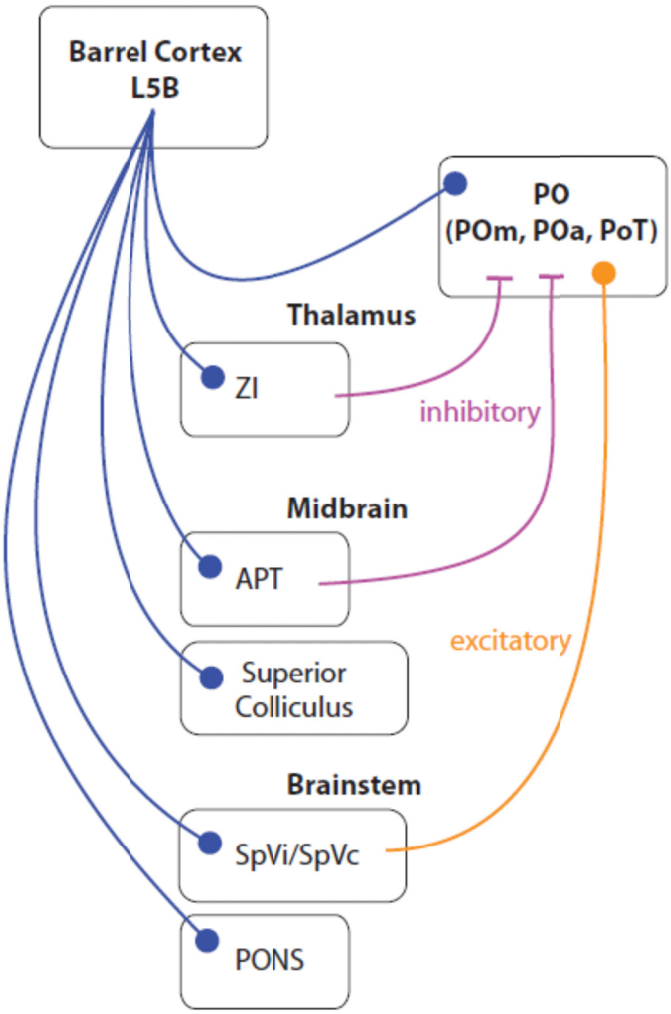

Figure 6: BC L5B efferent projections including secondary projections to PO.

Putative cortico-subcortical driver pathway indicated in blue; inhibitory and excitatory secondary projections in magenta and orange respectively. ZI: zona incerta; APT: anterior pretectum; SpVi/SpVc: spinal trigeminal nuclei intermedialis and caudalis; PONS: pontine nuclei.

Superior Colliculus (SC) (Wise and Jones 1977a, 1977b), a region involved in multisensory integration and premotor functions (Cohen and Castro-alamancos 2010). The brainstem is densely innervated by L5B in the pontine nuclei (PONS) (Wise and Jones 1977b; Leergaard et al. 2000; Leergaard and Bjaalie 2007), which in turn provide the main input to the cerebellar cortex via mossy fibers. Additionally L5B neurons project to the trigeminal nuclei (Wise et al. 1979; Matyas et al. 2010; Smith et al. 2015), thereby influencing the ascending somatosensory pathways. There seem to be L5B subgroups, i.e. not every individual neuron innervates all targets (personal communication Marcel Oberländer, (Bourassa et al. 1995; Deschênes et al. 1998; Veinante, Lavallee, et al. 2000)). L5B neurons generally seem to innervate their subcortical target areas with sparse but particularly large boutons (Bourassa et al. 1995; Deschênes et al. 1998; Aronoff et al. 2010) – a rather unusual property in the mammalian brain, especially for boutons of cortical origin. So far, the properties of L5B synapses have only been investigated in detail in POm, where they can evoke large EPSPs (>10 mV), but have strong paired-pulse depression, matching driver characteristics defined by Sherman et al (Reichova and Sherman 2004; Groh et al. 2008).

The (Somatosensory) Thalamus

Originally, the thalamus was viewed as the gateway to cortex, where relay neurons serve as a way station of signals from periphery and cortex. Provocatively stated, at most some signal filtering and adaptation was thought to happen in thalamus while perceptual processing only happens in cortex. This view is changing, as it becomes more and more clear that thalamic neurons not only shape and gate incoming signals but also participate in post-cortical processing in form of cortico-thalamo-cortical loops and transcortical relays (Zacksenhouse and Ahissar 2006; Theyel et al. 2010; Yu et al. 2015). In fact, corticothalamic synapses typically outnumber synapses from the periphery by an order of magnitude (Guillery 1969; Erişir et al. 1997; Alitto and Usrey 2003). Interestingly, thalamic relay neurons are not interconnected with each other, demonstrating a strong parallelization of thalamocortical pathways (Sherman 2016). Inhibition and gating is also a common concept in thalamus. Thalamic inhibitory and excitatory neurons tend to be separated into separate nuclei – at least in rodents. Thalamic relay neurons have a high T-type calcium (Ca) channel concentration. The channel is inactivated at resting membrane potential and above, but de-inactivated by hyperpolarization. When opened T-type Ca-channels lead to long-lasting low-threshold Calcium spikes (LTS), often causing bursts of action potentials (Destexhe et al. 1998). These channels allow thalamic neurons to operate in two modes, depending on previous inputs: EPSPs from resting or already depolarized membrane potentials lead to single spikes (tonic mode), if threshold is reached. EPSPs during hyperpolarized membrane potentials can in contrast cause LTS and subsequently fast

bursts of 2-5 APs (phasic or burst mode) (Fanselow et al. 2001; Mease et al. 2014). Thereby thalamic neurons can, depending on resting membrane potential, dynamically switch between linear representation of stimulus features in tonic mode or high detectability of weak stimuli in burst mode (Sherman 2001).

There are two general types of thalamic nuclei: First-order/lemniscal nuclei (VPM in somatosensory, lateral geniculate nucleus in visual, ventral division of medial geniculate nucleus in auditory system) that fit better in the classical view of the thalamus, being driven by the periphery and modulated by cortex (In this thesis modulatory input refers not to neuromodulators like Acetylcholine or Dopamine but to weak glutamatergic inputs in contrast to driver inputs, according to the definitions established by Sherman et al. (Sherman 2016)). On the other hand there are higher-order/paralemniscal thalamic nuclei (POm in somatosensory, pulvinar nucleus in visual, dorsal division of medial geniculate nucleus in the auditory system), that seem to have reverse organization in that they are mostly driven by cortex (Sherman 2005; Bertram 2010). This thesis is about the somatosensory thalamus, therefore I will describe properties of VPM and POm in more detail.

Structure and Function of VPM

VPM is a lemniscal nucleus, linking PrV of the brainstem to barrel cortex (Erzurumlu et al. 1980). In parallel to brainstem nuclei, neuronal clusters form barrelloids, reflecting the whisker map in VPM (Van Der Loos 1976; Haidarliu and Ahissar 2001) (Figure 4). There is evidence for subdividing VPM in 3 subnuclei (head, core (VPMdm), tail (VPMvl)), whereas VPMvl gives rise to the extralemniscal pathway to S2 (Pierret et al. 2000; Yu et al. 2006). The best studied area however is the dorsomedial core area, where neurons respond only to a single whisker, while neurons in the head and ventrolateral tail regions are thought to have multi-whisker RFs (Veinante and Deschênes 1999). VPMdm receives innervation from PrV (Erzurumlu et al. 1980), the GABAergic thalamic reticular nucleus (Rt) (Shosaku et al. 1984) and L6 of barrel cortex (Hoogland et al. 1987; Mease et al. 2014), the barrelloid tail region also from SpVi (Pierret et al. 2000), the head region on the dorsomedial border to POm also from motor cortex (Urbain and Deschênes 2007b). VPMdm neurons respond very reliably and with short latencies (5-10 ms) to whisker deflections (Diamond, Armstrong-James, and Ebner 1992), however individual neurons respond best to particular kinematic whisker parameters like velocity or angle of deflections (Ito 1988; Timofeeva et al. 2003; Petersen et al. 2008). Additionally VPM neuron activity is modulated by whisker self-motion in air (Khatri et al. 2010; Moore et al. 2015; Urbain et al. 2015). VPM axons heading to L4 and L6 of barrel cortex (Chmielowska et al. 1989; Meyer, Wimmer, Hemberger, et al. 2010; Constantinople and Bruno 2013) give off collaterals at the reticular nucleus, which in turn provides inhibition to VPM and POm, establishing an intrathalamic negative feedback loop (Crabtree et al. 1998; Desîlets-Roy et al. 2002)

and the only possibility how thalamic relay neurons can influence each other. Barrel cortex L6 innervation leads to a complex pattern of hyperpolarization (probably indirectly through Rt) and then depolarization, thereby modifying the tonic vs. burst mode of VPM firing (Mease et al. 2014). L6 activation switches VPM to tonic mode and subsequently its neurons can follow higher frequency whisker stimulation than without L6. In summary, the major VPM function is transmitting kinematic whisker signals to barrel cortex, either in a fine-tuned tonic or in a strong all or nothing burst fashion.

Structure and (Proposed) Functions of POm

Historically POm is called medial division to distinguish it from intermediate (POi) and lateral (POl) divisions of the posterior group found in cat and associated with visual processing (Naito and Kawamura 1982). Even so POi and POl have never been identified in rodents, the term POm is often used interchangeably for the whole rodent PO (Diamond 1995), causing some confusion. PO is likely subdivided into multiple subregions, with varying nomenclature: The anterior or medial PO is called angular nucleus by some (Deschênes et al. 1998), ventrolateral or ventral anterior nucleus by others (Zakiewicz et al. 2014, 2015), the posterior region is sometimes called the posterior triangular nucleus (PoT) (Gauriau 2004). If and how the different nuclei have different projection patterns and physiologies is not clear. As examples for different functions in different areas of PO, signaling of specifically noxious stimuli was reported for PoT (Gauriau 2004), sensorimotor signaling in POm lateral (Ahissar et al. 2000). For the purpose of this thesis, trying to be consistent with the most common names we divided PO in 'anterior PO' (POa), 'POm lateral' and 'POm medial' part (intermediate PO), as well as 'PoT' (posterior PO). One goal of this thesis is to investigate how barrel cortex L5B projections into these (sub)nuclei are organized and distributed. Previous studies on PO however mostly focused on the lateral intermediate part, which is mostly just named POm.

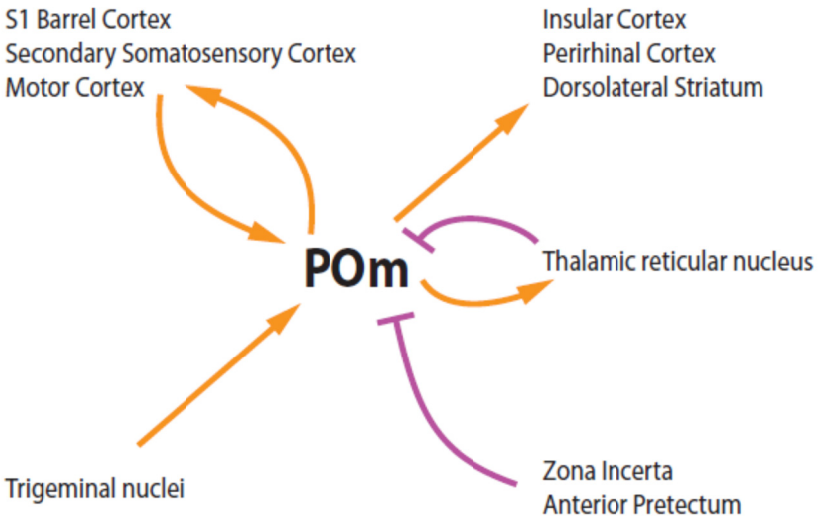

Figure 7: POm Connectivity

Excitatory connectivity indicated in orange, inhibitory in magenta.

(Lateral) POm is a 'higher-order' or paralemniscal thalamic nucleus, defined by its main driver input from cortex (Sherman 2005). POm input and output connectivity is far more complex than that of VPM (Figure 7). POm receives driver input from L5B of barrel cortex, deep layers of secondary somatosensory cortex, as well as SpVi in brainstem (Veinante, Jacquin, et al. 2000; Groh et al. 2008; Liao and Yen 2008; Liao et al. 2010). While L5B boutons cover most of POm, SpVi innervates only approximately one third of its volume (Groh et al. 2014). Furthermore there are modulatory inputs from L6 of barrel cortex (Bourassa et al. 1995; Deschênes et al. 1998), deep layers of secondary somatosensory cortex (Liao et al. 2010) and motor cortex (Cicirata et al. 1986; Alloway et al. 2008). POm is under inhibitory control arising from Rt (Crabtree et al. 1998; Bokor et al. 2005), ZI (Trageser and Keller 2004) and APT (Giber et al. 2008; Murray et al. 2010). POm activity can thereby be influenced by barrel cortex in numerous ways: monosynaptically from L5B and 6 and putatively disynaptically via secondary somatosensory cortex, motor cortex, SpVi, Rt, ZI and APT. POm neurons send their own axons to many of their input regions, reciprocally innervating barrel cortex, secondary somatosensory cortex, motor cortex and Rt (Carvell and Simons 1987; Crabtree et al. 1998; Deschênes et al. 1998; Meyer, Wimmer, Hemberger, et al. 2010). Notably the POm to secondary somatosensory cortex innervation has driver characteristics (Lee and Sherman 2008; Theyel et al. 2010). Furthermore POm innervates the dorsolateral striatum (Smith et al. 2012; Alloway et al. 2014), as well as insular and perirhinal cortices (Deschênes et al. 1998). It is not clear if all of PO receives inputs from the aforementioned areas, or if subnuclear organization correlates with specific input patterns.

POm neurons respond to whisker deflections in anesthesia with variable and long latencies of around 25 ms and a modest spike rate increase (Diamond, Armstrong-James, and Ebner 1992). Lesioning ZI however, reduces response latencies and increases response magnitudes, suggesting that the ascending pathway through POm is tightly controlled by ZI (Trageser and Keller 2004; Masri et al. 2006; Trageser et al. 2006; Urbain and Deschênes 2007a). Typically, POm neurons have RFs encompassing more than one whisker. As POm's main input structures (BC L5B and SpVi) also have multi-whisker RF properties, this property seems to be derived rather than emergent and hints at somatotopically organized inputs. Spontaneous activity is coupled to cortical up and down states in anesthesia (Diamond, Armstrong-James, Budway, et al. 1992; Slézia et al. 2011). In awake animals, POm spike rates modestly increase during whisking and are weakly tuned to whisking phase (Moore et al. 2015; Urbain et al. 2015).

Barrel cortex L5B axons have sparse but large (>3 µm diameters) and powerful boutons in POm. Electrically stimulating a single bouton triggers huge excitatory postsynaptic potentials (EPSPs >10 mV), which suffice to drive the postsynaptic neuron to spike (Groh et al. 2008). EPSP sizes allow

isolation of individual EPSPs in vivo, making detailed input-output analyses possible. Interestingly, POm directly innervates L5B, thereby potentially constituting a closed loop circuit (Mease et al. 2015). A further characteristic of L5B synapses in POm is their prominent paired-pulse depression. L5B synapses can thereby function in two different modes: Single synapse driving if the synapse is recovered or integrative mode if firing rate is >2 Hz (Groh et al. 2008). In the integrative mode EPSPs are smaller and therefore multiple EPSPs from barrel cortex or peripheral sources (Groh et al. 2014) have to be integrated to reach threshold. It was observed that during typical spontaneous activity the synapse is mostly in a depressed state (integrative mode), only occasionally inter spike intervals are long enough for the synapse to recover and switching to driving mode. In functional terms, this led to the theory that in driving mode L5B neurons can very effectively transmit a very strong signal at times of relatively low activity (Novelty or surprise detection) and more finely scaled signals during phases of higher activity (e.g. attentive states) in integrative mode. Presynaptic paired-pulse depression, together with the postsynaptic nonlinear biophysical properties of high T-type Ca-channel concentrations, makes this synaptic connection highly dynamically controlled.

POm function is a matter of debate, due to its unreliable responses to whisker deflections (Diamond, Armstrong-James, and Ebner 1992; Diamond, Armstrong-James, Budway, et al. 1992). Fitting into the concept of higher-order thalamic nuclei, it has been shown that POm can function as a cortico-thalamo-cortical (“transthalamic”) relay from barrel cortex to secondary somatosensory cortex (Theyel et al. 2010), however the relayed information content remains unclear. Stimulation of POm terminals can enhance and prolong BC sensory responses, showing POm has influence on BC signal processing (Mease et al. 2015). It has been demonstrated, but subsequently contested, that POm transforms stimulus frequencies into a rate code (Ahissar et al. 2000, 2008, Masri et al. 2008a, 2008b). Additionally there are reports that nociceptive signaling is mediated by POm (Murray et al. 2010). Another model takes the inhibitory control ZI has over POm into account, demonstrating that activating motor cortex disinhibits POm, leading to more robust whisker responses (Trageser and Keller 2004; Urbain and Deschênes 2007a). It was hypothesized that POm might therefore be disinhibited during whisking behavior, however, recently it was shown in awake animals that ZI rates did not change substantially during whisking (Moore et al. 2015). Finally, a role of POm in sensorimotor learning has been proposed, as POm signals to dorsolateral striatum (Smith et al. 2012; Alloway et al. 2014) and POm stimulation induces long term potentiation in barrel cortex (Gambino et al. 2014).

Goals

The role of higher-order thalamus in somatosensory processing is still unclear. Its major drive comes from BC L5B which has been demonstrated in vitro. In vivo however, due to the pathway's paired pulse depression and substantial spontaneous firing of L5B neurons the connection could be functionally less important. The focus of this thesis is to describe this pathway from cortex to thalamus in detail. First, we investigated the organization of the corticothalamic innervation from barrel cortex L5 by quantitative anatomical methods. Using whole-brain reconstructions of bouton locations from anterograde tract tracer injections, we report substructures in PO and quantify the synaptic bouton parameters in thalamus. Using dual injections we determine the somatotopic organization and whisker map orientation of the projections. Secondly we addressed the corticothalamic signaling efficacy and gain of these projections in POm in anesthetized mice *in vivo*. Using intra- and juxtacellular electrophysiology and optogenetics we ask how cortical signals are transformed in POm and how dominant those signals are in POm in comparison to VPM. We investigate both how spontaneous cortical oscillations are transformed in POm, as well as how cortical whisker evoked activity shapes POm and VPM responses *in vivo*.

Manuscript No 1: Organization and somatotopy of corticothalamic projections from barrel cortex layer 5B

Organization and somatotopy of corticothalamic projections from barrel cortex layer 5B

Anton Sumser, Bert Sakmann, Alexander Groh

In preparation

Author Contributions:

A.S. designed the study together with A.G. and B.S.; A.S. performed all injections, post-processing and imaging, developed all analysis programs and analyzed the data including figure generation; A.S. wrote the manuscript with help of all authors.

Organization and somatotopy of corticothalamic projections from L5B in barrel cortex

Anton Sumser[1,2,3], Bert Sakmann[1,3], Alexander Groh[1]

[1]Institute for Neurosciences, Technische Universität München, Biedersteiner Str. 29 – Bau 601, D-80802 Munich, Germany; [2]Graduate School of Systemic Neurosciences, Ludwig-Maximilians Universität München, Grosshaderner Str. 2, D-82152 Martinsried, Germany; [3]Max Planck Institute for Neurobiology, Am Klopferspitz 18, D-82152 Martinsried, Germany.

Neurons in cortical layer 5B (L5B) connect the cortex to various subcortical areas. Possibly the best studied L5B cortico-subcortical connection is formed between L5B neurons in the rodent barrel cortex (BC) and the posterior medial nucleus of the thalamus (POm). L5B neurons sparsely innervate POm where they form the largest known synapses of cortical origin. However, the distribution and organization of L5B giant boutons within POm and other target nuclei is not known. It is therefore unclear if this descending pathway retains somatotopic, i.e. body map organization – a hallmark of ascending pathways of sensory systems. Here we investigated the organization of the descending L5B driver pathway by multicolor anterograde labeling of cortical bouton fields in the thalamus and the anterior midbrain, originating from few (2-3) barrels in the barrel field. Subsequent large-scale confocal scanning microscopy and slice alignment enabled us to reconstruct the projection fields of adjacent BC L5B areas. In total we reconstructed the 3D location of more than 110,000 large boutons from seven such dual injection experiments. We found that L5B in BC targets 6 thalamic and midbrain areas in the posterior group thalamic nuclei (PO), the zona incerta (ZI) and the anterior pretectum (APT). Bouton numbers, density and projection volume were specific for the individual target nucleus. Common to all target nuclei is the maintenance of topology from different barrel columns in BC, albeit with a nucleus-specific varying precision. Bouton and soma density estimates revealed low convergence and divergence, illustrating that the L5B corticothalamic pathway is highly parallelized. The spatial organization of boutons and whisker map organization revealed the subdivision of PO into four distinct subnuclei (anterior, lateral, medial and posterior). In conclusion, corticofugal L5B neurons establish a widespread cortico-subcortical network via sparse but somatotopically organized parallel pathways.

Introduction

A characteristic feature of sensory systems is the topographic organization of their ascending pathways from the sensors to the cortex. This is particularly evident in the rodent whisker system in which the arrangement of whisker follicles on the snout of the animal (1) is mapped at each synaptic station up to the cortex where the whisker map forms the cortical barrel field of rodents (2). Neurons in the respective structures (i.e. barrellettes, barrelloids, barrels) respond best to deflections of their principal whisker (1). While this strict topographic organization is well-established for ascending pathways up to the cortex (1), it is less clear to which extend this map organization continues beyond the primary sensory cortex via descending projections to subcortical structures.

A major target of descending cortico-efferent projections is the thalamus, which is innervated by the cortex via two distinct corticothalamic pathways. Neurons in cortical layer 6 (L6) provide the numerically largest input to the primary sensory thalamus (3), while 5B thick-tufted neurons (L5B) innervate the higher-order thalamus with fewer but uniquely large driver synapses (4–6). The L6 feedback pathway is somatotopically organized (4). However, the organization and somatotopy of the L5B driver pathway is unclear. The lateral part of the posterior group (PO) in thalamus (POm) is the best described recipient of L5B synapses, where it has been shown that cortical L5B neurons comprise the dominant input (7–9). Receptive field studies support somatotopic organization of POm neurons even though an anatomical whisker map has not been shown (10). If somatotopic organization is continued in other than the most lateral part of PO is even less clear. L5B neurons also project to ventral thalamus, midbrain and brainstem (5, 6, 11, 12), however with undetermined organization. In this study we investigate if cortico-subcortical projections to thalamus and

anterior midbrain are somatotopically organized using a quantitative anatomical approach.

We labeled barrel cortical boutons using dual color anterograde tract tracing and subsequently imaged and reconstructed the 3D location of giant L5B boutons in the whole thalamus and the anterior midbrain. We found discrete bouton clouds in 4 areas of dorsal thalamus, one in ventral thalamus (zona incerta) and another in the anterior pretectum. L5B projections to each of those areas were somatotopically arranged, thereby mapping the whisker pad via cortico-subcortical projections. The somatotopic precision, map orientation and numbers of boutons were nucleus specific and revealed the subdivision of PO into four distinct L5B target areas. In summary, somatotopic maps can continue beyond the cortex via somatotopically organized cortico-subcortical projects from L5B neurons.

Results

Labeling of L5B neurons and boutons

We investigated cortico-subcortical projection patterns by injecting two different AAV constructs in two small areas in mouse BC of 7 mice (Figure 1A). Infected cells subsequently expressed the bouton marker Synaptophysin fused to either GFP or mOrange (Figure 1B, C) (13). Injections were targeted to L5 and labeled on average 98 +/- 61 L5B neurons (mean +/- standard deviation) in approximately 2.6 +/- 1.4 columns. Dual injections were always non-overlapping, the respective borders 288 +/- 80 µm (~2 column diameters) apart. Via large scale mosaic confocal fluorescence microscopy we acquired images (Figure 2 A-D) of the whole thalamus and adjacent midbrain regions, which were then used to semi-automatically extract the position and apparent diameters of giant (>1.5 µm) putative synaptic boutons (Figure 2E, F).

Spatial organization of bouton clouds

In the thalamus and anterior midbrain we find 6 target areas containing spatially distinct bouton clouds. Based on cytoarchitecture (Neurotrace and Cytochrome C Oxidase), these target areas correspond to 4 separate areas in PO, one in ZI and another in APT (Figure 1D-E). In dorsal thalamus, four clouds form a geometry resembling a ring (Figure

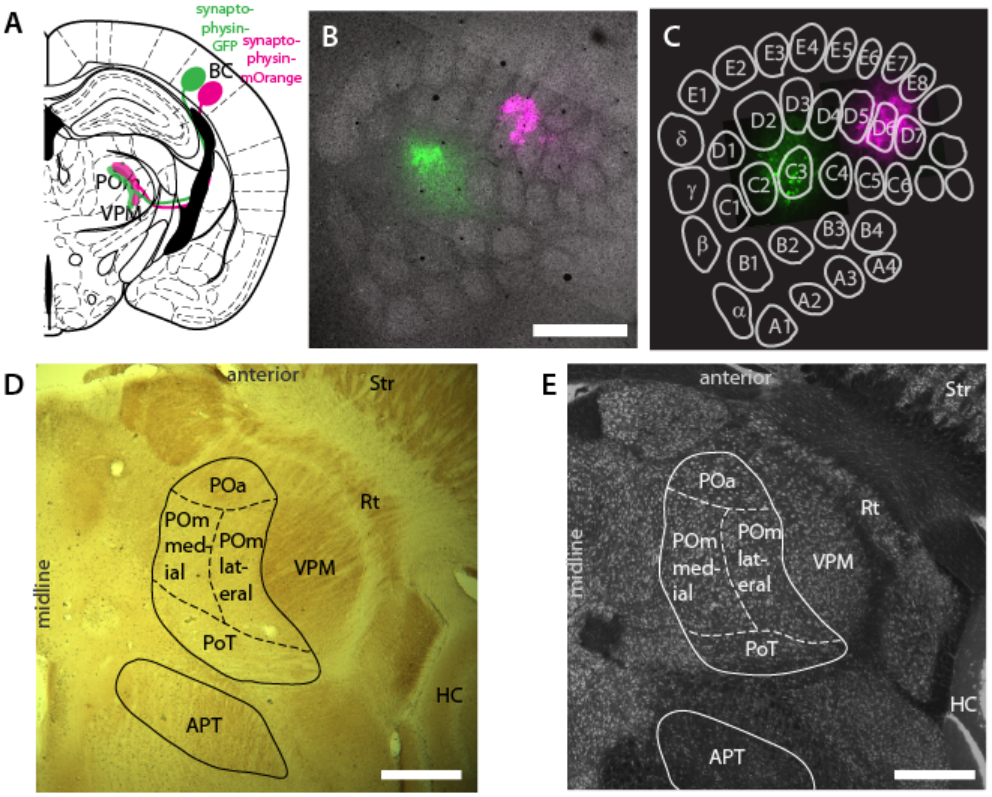

Figure 1: Experiment schematics, Injections and nucleus borders

Corticothalamic projections from barrel cortex were labeled with virus-mediated expression of two fluorescent proteins.
A: Experimental schematic, showing dual injection (green/magenta) of viral particles into BC and termination fields in thalamus in a coronal view (modified from (13)). B: Merged confocal fluorescence image of tangentially sliced BC at the level of layer 4. Barrels visualized in grey (Streptavidin-647 staining), injection areas for viruses expressing SP-GFP in green, SP-mOrange in magenta. Scalebar 500 µm. C: Delineation of Barrel field from B and injection sizes at the level of L5B as green and magenta colored somata and neuropil respectively. D: Example image showing thalamic areas in horizontal slice plane, stained for Cytochrome C Oxidase. Delineations of nuclei borders investigated in this study (with large boutons). Ventral posterior medial nucleus (VPM), thalamic reticular nucleus (Rt), Striatum (Str), Hippocampus (HC) indicated for orientation. Zona incerta is not shown, as it is located ventrally. Scalebar 500µm. E: Example image at a similar level as in D, but stained for neuronal somata by Neurotrace. Scalebar 500 µm.

2F), oriented along the horizontal plane and elongated rostrally. This anterior area is at the border between anterior PO and ventral lateral nucleus (VL), according to Paxinos mouse brain atlas (14). Inputs to VL are reported to come from basal ganglia and most tracing studies from BC do not report projections here. Two studies named the same projection area that we report here as VL, based on fitted atlas geometry (15, 16). However as PO extends into this area in the Allen Brain Institute atlas (17), we call this anterior PO (POa). The lateral and medial parts of the ring are also both in PO. To keep in established nomenclature we call these areas POm lateral and POm medial. The posterior area is at the atlas border of PO and the posterior triangular nucleus (PoT). Boutons are sparser in PoT. In ventral thalamus the dorsal ZI is labeled with many giant boutons, however as the area of ZI is prone to tissue damages during slicing, fewer data points are available (Figure 2H, 3C,G). Dense projections were additionally found in APT (Figure 2H, 3D,H). Table 1 lists the center of mass of the bouton clouds for each nucleus in Paxinos coronal mouse brain atlas equivalent coordinates (14). In contrast to some earlier reports (16, 17) we found only weak or no labeling in the ventral posterior lateral nucleus (VPL, not shown). As reported before, we found a few big boutons in the most posterior area of VPM

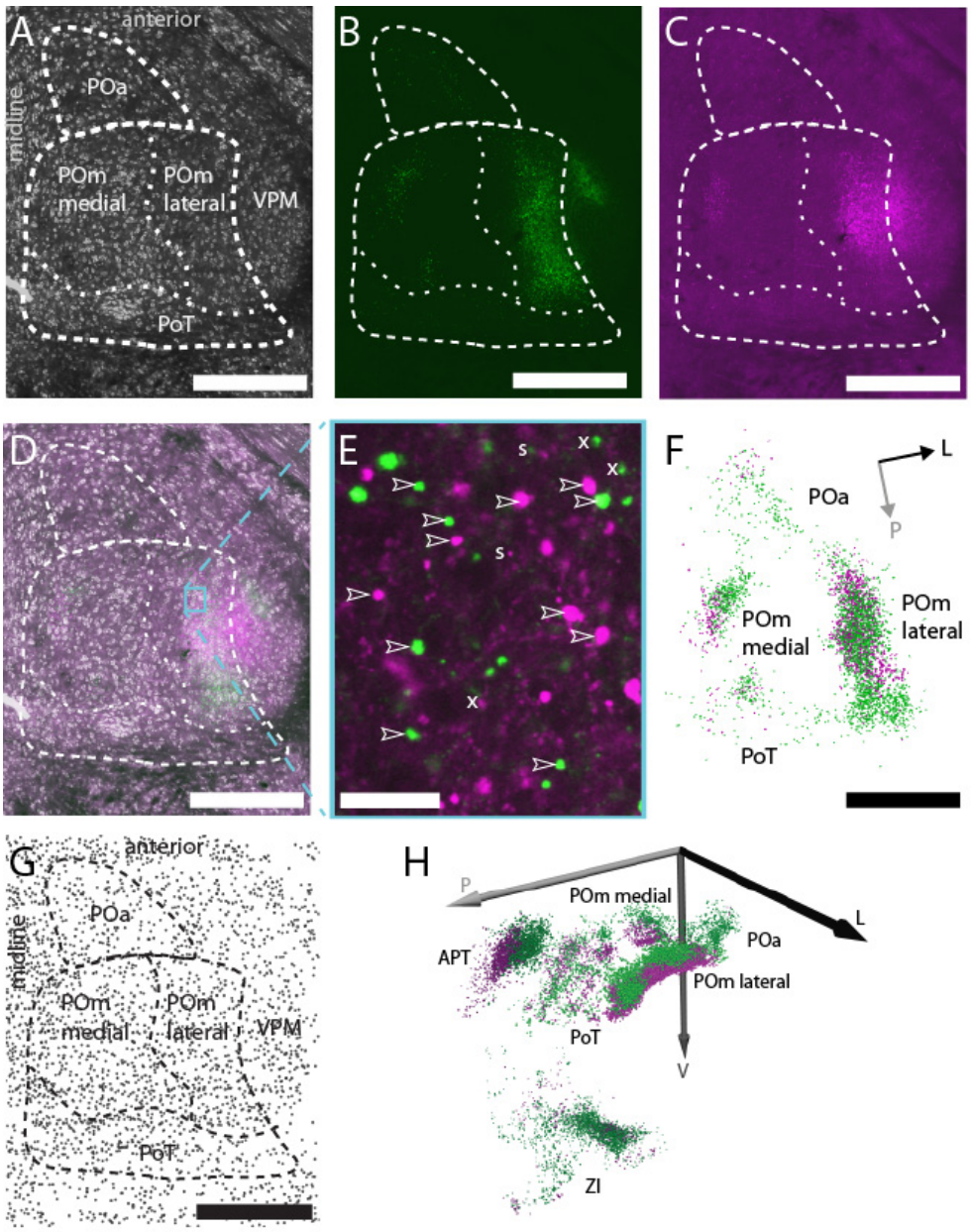

Figure 2: Example images and bouton cloud reconstruction

Confocal microscopy example images and bouton reconstruction. Scalebar A-D, F-G: 500 µm. A: Confocal image of dorsal thalamus; Neurotrace channel showing cell somata. B: GFP channel of the same region as A. C: mOrange channel of the same area as A. D: Merged images A-C. E: Zoom in into area shown in D (only GFP (green) and mOrange (magenta) channels). Arrowheads mark examples of boutons whose locations and diameters are extracted for terminal field reconstructions. 's' marks examples of puncta that are excluded from reconstructions due to their small size; 'x' marks examples of boutons not extracted, because brightness maximum is in an adjacent z-section. Overall brightness was enhanced here to increase visibility of dim signals. Scalebar 25µm. F: Reconstructed green and orange (shown in magenta) fluorescent boutons from B and C respectively. Sphere diameters represent bouton sizes scaled 2x to increase visibility. G: reconstructed somata locations from the image in A. H: All reconstructed boutons from the same experiment as A-G in a 3D view; colors for each nucleus slightly altered to increase visibility.

((18), not shown) but due to the low numbers of boutons (less than 3 boutons per L5B on average), VPM and VPL were not included in further analyses. In summary we report 6 separate areas receiving substantial numbers of L5B giant boutons, 4 of which are in PO. Besides the anterior midbrain and thalamus we found additional giant bouton clouds in superior colliculus and brainstem which will be presented in a separate study.

Bouton cloud geometries

Bouton clouds have distinct shapes in each of the reported areas. Bouton cloud shapes in POm lateral are approximating a straight rod oriented parallel to the anterior-posterior (AP) axis (Figure 3B, F). Bouton clouds in POm medial form a curved rod ('banana') with its main axis approximately parallel to the AP axis and its ends pointing laterally. Bouton clouds in PoT are shaped like a sheet where the anterior end is slightly elevated from the horizontal plane. POa bouton clouds are roughly spherical, with an extension in the direction of POm lateral, however POa bouton cloud shapes were variable over experiments. In ventral thalamus, ZI boutons lie roughly in the horizontal plane, often with inhomogeneous density distribution (Figure 3C,G). The majority of boutons were in the dorsal part of ZI. Bouton clouds in APT are shaped like slightly prolate spheroids, sometimes with low density extensions (Figure 3D,I).

Bouton cloud quantifications

Using full 3D reconstructions of giant boutons in thalamus and anterior midbrain, we were able to quantify size and numbers of individual boutons, as well as volumes and densities of bouton clouds in the respective nuclei. Estimated mean bouton diameters were 2.7 +/- 0.6 µm and 3.0 +/- 0.6 µm (GFP and mOrange labeled boutons, respectively; interval based on standard deviation). Bouton diameters were comparable across nuclei with a mean of 2.4-3 µm (GFP, Figure 4A, mOrange: 2.7-3.3 µm, table 1).

We next estimated the average number of boutons per L5B neuron by normalizing bouton counts for the different nuclei with the number of fluorescently labeled somata in BC L5B (Figure 4B). Based on these estimates, L5B neurons make between 9.4 and 40.7 giant boutons depending on the nucleus. Nuclei fall in roughly two groups: POm lateral and APT are innervated by more than 30 boutons per L5B neuron, while POa, POm medial and PoT have less than

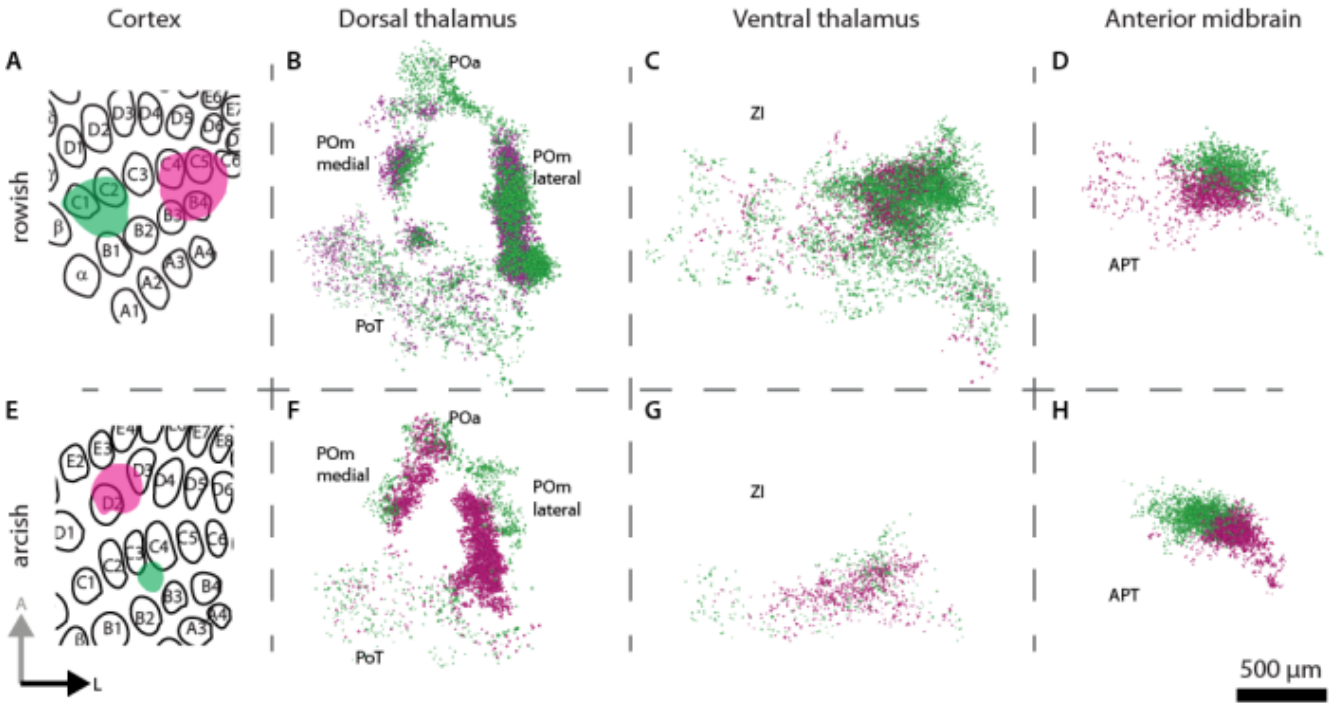

Figure 3: Thalamic Nuclei, termination field illustrations

Comparison of two experiments with rowish (A-D) and arcish (E-H) injection positions respectively, showing different relative bouton cloud positions in consequence. B-D, F-H at same scale and orientation; scalebar 500µm. A: Schematic of rowish injection locations in BC; Both injections mostly in C-row. B: Top view on bouton reconstructions in dorsal thalamus (PO) labeled by injections shown in A, showing the individual bouton clusters. In PO, GFP labeled boutons are located mostly above mOrange labeled boutons; 3D view in Fig. 2G. C: Top view on boutons in ventral thalamus (ZI) labeled by injections shown in A; 3D view in Fig. 2G. D: Top view on boutons in anterior midbrain (APT) labeled by injections shown in A; 3D view in Fig. 2G. E: Schematic of arcish injection locations in BC; Both injections mostly in arcs 2-3. F-G: as B-D for injections shown in E.

12 (Table 1). ZI bouton numbers range in between at approximately 23. The differences are significant (Wilcoxon signed rank, $p<0.05$) between these groups. Scaled to a L5B column, we estimate approximately 1100 boutons per column in the first group and 280 in the latter (Supplementary figure 1). When approximating bouton cloud volumes (see supplementary methods) in the respective nuclei, PO (excluding PoT) contains the smallest volumes with less than 1.4e-4 mm^3 per projection neuron while in PoT, APT and ZI boutons are spread over significantly larger volumes (Table 1 and Figure 4C). We measured the highest bouton densities in POm lateral and APT (4.2e5 +/- 0.5e5 and 3.6e5 +/- 0.7e5 mm^{-3} respectively, both significantly higher than all others (Table 1 and Figure 4D)). Estimating soma densities based on a subset of Neurotrace co-labeled experiments resulted in comparable densities of approximately 4e4 mm^{-3} in all nuclei, with the exception of ZI where density is lower at 2e4 mm^{-3} (Table 1 and Figure 4E). The ratio of bouton density and soma density gives an approximation of how many boutons are available to one target neuron on average. POm lateral and APT neurons have most with 9 boutons per soma, while neurons in all other (APT vs. ZI not significant) nuclei have significantly fewer (5 or less) boutons available. In summary, while bouton sizes were comparable in the respective nuclei, numbers and cloud volume differed specifically depending on target. POm lateral and APT are innervated very strongly by L5B.

Somatotopic precision

When looking at the bouton reconstructions in 3D, it is evident that the bouton clouds are mostly positioned next to each other and are not occupying the same volume (Figure 2H). To quantify the somatotopic precision of those projections we used an approach based on generalized quadratic linear models (GLM), as volume determination from point clouds is error-prone. Using GLMs we fitted the surface separating the bouton clouds best and then

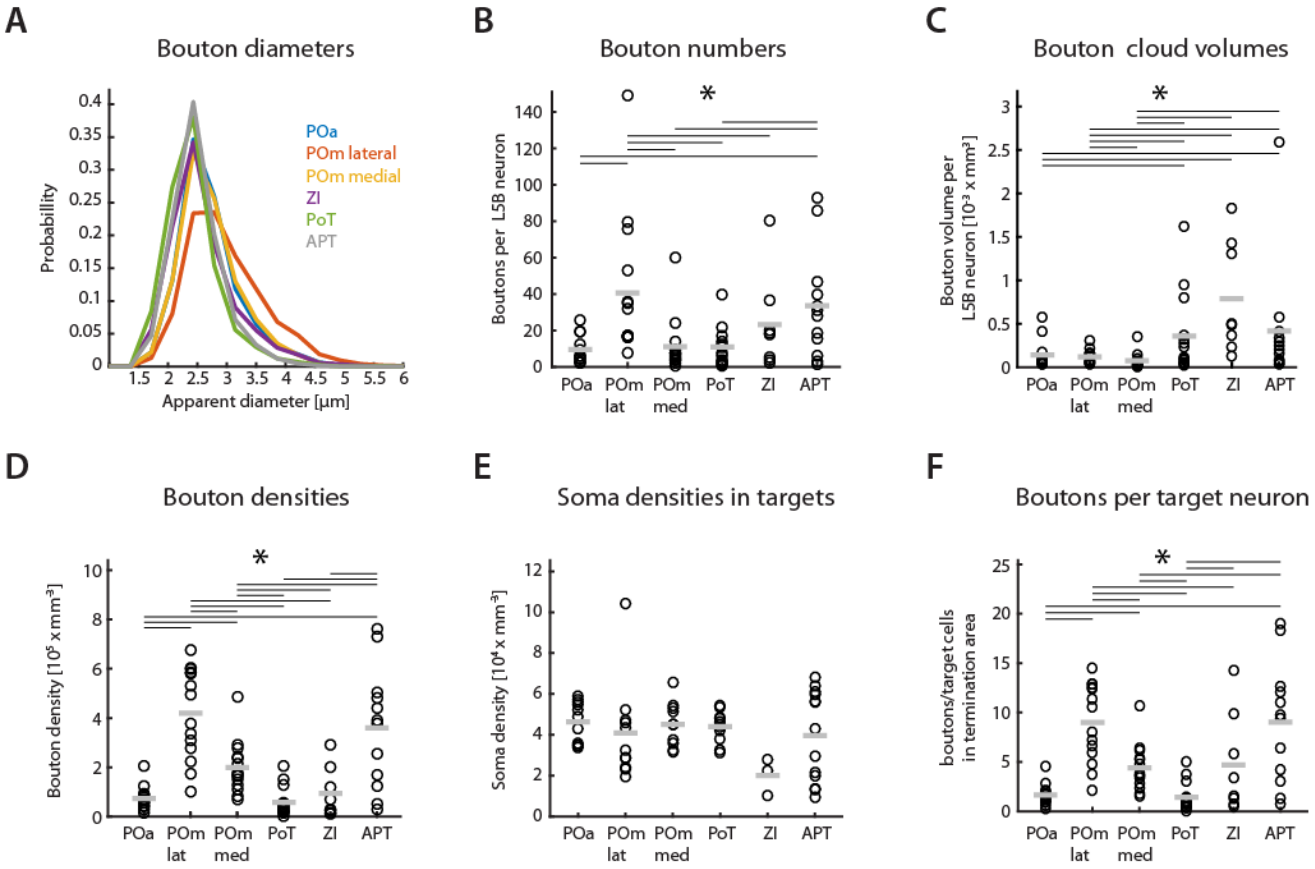

Figure 4: Quantifications

A: Histogram of bouton diameters (only GFP) in the respective nuclei, normalized to probability of occurence. B: Number of boutons in respective nuclei, normalized by number of labeled L5B neurons. Each injection represented as black circles, mean as grey line. Black lines above indicate which nuclei are significantly different from each other (Wilcoxon signed rank, $p<0.05$). C: Termination field volume in respective nuclei, normalized by number of labeled L5B neurons. Conventions as in B. D: Density of boutons in termination field, equaling the ratio of number per volume. Conventions as in B. E: Estimated soma densities from Neurotrace staining in a subset of experiments. F: Number of boutons for each target cell in respective nuclei, equaling the ratio between bouton and neuron density. Conventions as in B.

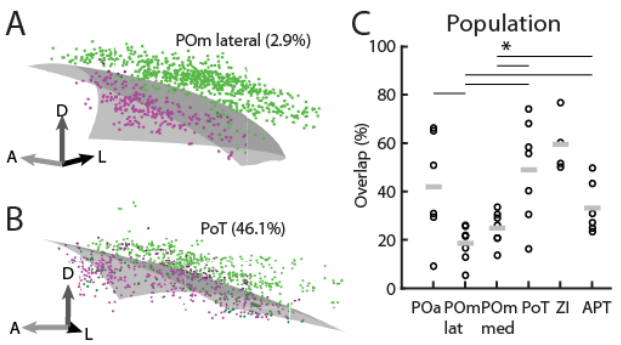

Figure 5: Overlap

Overlap between dual injection bouton clouds calculated by generalized linear model (GLM)
A: Low overlap example from POm lateral, showing a randomly selected subset of 1000 Boutons for clarity. Transparent grey surface shows (GLM) modeled surface that gives best separation of bouton clouds (green and magenta dots). Boutons on the opposite side of the surface (overlapping boutons) are plotted in a dark shade of green and magenta respectively. Twice the percentage of overlapping boutons gives an estimate of cloud overlap. B: High overlap example from PoT. Plot conventions as in A. C: Population data: Overlap estimates as in A,B for all nuclei. Each circle represents one experiment, grey bar shows mean. Lines indicate which nuclei are significantly different from each other (Wilcoxon signed rank, $p<0.05$).

calculated the percentage of boutons located on the opposite side (Figure 5A,B). The percentage is then proportional to the overlap, which can be used as an inverse proxy of somatotopic segregation. Even though injections were always non-overlapping, bouton clouds did overlap. Overlap percentages varied substantially between experiments and nuclei. POm (medial and lateral) and APT have mean overlaps of 20-30%, POa, PoT and ZI more than 40% (Figure 5C). There were no significant correlations between overlap and injection distances or rowish/arcish injections.

Whisker map transformation

Comparing the bouton cloud locations from rowish (Figure 3A-D) and arcish (Figure 3E-I) injections, we found that the relative bouton cloud positions varied for each nucleus depending on the injections. Using all seven pairs of dual injections, we tested if bouton cloud positions can be predicted from injections. We fitted linear models to the relative positions of bouton cloud centroids from relative injection locations in the barrel field. Using the models to predict virtual purely rowish and arcish injections, results in the rotation of barrel field projection geometries in thalamus and anterior midbrain. POm lateral and APT bouton clouds could be predicted quite accurately (prediction SEM 2° for POm lateral and 3° for APT). Prediction errors for the other nuclei were higher (SEM: 6° (POa), 7° (POm medial), 9° (PoT), 5° (ZI)). In POm lateral, rows A-E are arranged approximately from lateral to medial, arcs 1-7 from dorsal to ventral. In POm medial and PoT, projection arcs are oriented similarly while projection rows, point in the opposite direction. In APT, projection rows point posteriolaterally, arcs ventroposteriomedially. In ZI, projection rows point anterioventrally, arcs medially. In POa, projection arcs and rows both are oriented approximately in the posterior direction, arcs slightly ventrally; the projection barrel field is therefore strongly distorted (Figure 6). In summary each nucleus has its individual map organization in L5B projections. Taking the map orientations of PO together, rows are organized from outside to inside, e.g. A row projections encompassing B row projections, while arc projections are oriented downwards, e.g. arc 1 dorsal to arc 2 (Figure 7).

Nucleus		POa		POm lateral		POm medial		PoT		ZI		APT	
		Mean	SEM	Mean	SEM	Mean	SEM	Mean	SEM	Mean	SEM	Mean	SEM
Paxinos equivalent coordinates (mm)	lateral (bregma)	0.95		1.35		0.77		0.91		1.33		0.83	
	caudal (bregma)	1.25		2		1.73		2.28		2.43		2.71	
	ventral (pia)	3.2		3.25		3.2		3.34		4.28		3.14	
Bouton mean diameters (µm)	GFP	2.73	0.01	3.01	0.03	2.75	0.02	2.62	0.03	2.44	0.03	2.51	0.02
	mOrange	2.93	0.06	3.27	0.04	2.99	0.03	3	0.07	2.73	0.08	2.74	0.03
Boutons/L5B neuron		9.4	2.3	40.7	10.4	11.7	4.4	10.8	2.8	23.1	9.2	33.7	8.7
Boutons/column		271	47	1122	159	291	58	299	57	618	256	1022	209
Volume/L5B neuron (x10^-4 mm^3)		1.4	0.5	1.2	0.2	0.8	0.3	3.6	1.2	7.9	2.3	4.2	2
Volume/column (x10^-4 mm^3)		37.2	10.3	35.5	3.6	20.3	3.6	90.6	21.8	204.7	56.5	122.5	50.3
Bouton density (x10^4 mm^-3)		7.4	1.3	41.7	4.9	19.9	2.8	5.8	1.6	9.4	3.6	35.8	7
Soma density (x10^4 mm^-3)		4.4		4.64		4.52		4.09		2.01		3.97	
Boutons/Soma		1.7	0.3	9	1.1	4.4	0.6	1.4	0.4	4.7	1.8	9	1.8

Table 1: Nucleus specific bouton parameters

Discussion

Although POm clearly belongs to the whisker system on anatomical grounds and is responsive to whisker deflections (10), the function of POm in whisker processing is unclear (19–23). The main synaptic drive of POm originates in the barrel cortex in L5B (7, 8, 24, 25). Anatomical and physiological properties point to the possibility of substructures in PO, however not conclusively (26–29). Here, using a quantitative neuronal tract tracing approach, we find that L5B giant boutons cluster in four regions of PO. Additionally ZI and APT receive substantial input from L5B – two regions that were shown to inhibit POm (21, 30). Two-color labeling of L5B boutons, revealed that in each target nucleus, bouton clouds repeat the relative spatial arrangement of the whiskers on the animal snout. Thus, descending L5B projections are somatotopically arranged into whisker maps with target-specific orientation.

Methodological considerations

Synaptophysin-fluorophore fusion proteins have been used to label presynaptic boutons (17, 31). A fraction of the signal may stem from transport vesicles in axons, potentially leading to an overestimation of boutons. Clearly axonal signal was removed manually, however. Using a signal to noise approach, we selected only brightly labeled spots, thereby minimizing artifacts, on the expense of missing some boutons when background fluorescence was high. The sparseness and size of L5B boutons allowed us sample coarsely in z-direction (with 10 µm between optical sections) and thereby image the whole brain. To counteract signal loss through z-undersampling, we increased the pinhole. Consequently boutons span 2-3 z-sections, but could result in merging of closely neighboring boutons. In summary, this approach may underestimate L5B bouton counts. L6 also projects to POm (32) and was labeled in our experiments. However L6 innervation has a very different projection pattern, with very dense but small boutons in comparison to L5B (32). L6 boutons were either excluded by size (<1.5 µm), or poor signal to noise ratios because they appear as regions with high background, due to their very high density.

There was substantial variability of most bouton parameters (e.g bouton counts, cloud volume) across experiments. Varying background fluorescence in the experiments possibly influenced detectability of boutons and could account for some of the variance in bouton parameters over experiments. Another source of variability between injections might be explained by L5B subtypes: not every individual L5B neuron innervates all target areas simultaneously (6, 33) and septal L5B neurons might have different projection patterns than column neurons (34). Thereby small variations in injection sites relative to column centers may result in different bouton parameters in the target areas.

Substructures in PO

Bouton cloud reconstructions revealed four distinct input areas in PO which together form a ring in the horizontal plane. Each PO subnucleus has its characteristic, nucleus-specific organization of L5B boutons. Firstly, POm lateral has highest bouton densi-

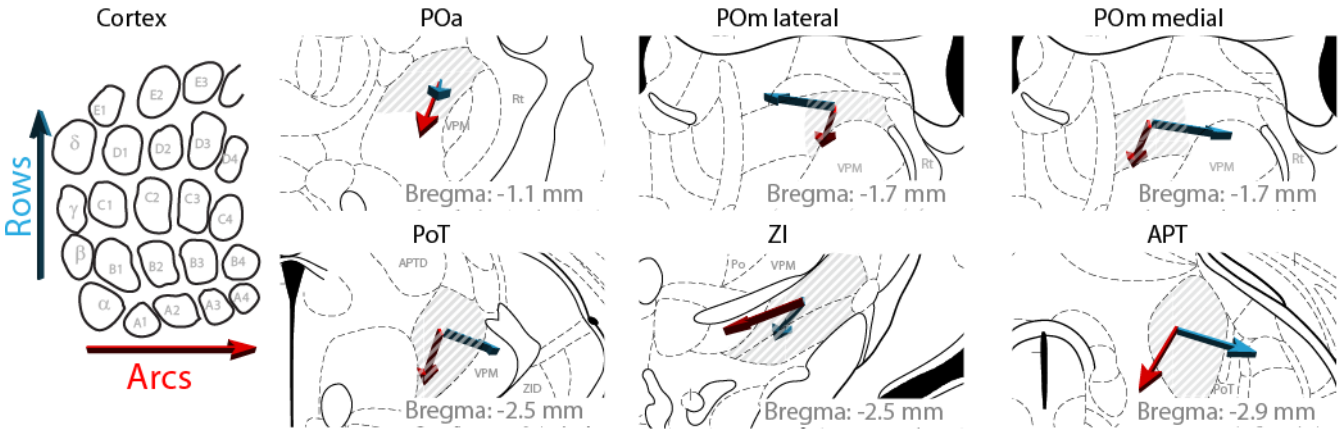

Figure 6: Schematics of map transformations

Illustration of barrel field projection map rotation in respective nuclei. Cortex panel shows a tangential schematic of barrel field with red and blue arrows showing arrangement of rows and arcs respectively. Schematics for respective nuclei show a modified cropped region from Paxinos coronal atlas (12), region of interest is striped. The POa region is actually labeled as VL in the atlas. Red and blue arrows show the 3-dimensional rotation of the projection map. Arrows are perspectively distorted for visualizing arrows coming out towards the viewer (posterior) or away (anterior). SEM of prediction: 2° (POa), 2° (POm lateral), 6° (POm medial), 6° (PoT), 3° (ZI) and 4° (APT).

ties, while PoT and POa densities are much lower (Figure 4D). Secondly, the corticothalamic map precision and orientation was specific for each PO subnucleus (Figure 5C) such that PO contains 4 differently oriented whisker maps. It remains unclear if the cortical projections into the 4 subnuclei are paralleled by inputs from other sources. For example the spinal trigeminal nucleus interpolaris innervates only approximately a third of PO, the distribution however does not colocalize with the divisions reported here (26). Previous physiological studies also hint at functionally different populations in PO (27, 28), but systematic functional studies are lacking.

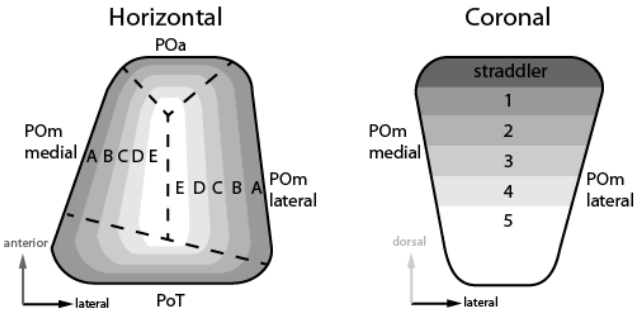

Figure 7: PO projection map

Horizontal (left)and coronal (right) schemata of the projection map in PO, showing outside-in organization of rows and dorsomedial orientation of arcs. For orientation, VPM would be located to the right in both panels.

Somatotopic precision

Bouton clouds from two-color injections demonstrate topographic projections. However, even though dual injections were always non-overlapping, subcortical bouton clouds overlap in nucleus specific amounts. The overlap variability between experiments also varied depending on the nucleus. POm lateral and medial had lowest overlaps (~20%) and lowest variation. This confirms previously reported corticothalamic projection map specificity (that included L6), suggested to be similar to that of VPM (35). POa and PoT have higher overlap and therefore less precise somatotopic projections. Overlap in POa and PoT furthermore was highly variable between experiments. Correlations between overlap and injection border distance were not significant. Therefore we assume a nonlinear relationship between injection distance and overlap. For other areas it has been previously reported that projection overlap is anisotropically higher along rows than along arcs (36), thereby the relative injection locations could influence projection overlap. Furthermore, due to the columnar organization of BC, L5B projections from neurons in the same column could have a far higher overlap than that from neurons in neighboring columns. In this case overlap would be scaled non-linearly, depending on the labeled column distance. In summary, in all nuclei we found segregated bouton clouds from dual injections indicating somatotopic projection organization. Somatotopic projections naturally entail a reproduced map from BC to target regions.

Projection maps

Abstracting from diverse relative injection locations, we were able to determine the rotation of the projection map. Interestingly, looking at the projections into PO together, projection arcs are always oriented approximately downwards (i.e. C4 projections are located ventrally of C2 projections), projection row directions however were variable: In the horizontal plane, the A row is located on the outside of the respective nuclei (e.g. lateral in POm lateral and medial in POm medial), while the other rows are on the inside (Figure 7). Consequently, injections in the same arc result in bouton rings stacked on top of each other, while injections in the same row form rings where one encompasses the other. PO neurons are mostly driven by BC L5B, therefore it can be expected that receptive fields of PO neurons map in a similar way than the L5B projection organization. This peculiar organization could have functional consequences. For example if other inputs would have a more regular projection map, inputs from different rows could be processed and integrated very differently. In summary, PO subnuclei receive cortical inputs in specific fashions and in toto produce a highly convoluted projection map.

Corticothalamic convergence and divergence

Corticothalamic driver convergence (i.e. the number of L5B neurons innervating one PO neuron) and divergence (the number of POm neurons innervated by one L5B neuron) is unknown. With the presented data set we can make a first quantitative estimation of corticothalamic driver convergence and divergence. For the example, in POm lateral we found on average approximately 41 boutons per L5B neuron, which is comparable to previously published single neuron reconstructions (6). Considering the unlikely scenario in which a L5B neuron makes only a single synapse with each of its postsynaptic target neurons in PO, L5B neurons would on average contact 41 POm lateral neurons. Furthermore, on average 9 L5B boutons are available for one POm neuron based on the ratio between bouton and soma densities. Again

assuming single contacts between neurons, a POm lateral neuron would thereby be innervated by 9 L5B neurons. However, single contacts between L5B and POm lateral neurons are unlikely since L5B axons form multiply dense bouton clusters (6). Multiple contacts between L5B and postsynaptic PO neurons are further supported by recent functional convergence estimates of the pathway, suggesting approximately 2-3 independent L5B subthreshold inputs (8). Multiple contacts of the same neuron however cannot easily be discerned physiologically and would resolve the apparent discrepancy between anatomical and physiological estimations. In consequence, 2.5 presynaptic neurons sharing 9 synapses to innervate the postsynaptic neuron result in 3.6 contacts between individual L5B and POm lateral neurons on average. Finally, when of the 41 boutons made in POm lateral 3.6 go to one neuron, an average L5B neuron innervates approximately 11 (41/3.6) POm lateral neurons. Even though these values are very rough estimates, they show very low divergence and convergence, indicating that the pathway is highly parallelized.

Inhibitory nuclei

In addition to PO, L5B also projects substantially into the GABAergic nuclei ZI and APT. While both nuclei receive similar numbers of L5B boutons, the organization of L5B giant boutons are quite distinct between nuclei. APT receives dense bouton clouds, which are somatotopically arranged albeit with lower precision than POm lateral. In dorsal ZI, L5B boutons innervate a large area in a sheet shape, following the overall dimensions of the nucleus. Densities are lower than in APT and somatotopic precision is poor. Neurons in both regions are reported to inhibit POm, allowing for complex corticothalamic interactions (21, 30, 37). Whether L5B targeted ZI and APT neurons in turn directly inhibit POm, or have a disinhibitory effect via intermediate local inhibition is unclear. For example, motor cortex also innervates ZI, but has probably a disinhibitory effect on POm due to local inhibition between the subdivisions of ZI (21).

Functional considerations

We found that cortico-efferent projections from BC L5B are somatotopic and highly parallelized. This suggests that the signal pathway is organized in a labeled lines fashion. Projections to PO are divided into 4 areas with different properties, suggesting functionally distinct subdivisions of PO. However, taking PO as one structural nucleus reveals a peculiar outside-in projection map, suggesting alternative functional consequences. While the L5B to APT innervation is somatotopically arranged, L5B to ZI projections appear less structured, which might hint at different (dis)inhibitory influences on PO processing. Whether ZI and APT in turn project somatotopically to POm remains unknown, but ZI neurons seem to innervate a large area of POm, according to single neuron reconstructions of projecting ZI neurons (21). Somatotopic precision and cortico-subcortical projection properties to superior colliculus and brainstem are subject of a separate study.

Barrel cortex layer 5B corticothalamic projections constitute a highly parallel and topographically organized driver pathway that centers on the higher order nucleus PO. In consequence, signals from barrel cortex are topographically broadcasted via PO to multiple other cortical and subcortical areas on the basis of the whisker map.

Materials and methods

Ethical Approval

All experiments were done according to the guidelines of German animal welfare and were approved by the respective ethical committees.

Viral Tracers

Adeno associated viruses serotype 1/2 (AAV), were obtained from Genedetect (New Zealand). The constructs (Synaptophysin-GFP and Synaptophysin-mOrange) were a kind gift of Thomas Kuner (31). As Synaptophysin is targeted to presynaptic endings, fluorescent proteins accumulate there. Injection coordinates ranged between 2.8-3.35 mm lateral and 0.85-1.7 mm posterior to bregma and were centered at the level of L5 (0.7-0.8 mm below pia). Injection coordinates for dual labeling were on average 0.6 mm apart. In post-hoc reconstructed tangential slices we visualized the barrel field by a simple fluorescent Streptavidin staining protocol and determined injection centers between α and D6. In the range between 100 and 300 µm below the lower end of barrels, which we approximate as L5B, we counted 98 +/- 61 (mean +/- standard deviation) fluorescent somata in a volume of 0.009 +/- 0.007 mm^3 (corresponding to approximately 2.6 +/- 1.4 columns). Dual injection borders were 288 +/- 80 µm (~2 column diameters) apart. Consequently we achieved focal transfection of low numbers of L5 neurons in two separate areas of BC with constructs

that lead to fluorescent labeling enriched specifically in synaptic boutons.

Injection procedure

Seven C57/BL6 mice of both sexes at age 5 to 7 postnatal weeks at the time of injection were used in this study. An additional C57/BL6 mouse was used for horizontal Cytochrome C Oxidase labelling, which was not injected. Detailed injection procedures are described in supplementary text. In short: Anesthesia was induced by isoflurane, local analgesia by subcutaneously injected lidocaine. The head was fixed with earbars, stereotactically aligned and the head tilted to the left to allow pipette insertion perpendicular to the pia on the right hemisphere. Approximately 30-100 nl virus solution was slowly injected at a depth of 0.7-0.8 mm below pia by applying air pressure. Injection procedure was then repeated for the second injection with the other virus solution (Mean distance between injections: 0.6 +/- 0.1 mm (mean +/- standard deviation)). After 14-16 days incubation period, the mouse was exposed to a lethal dose of isoflurane and transcardially perfused with 4% paraformaldehyde.

Slicing and Histology

Slicing: The brain was embedded in ~2% agarose and then cut at various angles, always with 100µm thickness. First BC was cut tangentially (tilt ~22° to left and ~8° upward), then thalamus and midbrain either coronally (1 experiment), sagittally (2) or horizontally (4). Barrels were visualized with Streptavidin-Alexa647 (ThermoFisher). In a subset of experiments thalamic slices were stained for somata using Neurotrace 435 (Thermo Fisher). Cytochrome C Oxidase staining was achieved as described in (26).

Microscopy

Slices were imaged with an Olympus FV1000 confocal microscope outfitted with an automated stage for mosaic imaging. For cortical barrel field and thalamic overview imaging objective UPlan FL N 4x NA 0.13, for bouton imaging objective UPlanSApo 20x NA 0.85 (oil immersion) was used. Lasers: Neurotrace 435/455: 405 nm; SP-GFP: 488 nm; SP-mOrange: 559 nm; Streptavidin 647: 630 nm. Slides were always scanned in sequential mode, pinhole opened to 300 µm, zoom 1.5. Z-stepping for imaging boutons was set to 10 µm to allow effective scanning of large areas.

Analysis

Scanned slices were aligned with Amira (FEI, USA), bouton locations and diameters extracted with custom written algorithms in MATLAB (Mathworks, USA). We excluded signals with diameters smaller than 1.5 µm from the analysis (Figure 2E), ruling out L6 contributions. L6 of barrel cortex projects to thalamus, but with smaller boutons (32, 38). Quantitative analysis performed with MATLAB. Analysis details are described in supplementary text. Values are given as mean +/- standard error of the mean if not specified otherwise.

Further method details are outlined in supplementary text.

Acknowledgments

We want to kindly thank Arthur Konnerth for providing lab space and infrastructure and Thomas Misgeld for access to his confocal microscope. For funding we also want to thank Boehringer Ingelheim Fonds (A.S.) and Deutsche Forschungsgemeinschaft (A.G.) (GR 3757/1-1).

1. Bosman LWJ, et al. (2011) Anatomical Pathways Involved in Generating and Sensing Rhythmic Whisker Movements. *Front Integr Neurosci* 5(October):53.
2. Woolsey TA, van der Loos H (1970) The structural organization of layer IV in the somatosensory region (SI) of mouse cerebral cortex. The description of a cortical field composed of discrete cytoarchitectonic units. *Brain Res* 17:205–242.
3. Erişir A, Van Horn SC, Sherman SM (1997) Relative numbers of cortical and brainstem inputs to the lateral geniculate nucleus. *Proc Natl Acad Sci U S A* 94(4):1517–20.
4. Sherman SM (2016) Thalamus plays a central role in ongoing cortical functioning. *Nat Neurosci* 16(4):533–541.
5. Bourassa J, Pinault D, Deschênes M (1995) Corticothalamic projections from the cortical barrel field to the somatosensory thalamus in rats: A single-fibre study using biocytin as an anterograde tracer. *Eur J Neurosci* 7(1):19–30.
6. Veinante P, Lavallee P, Deschênes M (2000) Corticothalamic projections from layer 5 of the vibrissal barrel cortex in the rat. *J Comp Neurol* 424(2):197–204.
7. Groh A, de Kock CPJ, Wimmer VC, Sakmann B, Kuner T (2008) Driver or Coincidence Detector: Modal Switch of a Corticothalamic Giant Synapse Controlled by Spontaneous Activity and Short-Term Depression. *J Neurosci* 28(39):9652–9663.
8. Mease RA, Sumser A, Sakmann B, Groh A (2016) Corticothalamic Spike Transfer via the L5B-POm Pathway in vivo. *Cereb Cortex*:bhw123.
9. Sherman SM (2005) Thalamic relays and cortical functioning. *Prog Brain Res* 149:107–126.

10. Diamond ME, Armstrong-James M, Ebner FF (1992) Somatic sensory responses in the rostral sector of the posterior group (POm) and in the ventral posterior medial nucleus (VPM) of the rat thalamus. *J Comp Neurol* 318(4):462–76.
11. Wise SP, Jones EG (1977) Somatotopic and columnar organization in the corticotectal projection of the rat somatic sensory cortex. *Brain Res* 133(2):223–235.
12. Wise SP, Jones EG (1977) Cells of origin and terminal distribution of descending projections of the rat somatic sensory cortex. *J Comp Neurol* 175(2):129–57.
13. Meyer HS, et al. (2010) Cell Type-Specific Thalamic Innervation in a Column of Rat Vibrissal Cortex. *Cereb Cortex* 20(10):2287–2303.
14. Franklin KBJ, Paxinos G (2008) *Paxinos and Franklin's The mouse brain in stereotaxic coordinates*.
15. Papp EA, Leergaard TB, Csucs G, Bjaalie JG (2016) Brain-Wide Mapping of Axonal Connections: Workflow for Automated Detection and Spatial Analysis of Labeling in Microscopic Sections. *Front Neuroinform* 10(April):1–11.
16. Zakiewicz IM, Bjaalie JG, Leergaard TB (2014) Brain-wide map of efferent projections from rat barrel cortex. *Front Neuroinform* 8(February):5.
17. Oh SW, et al. (2014) A mesoscale connectome of the mouse brain. *Nature* 508(7495):207–214.
18. Liao C-C, Chen R-F, Lai W-S, Lin RCS, Yen C-T (2010) Distribution of large terminal inputs from the primary and secondary somatosensory cortices to the dorsal thalamus in the rodent. *J Comp Neurol* 518(13):2592–611.
19. Ahissar E, Sosnik R, Haidarliu S (2000) Transformation from temporal to rate coding in a somatosensory thalamocortical pathway. *Nature* 406(6793):302–306.
20. Moore JD, Mercer Lindsay N, Deschênes M, Kleinfeld D (2015) Vibrissa Self-Motion and Touch Are Reliably Encoded along the Same Somatosensory Pathway from Brainstem through Thalamus. *PLoS Biol* 13(9):e1002253.
21. Urbain N, Deschênes M (2007) Motor Cortex Gates Vibrissal Responses in a Thalamocortical Projection Pathway. *Neuron* 56(4):714–725.
22. Masri R, Bezdudnaya T, Trageser JC, Keller A (2008) Encoding of stimulus frequency and sensor motion in the posterior medial thalamic nucleus. *J Neurophysiol* 100(January 2008):681–689.
23. Yu C, Derdikman D, Haidarliu S, Ahissar E (2006) Parallel Thalamic Pathways for Whisking and Touch Signals in the Rat. *PLoS Biol* 4(5):e124.
24. Mease RA, Sumser A, Sakmann B, Groh A (2016) Cortical Dependence of Whisker Responses in Posterior Medial Thalamus In Vivo. *Cereb Cortex*:bhw144.
25. Reichova I, Sherman SM (2004) Somatosensory corticothalamic projections: distinguishing drivers from modulators. *J Neurophysiol* 92(4):2185–97.
26. Groh A, et al. (2014) Convergence of cortical and sensory driver inputs on single thalamocortical cells. *Cereb Cortex* 24(12):3167–79.
27. Trageser JC, Keller A (2004) Reducing the uncertainty: gating of peripheral inputs by zona incerta. *J Neurosci* 24(40):8911–5.
28. Gauriau C (2004) Posterior Triangular Thalamic Neurons Convey Nociceptive Messages to the Secondary Somatosensory and Insular Cortices in the Rat. *J Neurosci* 24(3):752–761.
29. Clascá F, Rubio-Garrido P, Jabaudon D (2012) Unveiling the diversity of thalamocortical neuron subtypes. *Eur J Neurosci* 35(10):1524–1532.
30. Bokor H, et al. (2005) Selective GABAergic control of higher-order thalamic relays. *Neuron* 45(6):929–40.
31. Wimmer VC, Bruno RM, de Kock CPJ, Kuner T, Sakmann B (2010) Dimensions of a Projection Column and Architecture of VPM and POm Axons in Rat Vibrissal Cortex. *Cereb Cortex* 20(10):2265–2276.
32. Deschênes M, Veinante P, Zhang ZW (1998) The organization of corticothalamic projections: Reciprocity versus parity. *Brain Res Rev* 28(3):286–308.
33. Rojas-Piloni G, et al. (2014) Cell type- specific subcortical targets of layer 5 projecting neurons in the rat vibrissal cortex. *Washington (DC): Society for Neuro- Science Meeting.*
34. Alloway KD (2008) Information Processing Streams in Rodent Barrel Cortex: The Differential Functions of Barrel and Septal Circuits. *Cereb Cortex* 18(5):979–989.
35. Alloway KD, Hoffer ZS, Hoover JE (2003) Quantitative comparisons of corticothalamic topography within the ventrobasal complex and the posterior nucleus of the rodent thalamus. *Brain Res* 968(1):54–68.
36. Alloway KD, Crist J, Mutic JJ, Roy S a (1999) Corticostriatal projections from rat barrel cortex have an anisotropic organization that correlates with vibrissal whisking behavior. *J Neurosci* 19(24):10908–10922.
37. Giber K, et al. (2008) Heterogeneous output pathways link the anterior pretectal nucleus with the zona incerta and the thalamus in rat. *J Comp Neurol* 506(1):122–40.
38. Mease RA, Krieger P, Groh A (2014) Cortical control of adaptation and sensory relay mode in the thalamus. *Proc Natl Acad Sci* 111(18):6798–6803.

Manuscript No 1: Supplemental Information

Organization and somatotopy of corticothalamic projections from barrel cortex layer 5B

Supplemental Information

Supplementary Figures

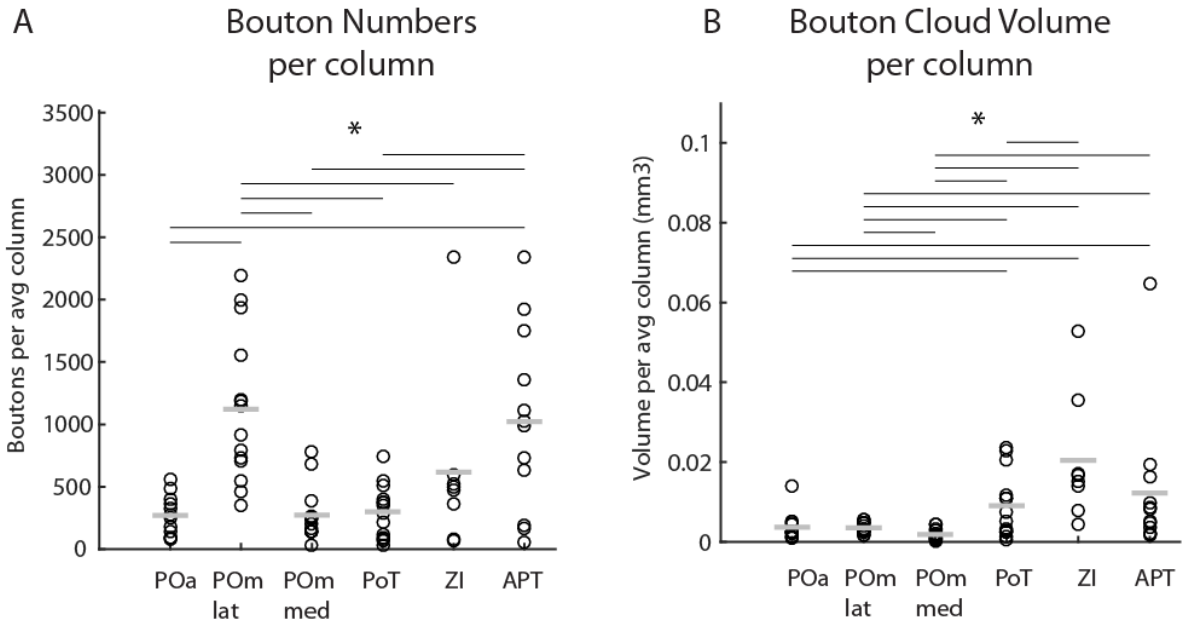

Supplementary Figure 1: Additional Quantifications

A: Number of boutons in respective nuclei, normalized by labeled volume relative to column. Each injection represented as black circles, mean as grey line. Black lines above indicate which nuclei are significantly different from each other (Wilcoxon signed rank, $p<0.05$).
B: Termination field volume in respective nuclei, normalized by labeled column. Conventions as in A.

Supplementary Methods

Injections

Seven C57/BL6 mice of both sexes at age 5 to 7 postnatal weeks at the time of injection were used in this study. An additional C57/BL6 mouse was used for horizontal Cytochrome C Oxidase labelling, which was not injected. Anesthesia was induced by exposing the animal to 1 Vol% isoflurane (Isofluran CP, cp-pharma, Germany) in O2, using an inhalator (Drägerwerk AG, Germany)). Body temperature was kept at 37°C using a heating pad and depth of anesthesia was monitored by visual inspection of breathing rate and lack of foot pinch reflex throughout the operation. Following deep anesthesia eyes were covered with eye and nose ointment (Bayer, Germany) to avoid drying and ~100 µl lidocaine (1%, LICAIN, DeltaSelect, Germany) was injected subcutaneously under the scalp. The mouse was then moved to a stereotactic frame (Customer constructed with elements of Anilam and Cartesian Research) and fixed with earbars. A small longitudinal cut exposed bregma and lambda, which was used to align the head stereotaxically. Following a small craniotomy at coordinates of BC (2.8-3.35 mm right, 0.85-1.7 mm posterior relative to bregma), the head was tilted 20° to the left to allow injection pipette penetration perpendicular to the pia. Viral particle solution was front loaded into pulled micropipettes (intraMARK, Blaubrand, Germany) and lowered to a depth of ~0.7-0.8 mm below pia. Approximately 50 nl virus solution was slowly injected by applying air pressure. Following the injection, the pipette was left at the injection location for 10 minutes to allow for diffusion and then slowly retracted. Injection procedure was then repeated for the second injection with the other virus solution. After completion, the skin above the skull was sutured with silk suture material (Perma-Hand, 6-0, Ethicon, USA). The animal was then transferred to its home cage, where it woke up. After 14-16 days incubation period, the mouse was exposed to a lethal dose of isoflurane and transcardially perfused with 4% paraformaldehyde (PFA) in phosphate buffered saline. The brain was removed and postfixated for 12 hours in 4% PFA at 4°C.

Slicing and Histology

Slicing: The brain was embedded in 2% agarose and then cut at various angles, using a vibratome (VT1000S Leica, Germany), always with 100µm thickness. First BC was cut tangentially (tilt ~22° to left and ~8° upward), then thalamus either coronally (1 experiment), sagittally (2) or horizontally (4). *Barrel visualization:* We found that Streptavidin Alexa-647 (ThermoFisherScientific, USA; typically used to fluorescently visualize biocytin-filled neurons) also clearly labels barrels. In short, we used the following protocol: 2x 10 min wash in phosphate buffer (PB); 1 h permeabilisation in 1% Triton-X (Sigma)/PB; 2 h 1 µg/ml Streptavidin-Alexa647 (Invitrogen/ThermoFisherScientific) in 0.5% Triton/PB; 4x 10min wash in PB; overnight wash in PB at 4°C. *Somata visualization:* In a subset of experiments thalamic slices were stained for somata using Neurotrace 435/455 (ThermoFisherScientific, USA), to facilitate alignment, nucleus border detection and soma counting. In short: 10 min wash in PB; 10 min 0.1% Triton-X/PB; 20 min in 200x diluted Neurotrace solution; 2x 10 min wash in 0.1% Triton-X/PB; 2x 10 min wash in PB. Cytochrome C Oxidase staining was achieved as described previously (1). *Embedding*: Following histological procedures, slices were embedded in SlowFadeGold or SlowFadeDiamond (ThermoFisherScientific, USA), the coverslip glued to slide by nail polish.

Microscopy

Slices were imaged with an Olympus FV1000 confocal microscope outfitted with an automated stage for mosaic imaging. For cortical barrel field and thalamic overview imaging objective UPlan FL N 4x NA 0.13, air, for bouton imaging objective UPlanSApo 20x NA 0.85, oil, was used. Lasers: Neurotrace-Alexa-435: 405 nm; Synaptophysin-GFP: 488 nm; Synaptophysin -mOrange: 559 nm; Streptavidin-Alexa-647: 630 nm. Slides were always scanned in sequential mode, zoom 1.5, 1024x1024 pixels, laser power and amplification adjusted such that maximum brightness was far from overexposure. Z-stepping for imaging boutons was set to 10µm to allow scanning of large areas with high x/y resolution at reasonable time and data storage demands. The resulting voxel size was 0.414x0.414x10 µm (XxYxZ). Potential signal loss by 10 µm stepsize was counteracted by increasing pinhole width to 300 µm. Most boutons could be seen in more than one z-section, leading to the conclusion that the scan parameters lead to a minimal loss in bouton numbers and a maximal coordinate imprecision of 5 µm. Not all the nuclei of interest could be scanned completely in all experiments, due to occasional tissue damage during slicing. Therefore the number of completely reconstructed experiments varies across nuclei.

Analysis

Mosaic tile images were stitched using Olympus inbuilt algorithms, without edge smoothing. Stitched stacks were then loaded into Amira 6 (FEI, USA) and aligned to each other (rigid alignment).

Stacks were loaded into Matlab 2015b (Mathworks, USA), where bouton locations and respective diameters were extracted using custom written algorithms. Pixel intensity values for each z-section were normalized to zero mean and standard deviation = 1 and 2-d gauss filtered (sigma=0.4 pixels). Then bouton candidates were found by looking for pixels with intensity higher than all their 8 neighbors (image dilation with center zero) and a minimal intensity of 2.5. Data snippets of 7x7 µm around each bouton candidate were extracted and background (defined as 10^{th} percentile of area around bouton) subtracted. Bouton candidates with a value lower than 2.5 following background subtraction were removed. Image snippets around boutons were interpolated by an upsampling factor of ~5 and diameter calculated as twice the shortest distance from peak to half-peak value. This allowed for robust diameter extraction even if multiple boutons are located close to each other, but underestimates diameter of ellipsoid boutons relative to spherical boutons. Diameters should be considered as apparent diameter estimations and deviate from real diameters, due to the influence of multiple factors: shape, point spread in confocal microscopy (no deconvolution was applied) and wavelength.

Bouton candidates that are visible in more than one z-section are only counted at their maximum intensity. Signals with diameters smaller than 1.5 µm or larger than 5 µm are removed. Following alignment of resulting bouton candidates in Amira (referenced to aligned slices), artifacts were

removed manually. Finally boutons were manually split into the respective nuclei, based on clustering.
Fluorophore expressing somata and Neurotrace labeled somata in thalamus were counted in Amira, using a sequence of filtering and opening-closing steps to smooth out darker cell nuclei and then counted by local maxima and connected component analyses.
Bouton cloud volumes were estimated using an alpha shape algorithm, after removing outliers. Outliers were defined as boutons for which the mean distance to their next 20 neighboring boutons was larger than 2 standard deviations of all mean distances. Alpha shape radius was empirically defined as two thirds of the smallest radius giving a single region with shrinkage factor of 0.8.
Estimation of overlap between bouton clouds was based on fitting a quadratic generalized linear model (GLM) with a step cutoff (i.e. the surface best separating the two bouton clouds). The percentage of incorrectly predicted boutons (positioned on the opposite side of the plane) then equals half of the overlap (two clouds with identical coordinates split by any surface would give 50% correct boutons, hence the factor 2).Barrel map orientation for each nucleus was calculated by first normalizing the vectors between both injection positions (in row/arc space) and the vectors between the median of both bouton clouds in each experiment and nucleus. The resulting relative directions of injection and cloud locations were then used to fit a linear model for each of the bouton space components. The set of linear models was then used to predict the relative direction of a vector between (virtual) bouton cloud locations for purely rowish and purely arcish (virtual) injections. The standard error of the mean angle between measured and predicted directions in each experiment gives an estimate of the predictability of the row and arc directions for each nucleus, low values indicating high predictability.

Supplementary references

1. Groh A, et al. (2014) Convergence of cortical and sensory driver inputs on single thalamocortical cells. *Cereb Cortex* 24(12):3167–79.

Manuscript No 2: Corticothalamic Spike Transfer via the L5B-POm Pathway in vivo

Corticothalamic Spike Transfer via the L5B-POm Pathway in vivo

Rebecca A. Mease, **Anton Sumser**, Bert Sakmann, Alexander Groh

Cerebral Cortex 2016

Author Contributions:

R.A.M, B.S. and A.G. designed the study, R.A.M. and A.G. performed experiments in Thy1-Chr2 animals; A.S. performed experiments in VGAT-Chr2 animals. R.A.M. and A.S. analyzed the data and generated figures; R.A.M. and A.G. jointly wrote the paper with the help of all authors.

Cerebral Cortex Advance Access published May 12, 2016

OXFORD

Cerebral Cortex, 2016, 1–15

doi: 10.1093/cercor/bhw123
Original Article

ORIGINAL ARTICLE

Corticothalamic Spike Transfer via the L5B-POm Pathway in vivo

Rebecca A. Mease[1,2], Anton Sumser[1], Bert Sakmann[1,3] and Alexander Groh[1,2]

[1]Institute for Neuroscience of the Technische Universität München, 80802 Munich, Germany, [2]Department of Neurosurgery, Klinikum rechts der Isar, Technische Universität München, 81675 Munich, Germany and [3]Max Planck Institute for Neurobiology, 82152 Martinsried, Germany

Address correspondence to Alexander Groh. Email: alexander.groh@gmail.com

Abstract

The cortex connects to the thalamus via extensive corticothalamic (CT) pathways, but their function in vivo is not well understood. We investigated "top-down" signaling from cortex to thalamus via the cortical layer 5B (L5B) to posterior medial nucleus (POm) pathway in the whisker system of the anesthetized mouse. While L5B CT inputs to POm are extremely strong in vitro, ongoing activity of L5 neurons in vivo might tonically depress these inputs and thereby block CT spike transfer. We find robust transfer of spikes from the cortex to the thalamus, mediated by few L5B-POm synapses. However, the gain of this pathway is not constant but instead is controlled by global cortical Up and Down states. We characterized in vivo CT spike transfer by analyzing unitary PSPs and found that a minority of PSPs drove POm spikes when CT gain peaked at the beginning of Up states. CT gain declined sharply during Up states due to frequency-dependent adaptation, resulting in periodic high gain–low gain oscillations. We estimate that POm neurons receive few (2–3) active L5B inputs. Thus, the L5B-POm pathway strongly amplifies the output of a few L5B neurons and locks thalamic POm sub-and suprathreshold activity to cortical L5B spiking.

Key words: adaptation, barrel cortex, corticothalamic feedback, layer 5, POm, somatosensory system, thy-1, VGAT

Introduction

A major input to the mammalian thalamus originates in the cortex from corticothalamic (CT) projection neurons in Layers 5 (L5) and 6 (Hoogland et al. 1987; Sherman 2001; Killackey and Sherman 2003). L5 CT axons target "higher order" thalamic nuclei, where they form large ("giant") synapses with thalamic proximal dendrites (Hoogland et al. 1991; Sherman and Guillery 1996; Veinante, Lavallee, et al. 2000; Killackey and Sherman 2003). Anatomical studies suggest that while these synapses are large, they are also sparse (Bourassa et al. 1995). While counts of L5 CT inputs per POm neuron are lacking, these properties differentiate L5 CT synapses from L6 CT synapses, which are small and numerous (Sherman and Guillery 2006). In brain slices, unitary EPSPs evoked from a single L5B axon can trigger action potentials (APs) in target POm neurons (Groh et al. 2008; Seol and Kuner 2015). This cortical "drive" of POm has been supported by in vivo experiments, as blocking cortical activity showed that POm spiking is contingent upon intact barrel cortex (BC) (Diamond et al. 1992; Groh et al. 2014) and is correlated with cortical Up states (Slezia et al. 2011; Groh et al. 2014). However, the strength and adaptive properties of the CT driver pathway in vivo are unknown. Consequently, the efficacy of spike transfer from the cortex to the thalamus (the CT transfer function) has not been quantified in vivo, and it is unknown which—if any—L5B spike patterns of evoke spikes in POm in the intact brain.

Putative CT spike transfer in vivo is likely to depend strongly on the spiking rate of individual L5B neurons, as L5B-POm synapses are characterized by pronounced, fast depression (Reichova and Sherman 2004; Groh et al. 2008; Seol and Kuner 2015); also

see Li et al. (2003) for similar findings in the visual thalamus. Therefore, the strength of a synapse will depend on the spiking history of the upstream L5B neuron, and—as L5B neurons are the most spontaneously active neurons in the BC (de Kock et al. 2007; Oberlaender et al. 2012)—the transfer function of this pathway should adapt markedly. We hypothesized that frequency-dependent synaptic depression could toggle CT spike transfer between different functional modes (Groh et al. 2008): in keeping with the original definition of "driver synapses" (Sherman and Guillery 2006), we refer here to "driver mode" as a fail-safe transfer mode between pairs of L5B and POm neurons, in which a single presynaptic L5B spike evokes one or more POm spikes. From in vitro measurements, this high gain mode is predicted to only occur for L5B spiking frequencies less than approximately 2 Hz, when the synapses are partially or fully recovered (Groh et al. 2008). In contrast, at higher frequencies, each L5B synapse would be depressed and the pathway would operate in a low gain mode, in which several coincident inputs are integrated to evoke POm spiking.

We address the properties of CT spike transfer in vivo by combining optogenetic manipulations with recordings of L5B and POm sub- and suprathreshold activity in urethane anaesthetized mice. The results show that POm is driven by very sparse CT input most likely of L5B origin. Furthermore, the L5B-POm pathway is not in a constant and stable state of depression, resulting in periodic transitions in CT gain following cortical Up and Down state activity.

Methods

Ethical Approval

All experiments were done according to the guidelines of German animal welfare and were approved by the respective ethical committees.

In Vivo Electrophysiology

Animal preparation and recordings were done with 6- to 8-week-old thy1-ChR2 (line 18) or VGAT-ChR2-EYFP line 8 (Jackson Labs) mice anesthetized with 1% Isofluorane in O_2 (SurgiVet Vaporizer) for the photostimulation experiments or urethane (1.3 µg/g body weight) for simultaneous LFP and juxtacellular recordings. Typically one or 2 experiments (simultaneous L5B/POm recordings, simultaneous L5B/L5B recordings, single L5B or POm recordings) were done per animal. Recordings were made from a total of 56 mice: 22 animals for intracellular POm recordings, 8 animals for simultaneous POm/L5B juxtasomal recordings, 5 animals for simultaneous L5B/L5B juxtasomal recordings, 5 animals for single L5B juxtasomal recordings, 10 animals for single juxtasomal POm recordings, 4 for VGAT POm juxtasomal recordings, and 2 for VGAT cortical juxtasomal recordings.

Depth of anaesthesia was continuously monitored by eyelid reflex, respiration rate, and cortical LFP, and additional urethane (10% of the initial dose) was given when necessary. Respiration rates were usually between 100 and 140 breaths per minute. In the case of isoflurane anaesthesia, concentration of anesthetic was adjusted to reach steady respiration rates around 100 breaths per minute. The skull was exposed, and small craniotomies above BC and POm were made (dura intact). For VGAT photostimulation experiments, the skull above BC was additionally thinned to permit better light penetration into the tissue. The head was stereotaxically aligned (Wimmer et al. 2004) for precise targeting of POm. Target coordinates relative to bregma were (lateral/posterior/depth; in mm) as follows: BC L5B: 3.0/1.1/0.7; POm: 1.25/1.7/2.8-3.0; Motor Cortex: 1.0/-1.0/0.6)

In vivo juxtasomal recordings and biocytin fillings were made as described in Pinault (1996). In brief, 4.5–5.5 MΩ patch pipettes were pulled from borosilicate filamented glass (Hilgenberg, Germany) on a DMZ Universal puller (Zeitz Instruments, Germany). Pipettes were filled with (mM) 135 NaCl, 5.4 KCl, 1.8 $CaCl_2$, 1 $MgCl_2$, and 5 HEPES, pH adjusted to 7.2 with NaOH, with 20 mg/mL biocytin added. Bath solution was identical, except for biocytin. Single units were found by the increase of pipette resistance (2–2.5 times of the initial resistance) measured in voltage clamp mode. A L5B and a POm cell were recorded simultaneously with a ELC-01X amplifier (NPI Electronics, Germany) for POm and a Axoclamp 2B (Molecular Devices, USA) for L5B. Unfiltered and band-pass filtered signals (high pass: 300 Hz, low pass: 9000 Hz) were digitized at 20 kHz with CED Micro 1401 mkII board and acquired using Spike2 software (both CED, Cambridge, UK). Typically, recordings consisted of 1 single unit which was filled at the end of the experiment with biocytin using current pulses (Pinault 1996). Whole-cell single neuron current clamp recordings in POm were done using the "blind patching" approach as described in Margrie et al. (2002). Pipette solution was (in mM) 130 K-gluconate, 10 HEPES, 10 Na-phosphocreatine, 10 Na-gluconate, 4 ATP-Mg^{2+}, 4 NaCl, 0.3 GTP, 0.1 EGTA, 2 mg biocytin, osmolarity approximately 300, and adjusted to pH 7.2 with KOH.

Cell Selection Criteria and Cell Reconstructions

For all L5B recordings, we used a combined photo- and sensory stimulation protocol to validate neurons' locations: L5B neurons were accepted for analysis if 1) photostimuli applied to the cortical surface resulted in rapid, unadapting spiking responses that persisted for the duration of a long photostimulus (3 s), and (2) each neuron responded within 100 ms to whisker stimulation, as the majority of L5B neurons in BC respond to whisker stimulation within this time period (de Kock et al. 2007). This protocol ensured that each putative L5B neuron was both in L5B (photostimulation) and in BC (sensory response). In addition to these physiological parameters, L5B and POm neurons were also filled with biocytin for reconstruction of the locations and morphologies (Fig. 1 and see Supplementary Fig. 1).

After the experiments, mice were euthanized with an overdose of ketamine/xylazine and transcardially perfused with 4% PFA in phosphate-buffered saline. Four hours after fixation, the brain was cut into 100 µm coronal slices and stained for cytochrome C to reveal the VPM/POm border and with DAB to reveal the soma and dendrite of the recorded neuron; both protocols are found in Groh and Krieger (2011).

Six POm neurons and 12 Chr2-L5B neurons were recovered and all showed dendritic parameters (Fig. 1 and see Supplementary Fig. 1 and Tables 1 and 2) consistent with previously published descriptions of these neurons (de Kock et al. 2007; Meyer et al. 2010).

Tracing L5B-ChR2 Projections to POm

For retrograde labelling of POm-projecting cortical neurons, a retrograde tracer (50 nL Cholera toxin B—Alexa 647 conjugate, Invitrogen) was stereotaxically injected into POm of thy1-ChR2 mice as described in detail in Wimmer et al. (2004). After 4 days, the animals were killed with an overdose of urethane (3 µg/g body weight) and perfused transcardially with 4% PFA containing PBS. The brain was removed, and 100 µm coronal sections of the somatosensory cortex and thalamus were obtained

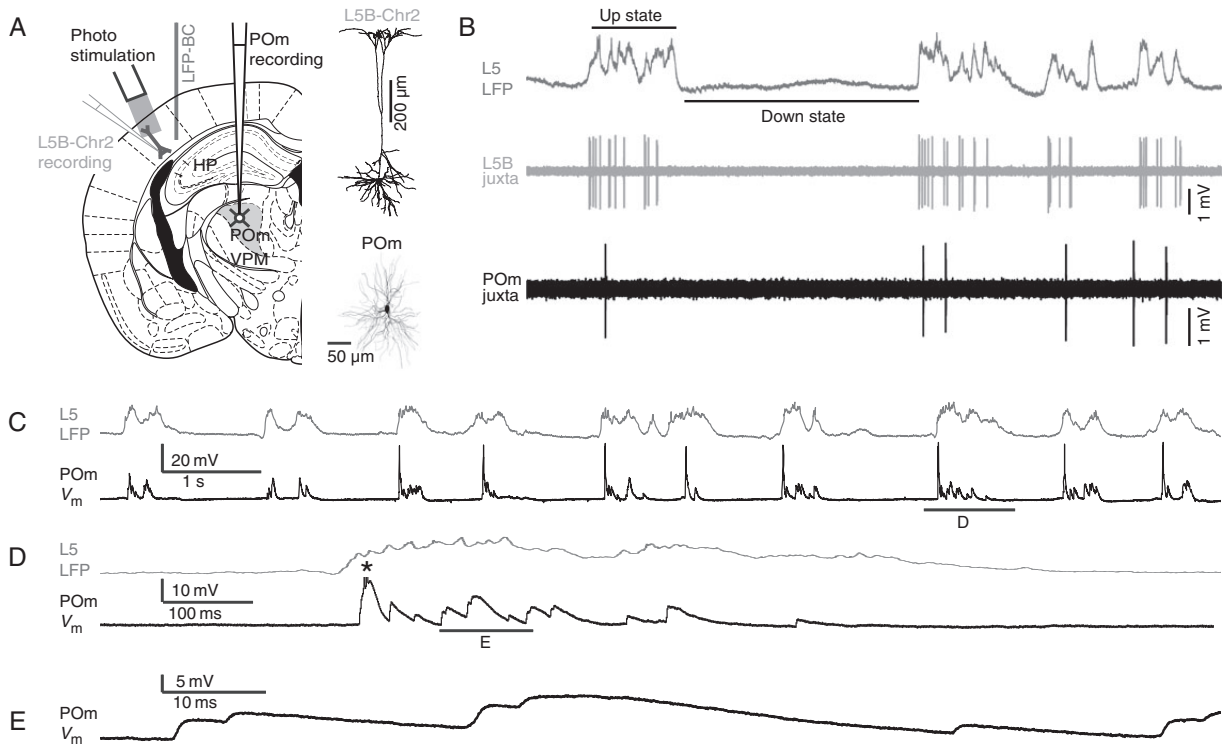

Figure 1. L5B-POm sub- and suprathreshold activity during cortical Up and Down states. (*A*) Left: Experimental setup scheme relative to coronal mouse brain slice, showing BC LFP recording, photostimulation of L5B, and recordings from individual neurons in L5B and POm. Mouse brain slice image modified from Paxinos (2001). Right: representative Neurolucida reconstructions of a L5B-Chr2 neuron (upper) and a POm neuron activated by cortical photostimulation (lower). Additional reconstructions and dendritic morphology parameters are shown in Supplementary Figure 1 and Tables 1 and 2. (*B*) Simultaneous cortical L5 local field potential (LFP, upper) and juxtacellular recordings from L5B (gray, middle) and POm (lower) neurons show L5B and POm spiking during cortical Up states. (*C*) Example of simultaneously recorded cortical L5 LFP and whole-cell patch clamp POm membrane voltage showing cortical Up states and associated POm EPSPs and APs. Resting membrane potential (RMP) = –62 mV. (*D*) Single Up state from *C* at higher time resolution shows a large "driver" EPSP and subsequent AP (truncated) at the start of an Up state and EPSPs of variable size throughout the Up state. (*E*) Short epoch from *D* showing summation of unitary EPSPs at higher time resolution.

on a vibratome (HR2, Sigmann Electronic, Germany). Fluorescence images were acquired using an Olympus FV1000 (Hamburg, Germany) confocal microscope with a ×20 oil objective (NA 0.9).

In Vivo Photostimulation Setup

Stimulation of ChR2 or VGAT neurons was achieved by a custom-built laser setup consisting of a solid state laser (Sapphire, Coherent, Dieburg, Germany) with a wavelength of 488 nm and a maximal output power of 20 mW. The sub-millisecond control of laser pulses was achieved by an ultrafast shutter (Uniblitz, Rochester, NY, USA). The laser beam was focused with a collimator into 1 end of a multimode fiber (Thorlabs, Grünberg, Germany; numerical aperture = 0.48, inner diameter = 125 µm). For ChR2-L5B neuron activation, the maximal output power at the end of the fiber was 1 mW, resulting in a maximal power density of approximately 32 mW/mm^2 on the brain surface. Shutter control was implemented with Spike2 software (CED, Cambridge, UK). The optical fiber was positioned at an angle of approximately 86° (from the horizontal plane) and at a distance of approximately 100 µm to the cortical surface. For each neuron, we recorded an average of 72 ± 58 or 74 ± 47 trials for juxtasomal and intracellular recordings, respectively. For BC VGAT photostimulation, the optical fiber was positioned at the same angle, but at a distance of approximately 2.5 mm to increase the stimulated area to a disc with a diameter of approximately 800 µm above BC. For robust cortical inhibition (see Fig. 3C), we used a 40 Hz series of laser pulses (12.5 ms on, 12.5 ms off) for 1 s with an approximate power density at the pia of 8.4 mW/mm^2, based on the study by Zhao et al. (2011). For each neuron, we recorded an average of 53 ± 18 trials (1 s photostimulation trains).

Cortical LFP Recordings

To monitor cortical state, we acquired L5 local field potentials (LFP) simultaneously with single neuron recordings. Depth-resolved LFPs were recorded with a 16-channel probe (Neuronexus probe model: A1X16-3mm-100-177, Neuronexus, MI, USA). The probe was inserted 1.5 mm from the pia and a Teflon-coated silver wire chlorided at the tip was used as reference in the bath solution above the craniotomy. Signals were amplified and filtered with an extracellular amplifier (EXT-16DX, NPI Elektronics, Tamm, Germany). LFPs were band-pass filtered with 0.01 or 0.1 Hz and 500 Hz corner frequencies and amplified 1000–2000 times. All signals were digitized at 20 kHz with CED Micro 1401 mkII board and acquired using Spike2 software (both CED, Cambridge, UK). Only LFPs recorded at a depth of 750 µm, corresponding to L5B, were used for analysis. Same coordinates as above.

Muscimol Block of BC

To determine the specificity of L5B drive of POm, we blocked barrel cortex (n = 3, Fig. 3) via application of approximately 50 nL of

10 mM muscimol (Sigma Aldrich) injected to L5. Muscimol is a GABA-A receptor agonist and is widely used to locally inhibit neuronal activity in the intact brain (Letzkus et al. 2011; Xu et al. 2012). Under these conditions, muscimol spreads approximately 1 mm along the anterio-posterior axis (Letzkus et al. 2011), thus likely blocking activity in the entire barrel field, and possibly parts of S2 cortex known to form giant synapses with POm neurons as well (Liao et al. 2010). After establishing a whole-cell recording in POm, an injection pipette (Blaubrand) was lowered into BC to a depth of 800 µm below the pia, and the drug was slowly pressure injected into the cortex. Effects on the sub- and suprathreshold activity in POm were seen approximately 5–10 minutes after drug application. We monitored the LFP in motor cortex (MC) while recording from single POm neurons. Despite ongoing Up and Down state activity in MC, spikes and spontaneous large EPSPs in POm successively disappeared 5–10 min after muscimol injection into BC. This treatment was nonreversible in the time course of our experiments.

Data Analysis

Electrophysiology data were acquired using Spike2 software and then exported for analysis in Matlab version 9 (MathWorks, Natick, USA) using custom written software. Spike times were extracted by finding local maxima in the temporal derivative of recorded voltage traces (dV/dt) above a variable threshold (typically 40–50% of maximum dV/dt). Reported values are mean ± standard deviation, unless otherwise noted.

EPSP Extraction

We characterized POm sub- and suprathreshold responses to putative L5B spiking via whole-cell patch clamp recordings ($n = 38$ neurons; >50 000 EPSPs). EPSP amplitude was defined as the EPSP maximum, including all postsynaptic potentials such as low threshold calcium spikes. EPSP times and maxima were extracted by finding crossings in the first derivative of the membrane potential and validated and/or corrected by hand.

Identification of Up States

Up states were selected by hand as large deflections in the LFP. To further standardize transition points across recordings and Up transitions with different rates of change, each individual LFP transition trace was normalized to a height of 1 and the transition point was then set to be the time at which the trace reached 50% of this maximum (see Supplementary Fig. 3). For the display figures, the LFP signal was converted to a dimensionless z-score and then inverted so that positive deflections correspond to "Up states" (Hahn et al. 2006).

Model Construction

EPSP Adaptation

To predict the adaptation state of the L5B-POm pathway, including synaptic and intrinsic factors, we constructed a simple model combining intracellular EPSP measurements and L5B spontaneous spiking statistics. For "single input" POm neurons which 1) showed only one unadapted EPSP amplitude peak and 2) showed high correlation between EPSP amplitudes and inter-EPSP interval (IEI), we normalized all EPSP amplitude by the average unadapted EPSP amplitude. We then plotted normalized EPSP amplitude versus IEI for a subset of single input neurons ($n = 5$). We then fit a double exponential to this curve: $M_{\text{pred}}(t) = e^{1-t_{\text{ISI}}/\tau_1} + e^{1-t_{\text{ISI}}/\tau_2}$, where $\tau_2 = 550\,\text{ms}$, $\tau_2 = 550\,\text{ms}$, $t_{\text{ISI}} = t - sp_t$, and sp_t is the most recent L5B spike relative to t. Those t_{ISI} >2 s were truncated to 2 s, and we set $M_{\text{pred}} = 0$ for $t_{\text{ISI}} = 0$, corresponding to a completely depressed synapse. We then used this function to convert experimentally measured L5B spike trains (juxtacellular recordings) into predicted POm EPSP recovery state.

Predicting POm Suprathreshold Events

POm intrinsic properties are highly nonlinear and show significant intrinsic bursting. Our goal here was to predict the timing of POm output relative to cortical input, not the precise spike count dependent on bursting mechanisms. To this end, instead of predicting discrete spikes times, we predicted POm suprathreshold events, in which an "event" could consist of one or more spikes. We first used the predicted POm EPSP recovery state to look up the predicted EPSP amplitude for each L5B spike time (completely recovered amplitude = 1). We then added a scaled version of an unadapted EPSP at each time point corresponding to an input L5B spike. EPSPs were modeled as a difference of exponentials fit to unadapted (IEI >700 ms) isolated (no subsequent EPSPs within a 50 ms window) experimentally measured EPSPs: $\text{EPSP}(t) = e^{(1-t/\tau_1)} - e^{(1-t/\tau_2)}$, with $\tau_1 = 12.8\text{ms}$ and $\tau_2 = 4.8\text{ms}$. Time constant fitting was done using a minimum root mean-squared difference between the model EPSP and target normalized voltage trace (normalized to maximum of 1).

Predicted event rates were then found by finding regions of the predicted voltage trace V_{pred} greater than a threshold θ; subsequent regions above θ were combined, corresponding to a minimum interevent interval of 1.5 ms. Unsurprisingly, predicted rates were quite sensitive to θ. For $\theta < 1$, unadapted single EPSPs can drive POm events, whereas for $\theta \geq 1$, either coincident independent L5B inputs or closely spaced EPSPs driven by the same input L5B neuron are required to drive POm output spikes. Predicted event rates were calculated as the number of above threshold regions divided by the total length of the input L5B recording.

Estimating Input Number Based on Correlation

For POm whole cell recordings, we estimated input number based on the correlation coefficient r between POm EPSP amplitude and $\log_{10}$ inter-EPSP interval. This strategy follows from the assumption of strong depression of the L5B-POm synapses (Groh et al. 2008). Single inputs should have a large r with an upper limit set by background noise from synaptic release noise (Groh et al. 2008) and membrane potential fluctuations controlling driving force and availability of the T-channel. It should be noted that this estimate is based in functional rather than anatomical data, that is, active L5B inputs (large and depressing) during spontaneous Up and Down states. The contribution of anatomical L6 inputs is negligible under these experimental conditions, (see Velez-Fort et al. (2014)).

To explore the range of r expected for single and 2 input neurons, we predicted the EPSP size generated in response to our group of simultaneous recorded L5B spike trains ($n = 9$ pairs), and r between IEI and EPSP size calculated for different levels of noise. For single inputs, all spike trains ($n = 18$) were used, and for double inputs, the paired EPSP trains were combined.

To extrapolate the predicted r values for >2 inputs, we generated mock spike trains by drawing from experimentally generated interspike interval distributions from up to 5 independent L5B recordings and then combining the EPSP trains and IEIs as above.

Results

We first measured the cortical input and thalamic output of the L5B-POm pathway by recording simultaneously from L5B and

POm neurons ($n = 12$ pairs) in the juxtacellular configuration (Fig. 1A). These individual L5B and POm neurons in the paired recordings were most likely not connected, because POm is sparsely innervated by L5B (Bourassa et al. 1995). To record from a defined group of L5B neurons in BC, we used the ChR2-expressing thy1 mouse (line 18) that has been used to specifically photostimulate L5 neurons in vivo (Arenkiel et al. 2007; Stroh et al. 2013; Vazquez et al. 2014). This allowed us to confine our cortical data set to a relatively homogenous group of L5B neurons by searching for photo-responsive neurons in L5B during each experiment. Analysis of morphologies showed that ChR2-expressing neurons are thick-tufted L5B neurons (Fig. 1A, top; see Supplementary Fig. 1), consistent with previous descriptions of POm-projecting neurons' morphology (Killackey and Sherman 2003). To confirm that Chr2-positive neurons indeed included POm-projecting neurons, Chr2-positive neurons were labeled by retrograde tracer injections in POm (see Supplementary Fig. 2). Recordings in POm were directed by stereotaxic coordinates, photo-responsiveness to BC L5 stimulation, and confirmed post hoc for a subset of POm recordings ($n = 6$) with recovered dendritic morphologies (Fig. 1A, lower and see Supplementary Table 2). Single L5B ($n = 12$) and POm ($n = 15$) neurons and simultaneously recorded L5B neuron pairs ($n = 9$ pairs) which met the above criteria were included in some analyses. A further set of recordings were done in whole-cell configuration from single POm neurons ($n = 38$) to quantify photo-evoked and spontaneous EPSPs.

L5B and POm Activity During Cortical Up and Down States

Cortical neurons follow spontaneous "Up state" cortical oscillations which occur during anesthesia (Timofeev et al. 1996; Steriade 1997; Constantinople and Bruno 2011). If the L5B-POm pathway supports efficacious CT spike transfer in vivo, then we expect to see correlated cortical and thalamic activity during such Up states. To first determine the relation between cortical Up states, L5B spikes, and POm spikes, we recorded simultaneously from L5B and POm neurons ($n = 12$ cortical/thalamic simultaneous recordings), as well as local field potential (LFP) in L5 of BC to monitor cortical Up states (schematic shown in Fig. 1A). L5B spiking was tightly correlated with cortical Up states. Interestingly, POm spiking was correlated with cortical Up states in a similar but more selective fashion. Both L5B and POm spiking occurred exclusively during Up states and peaked during Up state onsets. However, in contrast to L5B spiking throughout the entirety of each Up state, POm spikes were sparser and nearly always occurred at Down-Up state transitions (Fig. 1B).

To understand the changes in subthreshold activity which might underlie this marked difference between cortical and thalamic spiking, we simultaneously recorded POm membrane potential in whole-cell configuration and cortical LFP from L5 in BC. All POm neurons ($n = 38$) had large EPSPs evoked during spontaneous cortical Up states (Fig. 1C). In contrast, EPSPs were entirely absent during cortical Down states, matching the lack of spiking in L5B (Fig. 1B).

Spontaneous EPSPs in POm as shown in Figure 1E varied widely in amplitude (from 0.5 mV to larger than 20 mV, see Supplementary Fig. 7 for population distribution), with a median amplitude of 4.4 mV (1st quartile 2.6 mV, 3rd quartile: 7.3 mV). Larger EPSPs (>8 mV) often showed stereotyped slow depolarizations consistent with low-threshold calcium spikes (LTS) characteristic of thalamic relay neurons (Jahnsen and Llinas 1984; Landisman and Connors 2007; Groh et al. 2008). Such EPSPs typically triggered one or more APs, and these large AP-triggering EPSPs most often occurred at the beginning of Up states (first event in Fig. 1D). Furthermore, EPSPs showed strong adaptation, meaning that larger EPSPs were often followed at short-time intervals by small amplitude EPSPs (Fig. 1E).

To quantify these initial observations, we next used the Up transitions in the LFP to align and pool spiking, EPSP, and LFP data across recordings (see Methods and see Supplementary Fig. 3). Figure 2 compares the population average activity patterns in L5B and POm during cortical Up states ($n = 16$ L5B and $n = 12$ POm, juxtacellular; $n = 22$, POm intracellular). In all experiments, L5B and POm spiking was tightly coupled to spontaneous Up state transitions (Fig. 2A) and absent during Down states. L5B spike rates (Fig. 2B) were higher than POm spike rates (Fig. 2C) by an approximate factor of 3 (mean spike rates: 1.9 ± 0.8 Hz and 0.63 ± 0.5 Hz, for L5B and POm, respectively, L5B, $n = 16$; POm, $n = 12$; 172–1964 Up states per recording, mean 583 ± 413).

Population EPSP analysis shows that POm EPSPs (Fig. 2D) and L5B spikes (Fig. 2B) follow a similar progression through the Up state: peaking at the beginning of the Up state and slowly declining for the duration, consistent with POm activity being dominated by large L5B EPSPs during spontaneous Up states. Mean spontaneous EPSP rate was 3.8 ± 2.1 Hz ($n = 38$), and EPSP amplitudes (Fig. 2E) peaked in the beginning and declined by approximately 40% throughout the Up state. The time course of this adaptation suggests that the strength of L5B-POm synapses is periodically modulated by cortical Up and Down states and the associated changes in L5B spiking, with the result that CT spike transfer is most effective at Up state transitions when the L5B-POm synapse is maximally recovered after L5B inactivity during preceding Down states.

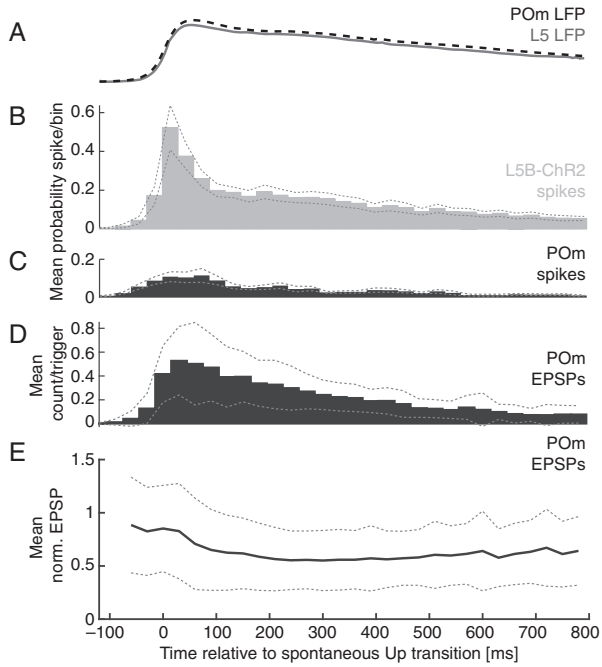

Figure 2. Summary of L5B-POm sub- and suprathreshold activity triggered on Up state transitions. (*A*) Mean LFP (from recordings in L5B in gray and POm in black dashed line) and histograms of (*B*) L5B (gray, $n = 16$) and (*C*) POm (black, $n = 12$) spikes triggered on spontaneous Up state transitions. Dotted lines show standard error of mean. See Methods and Supplementary Figure 3 for extraction of Up transitions. (*D*) Population mean spontaneous POm EPSP arrival histogram triggered on spontaneous Up states ($n = 22$ POm neurons). Dotted lines show SD. (*E*) Population mean normalized EPSP amplitudes ± SD for data in *D*.

Previous in vitro work suggested that POm neurons might be driven by single L5B spikes from single L5B neurons or, when the L5B-POm synapses are depressed, integrate 2 or more L5B spikes (Groh et al. 2008). Here, in the in vivo intracellular data set, we categorized POm APs by the number of EPSPs in the preceding 30 ms window. A population median of 45% of all APs (1st and 3rd quartiles, 21% and 0.61%, respectively) was driven by single EPSP (median amplitude = 8.7 mV; 1st and 3rd quartiles, 6.4 and 14.8 mV, respectively) and the remaining 55% by 2 or more EPSPs (median amplitude 5.0 mV, 1st and 3rd quartiles, 3.2 and 7.4 mV, respectively). Single EPSPs that triggered APs were nearly twice the amplitude of integrated EPSPs ($P < 0.05$, rank sum). This analysis suggests that, regardless of the number of anatomical L5B inputs, POm spikes can signal either the integration of 2 or more L5B spikes, or the occurrence of single L5B spikes, and that EPSP adaptation transitions L5B-POm spike transfer between the 2 modes.

EPSPs and Spiking in POm Depend on Cortical Input

The tight coupling of L5B spikes and POm EPSPs (Figs 1 and 2) suggests a causal relation between L5B in BC and POm activity. To test this causality, we inhibited BC pharmacologically and optogenetically. Spontaneous large EPSPs and APs in POm were abolished by muscimol injection into BC, with EPSP rates declining from approximately 3 to 0 Hz (Fig. 3A,B). While muscimol injection abolished Up states in BC (see Supplementary Fig. 4), Up states persisted in motor cortex (MC) (Fig. 3A, middle), suggesting that the drug remained relatively restricted to somatosensory cortex. Similarly, inhibiting BC in a more spatially and temporally specific manner via cell-type-specific photostimulation of inhibitory VGAT interneurons (Fig. 3C) (Zhao et al. 2011) immediately and reversibly abolished spontaneous POm spiking (Fig. 3D,E). These data show that in the anesthetized animal, cortical input —most likely of BC origin—is required for POm spiking. These data are in agreement with previous, less region-specific manipulations such as cortical cooling (Diamond et al. 1992) and cortical spreading depression (Groh et al. 2014).

EPSPs in POm Are Evoked by Photostimulation of L5B Neurons in BC

To directly confirm the L5B origin of large EPSPs in POm (Reichova and Sherman 2004; Groh et al. 2008), we photostimulated L5 neurons in BC and recorded subthreshold responses in POm, as before (Groh et al. 2014). Photostimulation with short (5 ms, <32 mW/mm^2) laser pulses applied to the surface of BC evoked sharp deflections in the L5 LFP and short latency, high probability spikes in L5B and POm neurons (Fig. 4A,B). To measure EPSP latencies and test whether EPSPs were unitary, we made whole-cell recordings of photo-evoked responses in POm (Fig. 4C). Under minimal stimulation conditions with low intensities, we

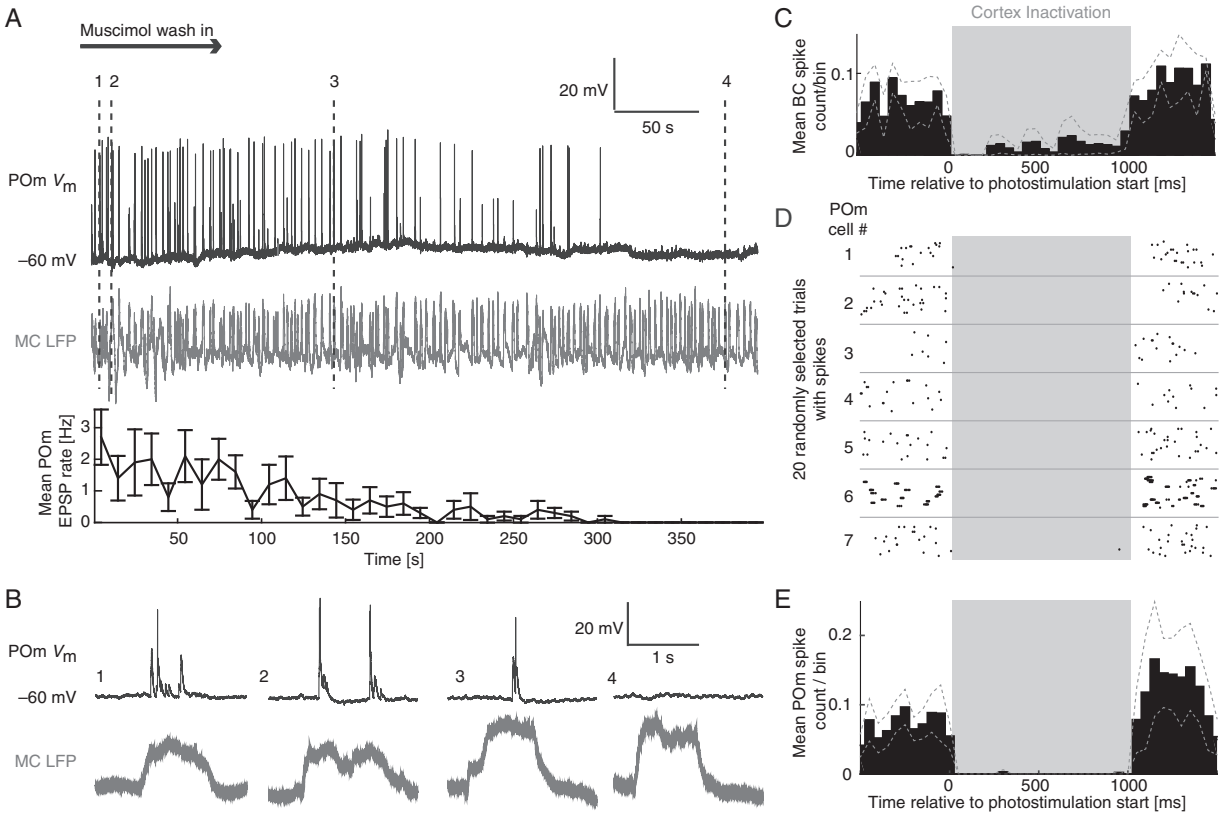

Figure 3. POm sub- and suprathreshold activities are suppressed by cortical inhibition. (*A*) Upper panel: POm whole-cell recording, (RMP = –60 mV), showing spiking and EPSPs during BC muscimol wash in. Middle panel: simultaneous LFP recorded in motor cortex maintained Up and Down states. Lower panel: Mean EPSP rate as a function of time; each data point is the average EPSP rate for ten 1 s bins, ± SEM. (*B*) Zoom of traces marked in A to show detail of motor cortex UDS and POm sub- and suprathreshold responses. (*C*) Population mean PSTH ($n = 4$) of infragranular (depth >730 µm from pia) BC neurons' spontaneous activity during cortex inactivation (VGAT photostimulation). Spontaneous rates decreased from 1.7 ± 0.5 to 0.21 ± 0.18 Hz (mean ± SEM) during cortex inactivation (VGAT photostimulation). (*D*) Example spike rasters from POm juxtacellular recordings ($n = 7$) aligned to cortex inactivation (VGAT photostimulation). (*E*) Population mean PSTH ($n = 7$) of POm cells shown in (*D*) with dashed lines showing SEM. Spontaneous rates decreased from 1.8 ± 0.4 to 0.03 ± 0.01 Hz (mean ± SE) during cortex inactivation (VGAT photostimulation).

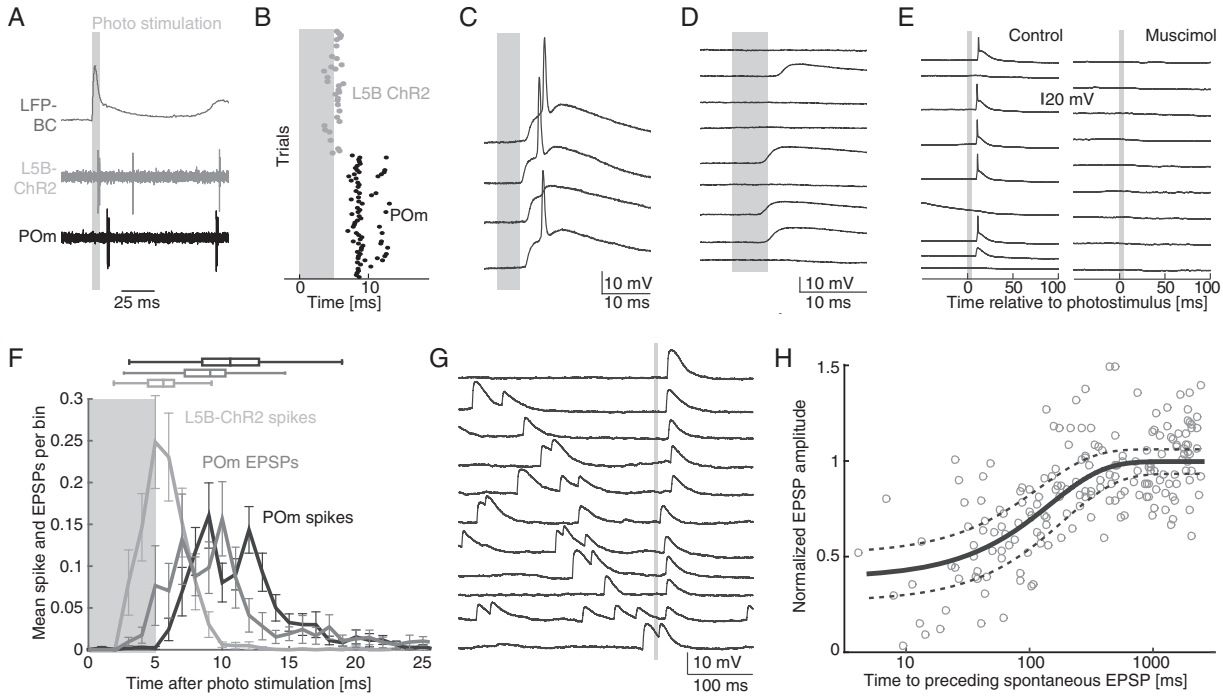

Figure 4. Photostimulation of L5B-POm pathway. (*A*) Example dual L5B/POm juxtacellular recording with photostimulation (gray bar) shows that both L5B and POm neurons sequentially respond to photostimulation. Simultaneously recorded cortical L5 LFP recording shown as the top trace. (*B*) Raster of spike responses to photostimulation for dual L5B and POm recording in A shows timing of first spikes: L5B approximately 5 ms and POm approximately 8 ms. (*C*) POm whole-cell responses to photostimulation: large EPSPs and APs and AP failure trials. RMP = −63 mV. (*D*) Same as C under minimal photostimulation conditions shows EPSP failures and large unitary EPSPs with amplitudes of >5 mV. (*E*) POm whole-cell recording of responses to L5B photostimulation before (left) and after (right) injection of muscimol into BC. RMP = −65 mV. (*F*) Population summary of response delays after photostimulation. Photo-evoked L5B (light gray) and POm (black) spikes. Median and 1st (1st quartile) and 3rd (3rd quartile) quartile spike latencies: L5B = 5.6 ms (1st quartile: 4.45 ms, 3rd quartile: 6.35 ms, $n = 1756$ spikes, 31 L5B neurons) and POm = 10.6 ms (1st quartile: 8.5 ms, 3rd quartile:12.75 ms, $n = 1367$ spikes, 38 POm neurons). The average delay from L5B spikes to POm spikes was 5 ms. Photo-evoked POm EPSP delays (dark gray) were 9.1 ms (1st quartile: 7.2 ms, 3rd quartile: 10.2 ms, $n = 1239$ EPSPs, 16 POm neurons). Thus, the delay between L5B spikes to POm EPSPs is 3.5 ms, ruling out polysynaptic activation. All medians were significantly different (rank-sum test). (*G*) Traces of evoked EPSPs preceded by spontaneous EPSPs in an example POm whole-cell recording, RMP = −62 mV; gray line shows time of photostimulation. Traces sorted by increasing interval between spontaneous and evoked EPSPs, showing that amplitudes of evoked EPSPs depend on the time to previous spontaneous EPSPs. (*H*) Photo-evoked EPSP amplitude versus $\log_{10}$ time to preceding spontaneous EPSP, population data ($n = 7$). To pool data across cells, photo-evoked EPSP amplitudes were normalized by mean isolated EPSP amplitudes per cell (no spontaneous EPSPs within 500 ms of light stimulus). Exponential fit (solid line) and error of fit (dashed line).

observed failure trials with no responses interspersed with successful trials consisting of large, unitary EPSPs (Fig. 4*D*). In addition, these EPSPs were blocked by muscimol injections into BC (Fig. 4*E*), confirming that these events were driven by cortical input.

Additional cortical input to POm originates in cortical layer 6 (L6) (Hoogland et al. 1987; Bourassa et al. 1995; Killackey and Sherman 2003). However, our L5B photostimulation protocol did not activate L6 neurons, which do not express ChR2 in the thy-1 mouse line (Arenkiel et al. 2007), and secondary activation of L6 via L5 cortico–cortico pathways was only seen for laser strengths approximately an order of magnitude greater than that we used for our photostimulation experiments (see Supplementary Fig. 5). Additionally, both spontaneous and photo-evoked POm EPSPs are incompatible with L6-evoked inputs: L6 inputs to the thalamus evoke EPSPs that 1) are about an order of magnitude smaller than EPSPs evoked by L5B inputs, 2) scale linearly with stimulation strength, and 3) are accompanied by simultaneous hyperpolarization (Reichova and Sherman 2004; Landisman and Connors 2007; Mease et al. 2014).

Finally, analysis of the response delays along the L5B-POm pathway strongly suggested monosynaptic activation (Fig. 4*F*). Photo-evoked L5B spikes occurred with a median delay of 5.6 ms (1st quartile: 4.45 ms, 3rd quartile: 6.35 ms, $n = 1756$ spikes, 31 L5B neurons), comparable to an earlier report by Arenkiel et al. (2007). Median photo-evoked EPSP onsets were 9.1 ms (1st quartile: 7.2 ms, 3rd quartile: 10.2 ms, $n = 1239$ EPSPs, $n = 16$ POm neurons) and median POm spike delays were 10.6 ms (1st quartile: 8.5 ms, 3rd quartile: 12.75 ms, $n = 1367$ spikes, $n = 38$ POm neurons) after photostimulus onset (Fig. 4*F*). In summary, the delays between photo-evoked L5B spikes and POm EPSPs or spikes were 3.5 and 5 ms, respectively, matching predictions from axon velocity measurements of this pathway (Kelly et al. 2001) and ruling out polysynaptic activation.

Interaction Between Evoked and Spontaneous POm Activity

These data strongly suggest that photo-evoked EPSPs in POm result from direct input from L5B (Fig. 4*C*,*D*,*F*). We reasoned that if both spontaneous and photo-evoked POm EPSPs and spikes are triggered by the same L5B inputs, spontaneous and evoked events measured in a single POm neuron should show statistical interaction due to synaptic depression (Reichova and Sherman 2004; Groh et al. 2008).

Spontaneous EPSPs did indeed affect subsequent photo-evoked EPSPs, in that the amplitudes of photo-evoked EPSPs decreased with the occurrence of spontaneous EPSPs

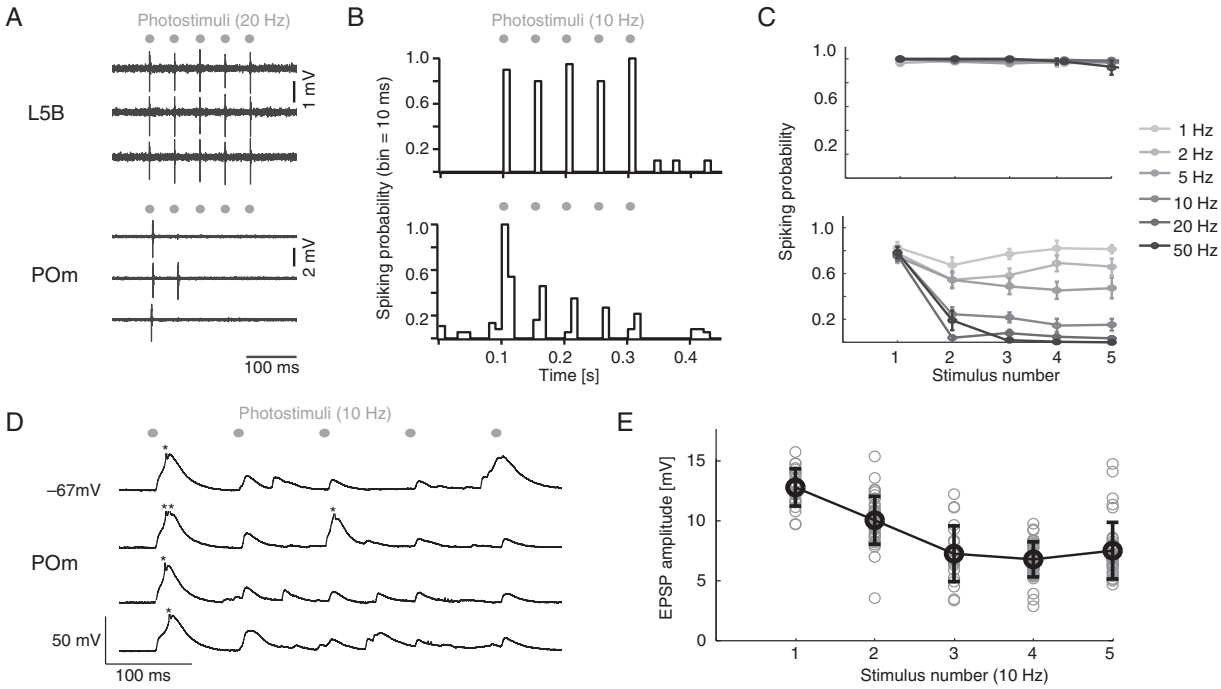

Figure 5. Photostimulation of L5B elicits frequency-dependent CT adaptation in vivo. (*A*) Example traces of juxtacellular recordings in a L5B neuron (upper) and a POm neuron (lower) photostimulated at 20 Hz. (*B*) PSTHs for juxtacellularly recorded spikes for a L5B neuron (upper) and a POm neuron (lower) photostimulated at 10 Hz. (*C*) Average spiking probabilities of 12 L5B-Chr2 (upper) and 15 POm neurons (lower) for photostimulus trains applied at different frequencies (1, 2, 5, 10, 20, 50 Hz). (*D*) Example traces of membrane voltage of a POm neuron during L5B photostimulation at 10 Hz, showing reduction of EPSP amplitudes over the stimulation train. RMP = –67 mV. Action potentials are truncated (*). (*E*) Scatter plot of EPSP amplitudes in POm in response to L5B stimulation at 10 Hz in a POm neuron. Single trials in gray, mean amplitudes in black. Error bars show SD. (*A–E*) As with single photostimulation pulses, individual pulses in the frequency trains were 5 ms long.

preceding the photostimulus (Fig. 4*G*). Consistent with frequency-
dependent depression of the L5B-POm pathway (Li et al. 2003; Reichova and Sherman 2004; Groh et al. 2008), population analysis of photo-evoked EPSPs showed that EPSP amplitude increased with time to preceding spontaneous EPSPs (Fig. 4*H*), showing significant interaction within a window of 500 ms. This timescale of adaptation matches that described previously in vitro (Groh et al. 2008). Similarly, on the suprathreshold level, spontaneous POm spiking decreased the probability of spiking responses to subsequent photostimuli (see Supplementary Fig. 6). Thus, in agreement with previous anatomical and functional data from the L5B-POm pathway (Hoogland et al. 1987; Diamond et al. 1992; Reichova and Sherman 2004; Groh et al. 2008), these in vivo interactions of spontaneous and evoked supra- and subthreshold activity suggest that both inputs originate in L5B of the BC.

Frequency-Dependent Adaptation of L5B-POm Pathway in vivo

The spontaneous and photo-evoked data show evidence of adaptation which should be strongly frequency dependent due to depression of the L5B-POm synapse (Reichova and Sherman 2004; Groh et al. 2008). We directly tested the in vivo frequency dependence of CT spike transmission with repeated (5) brief (5 ms) photostimuli presented at frequencies from 2 to 50 Hz (Fig. 5). L5B neurons spiked with high probability across the entire frequency range (Fig. 5*A–C*, upper panels), while POm spike responses decreased with stimulation frequency (Fig. 5*A–C*, lower panels). Thus, the efficacy of CT spike transfer strongly adapts according to the frequency of L5B input, with the most pronounced CT gain adaptation occurring for frequencies of 10 Hz and more (Fig. 5*C*). Examining subthreshold adaptation in whole-cell POm recordings (Fig. 5*D*,*E*) shows that photo-evoked EPSPs adapt significantly to high frequency stimulation, although with occasional recovery likely due to T-type calcium channel deinactivation. In sum, this rapid gain adaptation allows the L5B-POm pathway to operate dynamically according to the spiking patterns of L5B neurons, as in the spontaneous Up state data (Fig. 2).

EPSP Adaptation Across the L5B-POm Pathway

The variability in EPSP amplitudes in individual POm recordings was high, spanning almost an order of magnitude (see Supplementary Fig. 7). While some degree of variability was due to varying membrane potential at EPSP onset (see Supplementary Fig. 7*D*), we reasoned that a large amount of amplitude variation was due to different degrees of depression in L5B-POm synapses induced by variable intervals between spontaneous input L5B spikes. In a given POm recording, intervals between input L5B spikes can be inferred from inter-EPSP intervals (IEIs) in the recorded recipient POm neuron. Assuming strong depression at the L5B-POm synapse (Groh et al. 2008), in a POm neuron receiving input from a single L5B neuron, EPSP size should increase with long IEIs that allow the synapse to recover from depression. We found that a subset of neurons indeed matched this expectation (Fig. 6*A*). These neurons could be identified by a characteristically strong correlation between EPSP amplitude and IEI (Fig. 6*B*), whereas the remainder of recordings showed a weaker correlation (Fig. 6*C*,*D*).

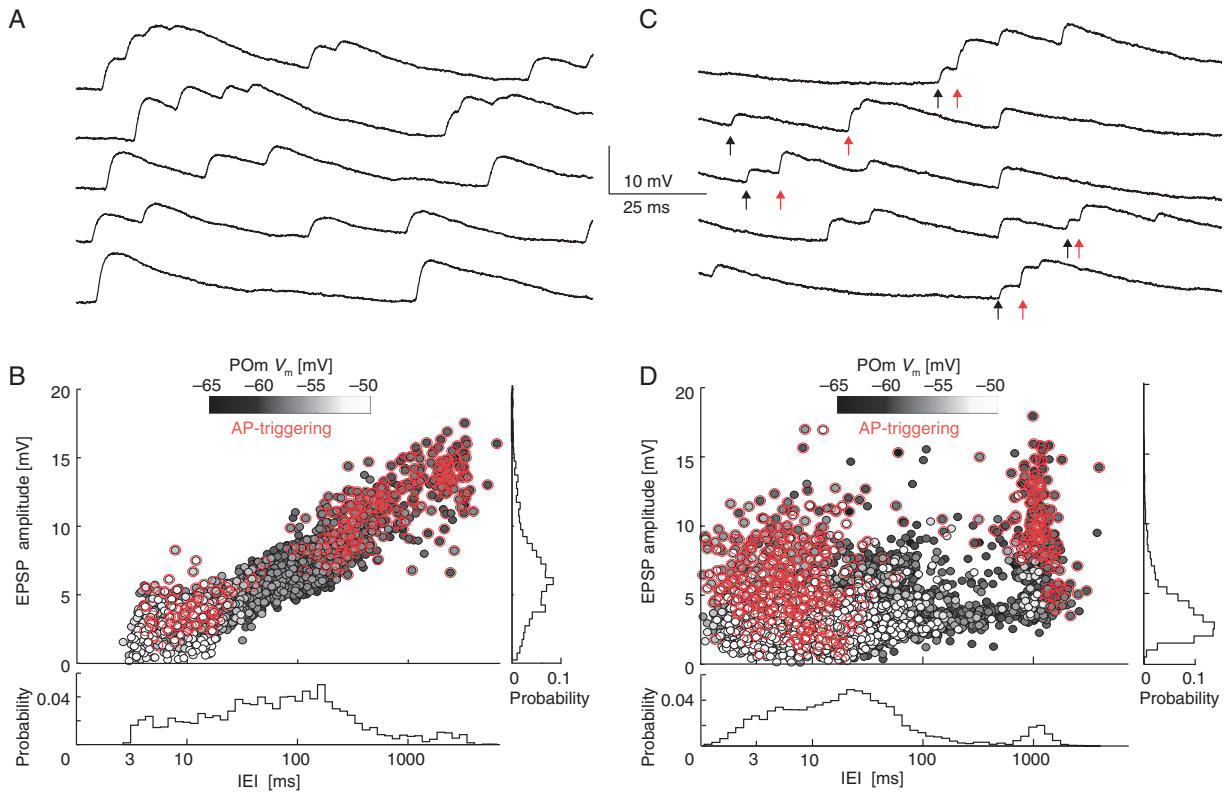

Figure 6. Adaptation of spontaneous POm EPSPs in "single" and "multiple" input neurons distinguished by correlation between EPSP amplitude and IEI. (*A*) Example spontaneous EPSPs; for this POm neuron, large EPSPs are always followed by smaller EPSPs at short IEIs, suggesting a single L5B input. RMP = −65 mV. (*B*) EPSP amplitude versus $\log_{10}$ IEI of the neuron shown in (*A*) displays strong correlation, $r = 0.89$, $n = 2031$ EPSPs. Marginal distribution to right shows EPSP amplitudes (first quartile, median, third quartile 4.3, 6.1, 8.1 mV). Marginal distribution of IEIs shown below (first quartile, median, third quartile: 21.3, 69.6, 177.5 ms). Grayscale shading of markers indicates membrane potential at event onset (lighter points are more depolarized). Red overlay highlights EPSPs that triggered action potentials. (*C*) Example traces showing multiple L5B inputs to POm. Arrows indicate large (unadapted) EPSPs (red) following smaller EPSPs (black). For this recording, approximately 45% of all recorded EPSPs were larger than would be predicted for adaptation of a single input. RMP = −67 mV. (*D*) EPSP amplitude versus $\log_{10}$ inter-EPSP intervals (IEI) during cortical Up state show poor correlation, $r = 0.349$, $n = 6549$ EPSPs in the neuron shown in (*C*). Marginal distribution of EPSP amplitudes shown to right (first quartile, median, third quartile: 2.2, 3.1, 4.8 mV); marginal distribution of IEIs shown below (first quartile, median, third quartile: 6.8, 18.8, 43.0 ms). Color conventions as in *B*.

We used this variation in adaptation to discriminate between POm neurons receiving different number of L5B inputs by calculating the correlation coefficient *r* between EPSP amplitude and $\log_{10}$IEI for each neuron. The logic is as follows: for a neuron with only one depressing input, EPSP amplitude should always be perfectly predicted by IEI (high *r*); in contrast, additional independent inputs will intersperse nonadapted EPSPs in the EPSP train and decrease *r*. A similar approach was used by Deschenes et al. (2003) to estimate the number of lemniscal inputs to VPM neurons.

Categorizing POm Neurons by Putative L5B Input Count

We used *r* to assign each POm neuron a category according to putative independent L5B input count. Nearly half (18/38) of the POm neurons showed a markedly simple relationship between EPSP amplitude and IEI: large EPSPs were always preceded by long IEIs, and small EPSPs occurred exclusively after short preceding IEIs (Fig. 6*A*). This reliable adaptation led to a high *r* between spontaneous IEI and EPSP amplitude (Fig. 6*B*). We categorized such neurons ($r > 0.6$) as "single input" neurons, as this high correlation could only arise if all observed EPSPs were driven by the same source L5B neuron (or if multiple L5B were always perfectly synchronized—a very unlikely situation). Single input recordings also had a clearly defined minimum IEI (~3 ms see Fig. 6*B* lower histogram). We interpret this minimum IEI as corresponding to the highest spiking rate of the single active input L5B neuron.

The remainder (20/38) of cells showed relatively weaker correlation ($r < 0.6$) between EPSP amplitude and preceding IEI (Fig. 6*C*,*D*) and were termed "multiple input" recordings. These recordings showed mixes of small and large EPSPs not unambiguously predicted by IEI (Fig. 6*C*, arrows), suggesting 2 or more active L5B inputs. In contrast to single input neurons, multiple input neurons showed a continuous distribution of IEIs approaching 0 ms (Fig. 6*D*, lower histogram), further suggesting that the EPSPs arose from multiple independent L5B inputs.

Predicting the CT Spike Transfer Function and the Number of Active L5B Inputs per POm Neuron

The data presented so far suggest that CT gain in the L5B–POm pathway is a function of synaptic depression. In the following, we use experimental data to construct a simple model to predict POm spiking in response to L5B spiking patterns.

The observation of "single input" POm neurons allowed us to quantify POm EPSP amplitude as a function of IEI and thereby the

in vivo adaptation of L5B-POm inputs. We used this adaptation curve (see Supplementary Fig. 8A) to predict POm EPSP amplitudes (unitless, with maximum of 1, corresponding to a completely recovered input) for L5B spikes recorded during Up states (Fig. 7A). Figure 7B shows the recovery of EPSP amplitudes towards 1 between L5B spikes, and the subsequent "adaptation" to 0 at the time of each L5B spike. The time course of predicted EPSP amplitude (Fig. 7C, lower)—the effective CT subthreshold gain—closely followed the in vivo Up state in the LFP (Fig. 7C, upper), supporting our experimental finding that CT gain is controlled by L5B spiking history.

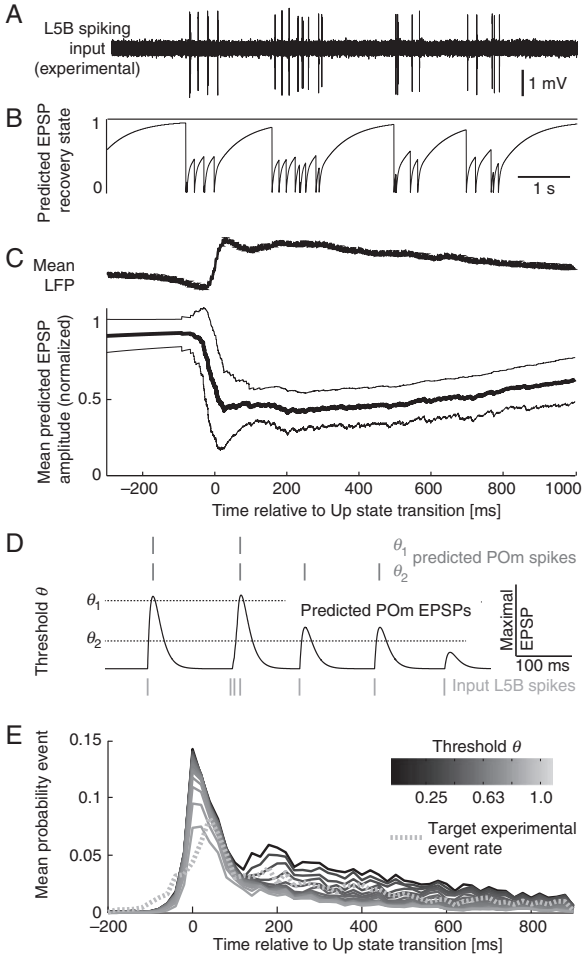

Figure 7. Simple predictive model for EPSP adaptation state. (*A*) Experimental L5B juxtacellular spikes during Up states taken as input to the model. (*B*) L5B spike history is translated into EPSP recovery state as a function of time by using the adaptation curve shown in Supplementary Figure 8A as a lookup table. (*C*) Mean cortical Up state transitions (upper) used as a reference signal for L5B-POm adaptation state. Mean ± SD adaptation state (lower, bold line and thin lines, respectively) triggered on cortical Up state transitions shows that recovery (=CT gain) of the L5B-POm pathway follows a similar course as cortical Up states. (*D*) Predicted POm EPSPs for a juxtacellular recording of L5B spontaneous spiking. Threshold lines indicate the degree of depolarization over which POm spiking is expected. L5B spikes preceded by a long silent interval trigger EPSPs exceeding spike threshold. (*E*) Predicted population POm spike event rates in response to experimental spike patterns of single L5B neurons during Up states. Population average predicted event probability shown over a range of thresholds (gray scale), triggered on Up state transitions. For comparison, experimentally measured mean POm event rate is overlaid (dashed line).

By using instantaneous EPSP adaptation state controlled by L5B spikes (Fig. 7B) as a multiplier for a template POm EPSP sampled from whole-cell recordings (see Methods), we could create predicted EPSP trains in response to experimentally measured L5B spike trains (Fig. 7D). Using these simulated EPSP trains, we next predicted POm spiking events to input L5B spiking patterns using a variable threshold θ (dashed lines in Fig. 7D). The time course of predicted POm spiking event times during Up states was similar to the observed experimental time course (Fig. 7E). Furthermore, predicted POm event rates best matched experimental values (~0.5 Hz) for θ corresponding to EPSPs recovered to 60–80% of maximal amplitude (see Supplementary Fig. 8). These predictions are consistent with a situation in which POm spiking during Up states are driven largely by L5B inputs, with temporal dynamics determined by subthreshold EPSP adaptation.

Estimating L5B Functional Convergence in POm

We next used 2 approaches—simulated EPSP trains and ratios of experimentally measured spike and EPSP rates—to estimate the number of L5B inputs converging on single POm neurons.

The logic of the simulated EPSP approach is to calculate r values from model-generated EPSP trains in response to defined numbers of L5B input patterns and compare those with the experimental r values from our intracellular data set (Fig. 8A). r values depend on 1) the number of L5B inputs, with r decreasing as the number of active inputs increase and 2) the variation in experimentally measured EPSP amplitude at a given IEI (EPSP noise). To first test this approach, we made simultaneous recordings from pairs of L5B neurons ($n = 9$ pairs) and used these spike patterns to generate simulated EPSP trains. We then calculated r values from simulated EPSP trains (see Supplementary Fig. 8B) from either 1) single L5B neurons ($n = 18$, Fig. 8B black) or 2) from pairs of L5B neurons ($n = 9$, Fig. 8B, red).

Predicted r for single inputs was greater than that predicted for 2 simultaneous inputs, and r decreased with the addition of EPSP noise. At noise levels matching those observed in vivo (~15%), predicted r for single inputs was in agreement with the maximal r measured in experimental data ($r = 0.87$). For 2 L5B inputs, r values were very similar to the median of all experimental r values, suggesting that the number of active L5B inputs per POm neuron may be around 2. Furthermore, these results support the validity of using r to discriminate between POm neurons with single and multiple inputs.

To test for 3 or more L5B inputs, we created artificial L5B spike trains by bootstrap resampling (Efron and Tibshirani (1991), 500 repetitions) from in vivo L5B spike trains to simulate POm EPSP trains for up to 5 independent L5B inputs. As in the paired protocol, r decreased with input count and EPSP noise, and up to 4 inputs were discriminable by r value (Fig. 8C). The experimental median r value was between the simulated r values from 2 and 3 L5B inputs, suggesting that POm neurons receive between 2 and 3 active L5B inputs. Comparing the simulated r values from increasing numbers of L5B inputs to experimentally measured r values allows an estimation of the number of active L5B inputs converging onto individual POm neurons (Fig. 8D). We found that roughly half of the cells in our sample received 1–2 inputs, and the remaining, 3 or more inputs, resulting in a mean of 2.5 L5B inputs per POm neuron.

Next, we independently estimated L5B-POm convergence by comparing L5B spike and POm EPSP rates (Fig. 8D). From 500 bootstrap resamples of L5B spike trains, we calculate that 1, 2, 3, 4, and 5 L5B inputs should result in mean POm EPSP rates of 1.5 ± 0.8, 3.4 ± 1.2, 4.7 ± 1.2, 6.4 ± 1.6, and 8.3 ± 1.6 Hz, respectively. Thus,

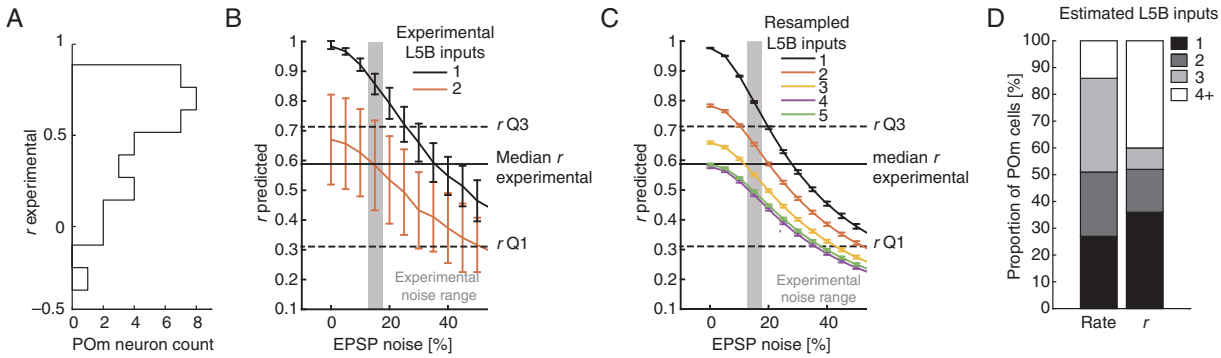

Figure 8. Estimating L5B to POm convergence. (*A*) Distribution of correlation coefficients between EPSP amplitude and $\log_{10}$IEI for 38 POm neurons (median: $r = 0.59$, 1st quartile: $r = 0.32$, 3rd quartile: $r = 0.72$, $n = 38$). (*B*) Mean ± SD of the correlation coefficient (r) between $\log_{10}$IEI and predicted EPSP amplitude for single (black) and paired experimental (red) L5B spikes, as a function of EPSP amplitude noise (additive Gaussian noise). Vertical gray bars and horizontal lines show experimentally measured noise level and correlation coefficient, respectively (median, first and third quartiles). POm EPSP noise was determined from unadapted EPSPs from "single input" whole-cell recordings: median noise value at given IEIs was 15% (1st quartile: 13%, 3rd quartile: 18%). (*C*) As in (*B*), but calculated for 1–5 artificial L5B spike trains resampled from interspike intervals (ISIs) of experimentally recorded L5B neurons. Each marker shows the mean predicted r, calculated for random combinations of 1–5 recorded neurons, 20 000 ISI draws. (*D*) Estimated distributions of L5B input count on POm neurons predicted by 2 different independent calculations: ratios between L5B spike and POm EPSP rates (rate) or correlation coefficient r between predicted EPSP amplitudes and IEI.

the mean experimental spontaneous POm EPSP rate of 3.8 ± 2.1 Hz ($n = 38$) measured here suggests that POm neurons on average receive input from 2–3 L5B neurons, in agreement with the estimation method using r. In summary, these estimates support a view in which L5B-POm functional convergence is sparse under conditions of slow cortical oscillations, with approximately 2.5 L5B neurons dominating the activity of postsynaptic targets in POm.

Discussion

The role of POm in the whisker system is not known, and recent independent demonstrations that whisker self-motion is poorly encoded in POm (Moore et al. 2015; Urbain et al. 2015) make POm even more puzzling. The absence of simple sensory modulation of POm activity highlights the possible importance of extra sensory inputs to higher order thalamus. Here, we investigate the input from cortical L5B to POm and ask how efficiently spikes can be transferred via this pathway in vivo. We determine the relation between the cortical activity patterns and CT gain and predict the convergence of L5B inputs on individual POm neurons.

We find that during low-frequency cortical oscillations typical for anaesthetized, sleeping, and "quietly wakeful" animals (Poulet and Petersen 2008; Constantinople and Bruno 2011; Vyazovskiy et al. 2011; Reimer et al. 2014), the POm membrane potential is characterized by the occurrence of large unitary ("giant") EPSPs (Fig. 1C–E). In combination with a set of control experiments incorporating cell-type-specific photostimulation (Figs 3 and 4), pharmacology (Fig. 3), and EPSP analysis, these data provide evidence that during the cortical Up state oscillations occurring in vivo, spiking in POm is mainly driven by L5B.

Specificity of BC L5B Synaptic Input to POm

Previous anatomical (Hoogland et al. 1987; Bourassa et al. 1995; Killackey and Sherman 2003), synaptic physiology (Reichova and Sherman 2004; Groh et al. 2008), and in vivo (Diamond et al. 1992; Groh et al. 2014) studies demonstrated large ("giant") EPSPs in POm of BC-L5B origin. In addition to L5B neurons in BC, other sources may contribute to the POm activity investigated here: somatosensory cortex 2 (S2, Liao et al. (2010)), motor cortex (Hooks et al. 2013), and SpVi (Chiaia et al. 1991; Veinante, Jacquin, et al. 2000). These inputs are well-established on anatomical grounds, but physiological data about their contribution to POm activity during Up and Down state activity are missing. Here, we provide evidence that in the absence of sensory stimulation, POm activity is dominated by L5B neurons in BC.

Firstly, optogenetic control of L5B activity in BC evoked (Fig. 4) or eliminated (Fig. 3) large, unitary EPSPs in POm. Photo-evoked EPSPs had response latencies incompatible with polysynaptic activation (Fig. 4). Furthermore, L5B spikes in BC and POm EPSPs show very similar patterns during Up and Down states (Fig. 2).

Secondly, SpVi neurons in the brainstem also make large synapses in POm (Chiaia et al. 1991; Veinante, Jacquin, et al. 2000; Lavallee et al. 2005), but these inputs exhibit almost no background firing during anesthesia (Furuta et al. 2010; Groh et al. 2014) and are thus unlikely to be the origin of cortical Up state evoked activity in POm. The photo-evoked EPSPs had average latencies of approximately 3.5 ms and are thus unlikely be triggered via multisynaptic activation of SpVi, which is activated by the cortex with much longer latencies of approximately 10 ms (Furuta et al. 2010).

Finally, L5B in S2 (Liao et al. 2010) and deep layers of motor cortex (Hooks et al. 2013) are additional sources of CT synapses in POm and may potentially contribute to the activity we describe here. While the optogenetic and pharmacological suppression of BC was relatively region specific, suggesting BC as the dominant input during Up and Down states (Fig. 3), better spatial control of cortical activity is needed to tease apart any potential contributions of S2 to POm activity.

The Gain of CT Transfer Function Is Dynamic

Synaptic depression is a well-established feature of the L5B-POm pathway (Reichova and Sherman 2004; Groh et al. 2008). However, the consequences of synaptic depression on CT spike transfer in vivo were unknown. L5B spontaneous spiking rates of 3–4 Hz predict that the L5B-POm pathway is in a constant state of depression which prevents high gain CT spike transfer. However, the present in vivo data show that CT gain is not constant, but rather follows cortical Up and Down states, peaking at the transition point and declining sharply during the early phase of the Up

state. Large single EPSPs occur mostly during the beginning phase of the Up state (Figs 1 and 2), especially the very large EPSPs that are most likely associated with the T-type Ca2+ channel currents and bursting (Jahnsen and Llinas 1984; Seol and Kuner 2015). By evoking these "driver" EPSPs, isolated L5B spikes (i.e., spikes preceded by a Down state) have the highest chance to trigger one or more POm spikes; estimates from the intracellular data suggest that nearly half of APs are triggered by such "driver" EPSPs. Subsequently, as EPSP amplitudes decline during the Up state (Figs 2 and 7), 2 or more EPSPs must be integrated to trigger POm spiking; such integration can occur in single input neurons for EPSPs separated by short IEIs, or in multiple input neurons for near coincident EPSPs.

These data demonstrate that the L5B-POm pathway shows pronounced frequency-dependent adaptation in vivo, and it is likely that synaptic depression is a main contributing mechanism. A simple model based on a few experimentally derived rules could recreate the time course and essential features of the L5B-POm spike transfer (Fig. 7), showing that the dynamics of POm spiking during Up states is largely explained by EPSP adaptation driven by L5B spontaneous spiking. Even though in vivo adaptation does not reach the extremes measured in vitro (Groh et al. 2008), we find that EPSP adaptation has functional consequences for CT spike transfer and underlies the dynamic gain of this pathway.

Given the complex nonlinear properties of POm neurons (Landisman and Connors 2007) and the voltage and time dependence of thalamic intrinsic mechanisms such as the T-type calcium and HCN channels (Jahnsen and Llinas 1984; McCormick and Pape 1990; Sherman 2001), it is noteworthy that EPSP adaptation is ensured by multiple intrinsic mechanisms in combination with presynaptic depression. The amplitudes of temporally isolated "driver" EPSPs in particular were decreased by depolarization (see Supplementary Fig. 7D), consistent with the presence of a T-type calcium component. In agreement with recent in vitro T-type calcium knockdown findings (Seol and Kuner 2015), these data suggest that the T-type calcium current contributes significantly to thalamic excitability to specifically enhance isolated or low frequency events. Thus, the interplay between multiple pre- and postsynaptic mechanisms strongly suggests that adaptation is a key feature of the L5B-POm pathway.

Finally, it remains to be determined exactly how the in vivo EPSP adaptation we report here interacts with changes in membrane potential elicited by modulatory inputs, in particular from CT L6 pathways (Lam and Sherman 2010; Mease et al. 2014; Crandall et al. 2015) and subcortical inhibition (Veinante, Lavallee, et al. 2000; Bartho et al. 2002; Trageser and Keller 2004; Lavallee et al. 2005; Bartho et al. 2007).

Expected L5B-POm Spike Transfer in the Awake Animal

In the awake rat, L5B neurons spike at 3–4 Hz (de Kock and Sakmann 2008, 2009; Oberlaender et al. 2012), predicting that this pathway may predominantly operate as an integrator of inputs. However, even at intermediate gains expected at these rates, only a few simultaneous L5B inputs would be needed to elicit POm spikes. This is a very different situation compared with thalamocortical connections, in which many synchronous thalamic inputs are required to trigger cortical spiking (Gabernet et al. 2005; Bruno and Sakmann 2006; Jia et al. 2014). Furthermore, in the awake animal, cortical spiking occurs in structured patterns (Luczak et al. 2007) with periods of inactivity, suggesting that CT spike transfer may in principle occur with high gain in the awake state. It is likely that inputs from higher order cortical areas such as S2 (Liao et al. 2010) and deep layers of motor cortex (Hooks et al. 2013) contribute substantially to POm spiking in the awake animal. Furthermore, L6 CT neurons—which probably contributed very little to POm activity in this study, due to "ultrasparse" spontaneous firing rates of approximately 0.1 Hz (Velez-Fort et al. 2014)—likely play a more important role during wakefulness. While recent reports show that POm neurons are indeed quite active in the awake animal (Moore et al. 2015; Urbain et al. 2015) and produce relatively complex spikes trains with long and short interspike intervals, the relationship between cortical and POm spiking described here remains to be investigated under nonanesthetized conditions.

Possible Role of the L5B-POm Pathway in Transferring Cortical Spike Output Through CT Circuits

It has been suggested that the majority of brain activity reflects "internal states," that is, spiking activity that is independent of sensory input, and that sensory inputs serve to modulate or suspend this activity (Llinas and Pare 1991; Raichle et al. 2001; Kenet et al. 2003; Ringach 2009; Destexhe 2011). In human fMRI studies, Raichle and colleagues (Zhang et al. 2008) report strong correlations between the cortex and the thalamus during spontaneous oscillations associated with the "default network state" (Raichle et al. 2001) of the resting brain. Spread of such internal cortical state throughout the cortico-thalamo-cortical network may employ CT signaling via higher order thalamic nuclei.

The idea that higher order nuclei route cortical activity to other cortical areas was first formulated by Sherman and colleagues (Sherman and Guillery 1996, 2006; Reichova and Sherman 2004). Here we provide evidence that in vivo, the higher order nucleus POm is indeed strongly activated by cortical input from L5B, particularly isolated L5B spikes occurring after periods of silence. However, a direct measure of CT convergence, that is, count of the number of anatomical L5B inputs per POm neuron, has yet to be achieved. Here, as an indirect first estimate of CT convergence, we find that during Up/Down state oscillations, each POm neuron receives functional input from a low number of active L5B neurons. Estimates from 2 different methods suggest that under these experimental conditions, approximately one-third of the POm neurons have only one active L5B input, with an average of 2.5 L5B input neurons per POm neuron (Fig. 8). Thalamus-projecting L6 neurons are ultrasparse firing (Velez-Fort et al. 2014) and evoke small and slow EPSPs (Reichova and Sherman 2004; Landisman and Connors 2007), making it unlikely that L6 inputs contributed significantly to this convergence analysis. However, it should be noted that both the level of functional CT convergence and the contribution of L6 input are most likely dependent on behavioral state.

These results suggest that single or synchronized spikes of a few BC L5B neurons can be amplified at the CT driver synapse and "broadcast" via POm simultaneously to motor, primary, and secondary sensory cortical via the widespread projections POm makes to various cortical areas (Deschenes et al. 1998; Meyer et al. 2010; Theyel et al. 2010). Consistent with this amplification and broadcasting idea is the net excitatory effect of POm on cortical networks (Bureau et al. 2006; Petreanu et al. 2009; Theyel et al. 2010; Viaene et al. 2011; Gambino et al. 2014; Jouhanneau et al. 2014) to enhance and prolong cortical sensory responses (Mease et al. 2016).

Supplementary Material

Supplementary material can be found at http://www.cercor.oxfordjournals.org/.

Funding

This work was supported by the Deutsche Forschungsgemeinschaft Sachbeihilfe (GR 3757/1-1) (R.A.M), the Max Planck Society (A.G., A.S., B.S., R.A.M.), the Institute of Advanced Studies at the TU München (A.G.), and Boehringer Ingelheim Fonds (A.S.). Funding to pay the Open Access publication charges for this article was provided by the Max Planck Society.

Notes

We thank Arthur Konnerth for providing lab space, infrastructure and support at the Institute for Neuroscience at the TU München, and Christiaan de Kock, Patrik Krieger, Randy Bruno and Erwin Neher for comments on earlier versions of this manuscript. Thy-1-ChR2 mice were a gift from Karl Deisseroth. *Conflict of Interest*: None declared.

References

Arenkiel BR, Peca J, Davison IG, Feliciano C, Deisseroth K, Augustine GJ, Ehlers MD, Feng G. 2007. In vivo light-induced activation of neural circuitry in transgenic mice expressing channelrhodopsin-2. Neuron. 54:205–218.

Bartho P, Freund TF, Acsady L. 2002. Selective GABAergic innervation of thalamic nuclei from zona incerta. Eur J Neurosci. 16:999–1014.

Bartho P, Slezia A, Varga V, Bokor H, Pinault D, Buzsaki G, Acsady L. 2007. Cortical control of zona incerta. J Neurosci. 27:1670–1681.

Bourassa J, Pinault D, Deschenes M. 1995. Corticothalamic projections from the cortical barrel field to the somatosensory thalamus in rats: a single-fibre study using biocytin as an anterograde tracer. Eur J Neurosci. 7:19–30.

Bruno RM, Sakmann B. 2006. Cortex is driven by weak but synchronously active thalamocortical synapses. Science. 312:1622–1627.

Bureau I, von Saint Paul F, Svoboda K. 2006. Interdigitated paralemniscal and lemniscal pathways in the mouse barrel cortex. PLoS Biol. 4:e382.

Chiaia NL, Rhoades RW, Bennett-Clarke CA, Fish SE, Killackey HP. 1991. Thalamic processing of vibrissal information in the rat. I. Afferent input to the medial ventral posterior and posterior nuclei. J Comp Neurol. 314:201–216.

Constantinople CM, Bruno RM. 2011. Effects and mechanisms of wakefulness on local cortical networks. Neuron. 69:1061–1068.

Crandall SR, Cruikshank SJ, Connors BW. 2015. A corticothalamic switch: controlling the thalamus with dynamic synapses. Neuron. 86:768–782.

de Kock CP, Bruno RM, Spors H, Sakmann B. 2007. Layer- and cell-type-specific suprathreshold stimulus representation in rat primary somatosensory cortex. J Physiol. 581:139–154.

de Kock CP, Sakmann B. 2008. High frequency action potential bursts (>or=100 Hz) in L2/3 and L5B thick tufted neurons in anaesthetized and awake rat primary somatosensory cortex. J Physiol. 586:3353–3364.

de Kock CP, Sakmann B. 2009. Spiking in primary somatosensory cortex during natural whisking in awake head-restrained rats is cell-type specific. Proc Natl Acad Sci USA. 106:16446–16450.

Deschenes M, Timofeeva E, Lavallee P. 2003. The relay of high-frequency sensory signals in the Whisker-to-barreloid pathway. J Neurosci. 23:6778–6787.

Deschenes M, Veinante P, Zhang ZW. 1998. The organization of corticothalamic projections: reciprocity versus parity. Brain Res Rev. 28:286–308.

Destexhe A. 2011. Intracellular and computational evidence for a dominant role of internal network activity in cortical computations. Curr Opin Neurobiol. 21:717–725.

Diamond ME, Armstrong-James M, Budway MJ, Ebner FF. 1992. Somatic sensory responses in the rostral sector of the posterior group (POm) and in the ventral posterior medial nucleus (VPM) of the rat thalamus: dependence on the barrel field cortex. J Comp Neurol. 319:66–84.

Efron B, Tibshirani R. 1991. Statistical data analysis in the computer age. Science. 253:390–395.

Furuta T, Urbain N, Kaneko T, Deschenes M. 2010. Corticofugal control of vibrissa-sensitive neurons in the interpolaris nucleus of the trigeminal complex. J Neurosci. 30:1832–1838.

Gabernet L, Jadhav SP, Feldman DE, Carandini M, Scanziani M. 2005. Somatosensory integration controlled by dynamic thalamocortical feed-forward inhibition. Neuron. 48:315–327.

Gambino F, Pages S, Kehayas V, Baptista D, Tatti R, Carleton A, Holtmaat A. 2014. Sensory-evoked LTP driven by dendritic plateau potentials in vivo. Nature. 515:116–119.

Groh A, Bokor H, Mease RA, Plattner VM, Hangya B, Stroh A, Deschenes M, Acsady L. 2014. Convergence of cortical and sensory driver inputs on single thalamocortical cells. Cereb Cortex. 24:3167–3179.

Groh A, de Kock CP, Wimmer VC, Sakmann B, Kuner T. 2008. Driver or coincidence detector: modal switch of a corticothalamic giant synapse controlled by spontaneous activity and short-term depression. J Neurosci. 28:9652–9663.

Groh A, Krieger P. 2011. Structure–function analysis of genetically defined neuronal populations. In: Fritjof H, Arthur K, Yuste R, editors. Imaging in neuroscience: a laboratory manual. Cold Spring Harbor: Cold Spring Harbor Laboratory Press.

Hahn TT, Sakmann B, Mehta MR. 2006. Phase-locking of hippocampal interneurons' membrane potential to neocortical up-down states. Nat Neurosci. 9:1359–1361.

Hoogland PV, Welker E, Van der Loos H. 1987. Organization of the projections from barrel cortex to thalamus in mice studied with Phaseolus vulgaris-leucoagglutinin and HRP. Exp Brain Res. 68:73–87.

Hoogland PV, Wouterlood FG, Welker E, Van der Loos H. 1991. Ultrastructure of giant and small thalamic terminals of cortical origin: a study of the projections from the barrel cortex in mice using Phaseolus vulgaris leuco-agglutinin (PHA-L). Exp Brain Res. 87:159–172.

Hooks BM, Mao T, Gutnisky DA, Yamawaki N, Svoboda K, Shepherd GM. 2013. Organization of cortical and thalamic input to pyramidal neurons in mouse motor cortex. J Neurosci. 33:748–760.

Jahnsen H, Llinas R. 1984. Ionic basis for the electro-responsiveness and oscillatory properties of guinea-pig thalamic neurones in vitro. J Physiol. 349:227–247.

Jia H, Varga Z, Sakmann B, Konnerth A. 2014. Linear integration of spine Ca2+ signals in layer 4 cortical neurons in vivo. Proc Natl Acad Sci USA. 111:9277–9282.

Jouhanneau JS, Ferrarese L, Estebanez L, Audette NJ, Brecht M, Barth AL, Poulet JF. 2014. Cortical fosGFP expression reveals broad receptive field excitatory neurons targeted by POm. Neuron. 84:1065–1078.

Kelly MK, Carvell GE, Hartings JA, Simons DJ. 2001. Axonal conduction properties of antidromically identified neurons in rat barrel cortex. Somatosens Mot Res. 18:202–210.

Kenet T, Bibitchkov D, Tsodyks M, Grinvald A, Arieli A. 2003. Spontaneously emerging cortical representations of visual attributes. Nature. 425:954–956.

Killackey HP, Sherman SM. 2003. Corticothalamic projections from the rat primary somatosensory cortex. J Neurosci. 23:7381–7384.
Lam YW, Sherman SM. 2010. Functional organization of the somatosensory cortical layer 6 feedback to the thalamus. Cereb Cortex. 20:13–24.
Landisman CE, Connors BW. 2007. VPM and PoM nuclei of the rat somatosensory thalamus: intrinsic neuronal properties and corticothalamic feedback. Cereb Cortex. 17:2853–2865.
Lavallee P, Urbain N, Dufresne C, Bokor H, Acsady L, Deschenes M. 2005. Feedforward inhibitory control of sensory information in higher-order thalamic nuclei. J Neurosci. 25:7489–7498.
Letzkus JJ, Wolff SB, Meyer EM, Tovote P, Courtin J, Herry C, Luthi A. 2011. A disinhibitory microcircuit for associative fear learning in the auditory cortex. Nature. 480:331–335.
Li J, Guido W, Bickford ME. 2003. Two distinct types of corticothalamic EPSPs and their contribution to short-term synaptic plasticity. J Neurophysiol. 90:3429–3440.
Liao CC, Chen RF, Lai WS, Lin RC, Yen CT. 2010. Distribution of large terminal inputs from the primary and secondary somatosensory cortices to the dorsal thalamus in the rodent. J Comp Neurol. 518:2592–2611.
Llinas RR, Pare D. 1991. Of dreaming and wakefulness. Neuroscience. 44:521–535.
Luczak A, Bartho P, Marguet SL, Buzsaki G, Harris KD. 2007. Sequential structure of neocortical spontaneous activity in vivo. Proc Natl Acad Sci USA. 104:347–352.
Margrie TW, Brecht M, Sakmann B. 2002. In vivo, low-resistance, whole-cell recordings from neurons in the anaesthetized and awake mammalian brain. Pflugers Arch. 444:491–498.
McCormick DA, Pape HC. 1990. Properties of a hyperpolarization-activated cation current and its role in rhythmic oscillation in thalamic relay neurones. J Physiol. 431:291–318.
Mease RA, Krieger P, Groh A. 2014. Cortical control of adaptation and sensory relay mode in the thalamus. Proc Natl Acad Sci USA. 111:6798–6803.
Mease RA, Metz M, Groh A. 2016. Cortical sensory responses are enhanced by the higher-order thalamus. Cell Rep. 14:208–215.
Meyer HS, Wimmer VC, Hemberger M, Bruno RM, de Kock CP, Frick A, Sakmann B, Helmstaedter M. 2010. Cell type-specific thalamic innervation in a column of rat vibrissal cortex. Cereb Cortex. 20:2287–2303.
Moore JD, Mercer Lindsay N, Deschenes M, Kleinfeld D. 2015. Vibrissa self-motion and touch are reliably encoded along the same somatosensory pathway from brainstem through thalamus. PLoS Biol. 13:e1002253.
Oberlaender M, de Kock CP, Bruno RM, Ramirez A, Meyer HS, Dercksen VJ, Helmstaedter M, Sakmann B. 2012. Cell type-specific three-dimensional structure of thalamocortical circuits in a column of rat vibrissal cortex. Cereb Cortex. 22:2375–2391.
Paxinos G. 2001. The mouse brain in stereotaxic coordinates/George Paxinos, Keith B.J. Franklin. San Diego, (CA): Academic Press.
Petreanu L, Mao T, Sternson SM, Svoboda K. 2009. The subcellular organization of neocortical excitatory connections. Nature. 457:1142–1145.
Pinault D. 1996. A novel single-cell staining procedure performed in vivo under electrophysiological control: morpho-functional features of juxtacellularly labeled thalamic cells and other central neurons with biocytin or Neurobiotin. J Neurosci Methods. 65:113–136.
Poulet JF, Petersen CC. 2008. Internal brain state regulates membrane potential synchrony in barrel cortex of behaving mice. Nature. 454:881–885.
Raichle ME, MacLeod AM, Snyder AZ, Powers WJ, Gusnard DA, Shulman GL. 2001. A default mode of brain function. Proc Natl Acad Sci USA. 98:676–682.
Reichova I, Sherman SM. 2004. Somatosensory corticothalamic projections: distinguishing drivers from modulators. J Neurophysiol. 92:2185–2197.
Reimer J, Froudarakis E, Cadwell CR, Yatsenko D, Denfield GH, Tolias AS. 2014. Pupil fluctuations track fast switching of cortical states during quiet wakefulness. Neuron. 84:355–362.
Ringach DL. 2009. Spontaneous and driven cortical activity: implications for computation. Curr Opin Neurobiol. 19:439–444.
Seol M, Kuner T. 2015. Ionotropic glutamate receptor GluA4 and T-type calcium channel Ca 3.1 subunits control key aspects of synaptic transmission at the mouse L5B-POm giant synapse. Eur J Neurosci. 42:3033–3044.
Sherman SM. 2001. Tonic and burst firing: dual modes of thalamocortical relay. Trends Neurosci. 24:122–126.
Sherman SM, Guillery R. 2006. Exploring the thalamus and its role in cortical function. Cambridge (MA): MIT Press.
Sherman SM, Guillery RW. 1996. Functional organization of thalamocortical relays. J Neurophysiol. 76:1367–1395.
Slezia A, Hangya B, Ulbert I, Acsady L. 2011. Phase advancement and nucleus-specific timing of thalamocortical activity during slow cortical oscillation. J Neurosci. 31:607–617.
Steriade M. 1997. Synchronized activities of coupled oscillators in the cerebral cortex and thalamus at different levels of vigilance. Cereb Cortex. 7:583–604.
Stroh A, Adelsberger H, Groh A, Ruhlmann C, Fischer S, Schierloh A, Deisseroth K, Konnerth A. 2013. Making waves: initiation and propagation of corticothalamic ca(2+) waves in vivo. Neuron. 77:1136–1150.
Theyel BB, Llano DA, Sherman SM. 2010. The corticothalamocortical circuit drives higher-order cortex in the mouse. Nat Neurosci. 13:84–88.
Timofeev I, Contreras D, Steriade M. 1996. Synaptic responsiveness of cortical and thalamic neurones during various phases of slow sleep oscillation in cat. J Physiol. 494(Pt 1):265–278.
Trageser JC, Keller A. 2004. Reducing the uncertainty: gating of peripheral inputs by zona incerta. J Neurosci. 24:8911–8915.
Urbain N, Salin PA, Libourel PA, Comte JC, Gentet LJ, Petersen CC. 2015. Whisking-related changes in neuronal firing and membrane potential dynamics in the somatosensory thalamus of awake mice. Cell Rep. 13:647–656.
Vazquez AL, Fukuda M, Crowley JC, Kim SG. 2014. Neural and hemodynamic responses elicited by forelimb- and photostimulation in channelrhodopsin-2 mice: insights into the hemodynamic point spread function. Cereb Cortex. 24:2908–2919.
Veinante P, Jacquin MF, Deschenes M. 2000. Thalamic projections from the whisker-sensitive regions of the spinal trigeminal complex in the rat. J Comp Neurol. 420:233–243.
Veinante P, Lavallee P, Deschenes M. 2000. Corticothalamic projections from layer 5 of the vibrissal barrel cortex in the rat. J Comp Neurol. 424:197–204.
Velez-Fort M, Rousseau CV, Niedworok CJ, Wickersham IR, Rancz EA, Brown AP, Strom M, Margrie TW. 2014. The stimulus selectivity and connectivity of layer six principal cells reveals cortical microcircuits underlying visual processing. Neuron. 83:1431–1443.
Viaene AN, Petrof I, Sherman SM. 2011. Properties of the thalamic projection from the posterior medial nucleus to primary and secondary somatosensory cortices in the mouse. Proc Natl Acad Sci USA. 108:18156–18161.

Vyazovskiy VV, Olcese U, Hanlon EC, Nir Y, Cirelli C, Tononi G. 2011. Local sleep in awake rats. Nature. 472:443–447.

Wimmer VC, Nevian T, Kuner T. 2004. Targeted in vivo expression of proteins in the calyx of Held. Pflugers Arch. 449:319–333.

Xu NL, Harnett MT, Williams SR, Huber D, O'Connor DH, Svoboda K, Magee JC. 2012. Nonlinear dendritic integration of sensory and motor input during an active sensing task. Nature. 492:247–251.

Zhang D, Snyder AZ, Fox MD, Sansbury MW, Shimony JS, Raichle ME. 2008. Intrinsic functional relations between human cerebral cortex and thalamus. J Neurophysiol. 100:1740–1748.

Zhao S, Ting JT, Atallah HE, Qiu L, Tan J, Gloss B, Augustine GJ, Deisseroth K, Luo M, Graybiel AM, et al. 2011. Cell type-specific channelrhodopsin-2 transgenic mice for optogenetic dissection of neural circuitry function. Nat Methods. 8: 745–752.

Manuscript No 2: Supplemental Information

Corticothalamic Spike Transfer via the L5B-POm Pathway in vivo

Rebecca A. Mease, **Anton Sumser**, Bert Sakmann, Alexander Groh

Supplemental Information

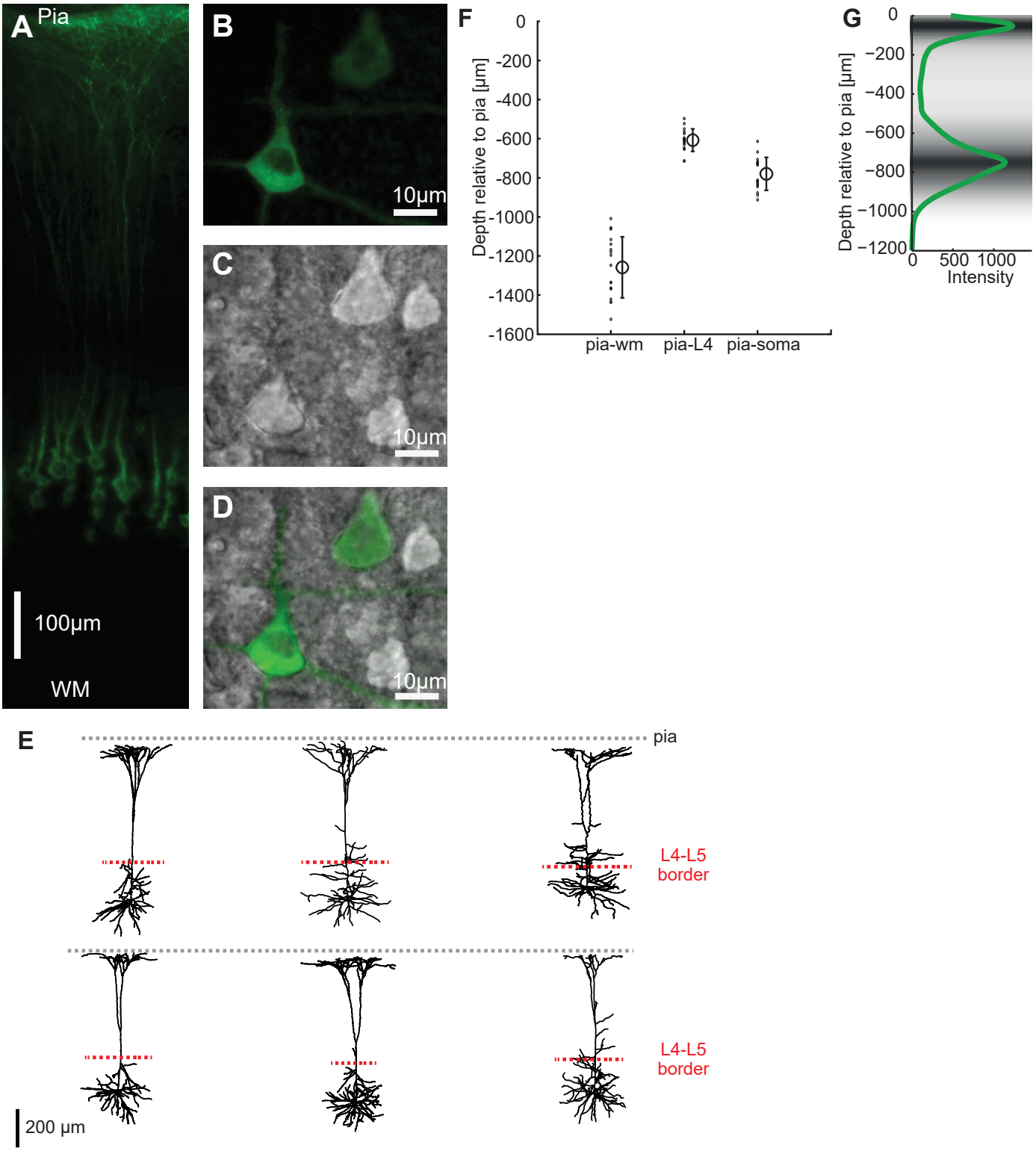

Figure S1. Identification of ChR2-positive neurons

(A) To characterize the morphology of Channelrhodopsin 2 (ChR2) positive neurons, cells were identified by their EYFP fluorescence in acute slices from ChR2 transgenic mice. Strongest expression is seen in L5 neurons and their apical dendrites. White matter (WM) and pia are indicated for orientation. These neurons were filled with biocytin for subsequent identification using morphological reconstructions (E).
(B) EYFP fluorescence of two ChR2 positive neurons (somata).
(C) Same field of view as in B but with difference interference contrast (DIC) optics for whole-cell recording and biocytin filling
(D) Same field of view as in B and C, overlay of DIC and fluorescence image to facilitate fluorescence guided whole-cell recordings.
(E) Dendritic morphology of six example ChR2-positive neurons. Reconstructions were done with Neurolucida and individual neuronal morphologies were scaled to the average pia to white matter distance (1259 µm) using Neuronregistrator 1D (Supplementary Methods). Black dashed lines indicate the pia; red dashed lines indicate the approximate L4/L5 border. See Supplementary Table 1 for a summary of cell morphologies.
(F) Soma location of ChR2 neurons in the cortical column: Distances between pia and white matter (pia-wm), pia and lower L4 (pia-L4), and pia and soma (pia-soma) for all reconstructed L5B-ChR2-positive neurons (n=12). Circles and error bars show mean ± standard deviation.
(G) Population average dendritic density plot showing dendritic total length / bin as a function of depth relative to the pia. Individual density profiles for each neuron were calculated with Rembrandt 3D with a bin size of 50 µm and visualized using Rothko (see Supplementary Methods).

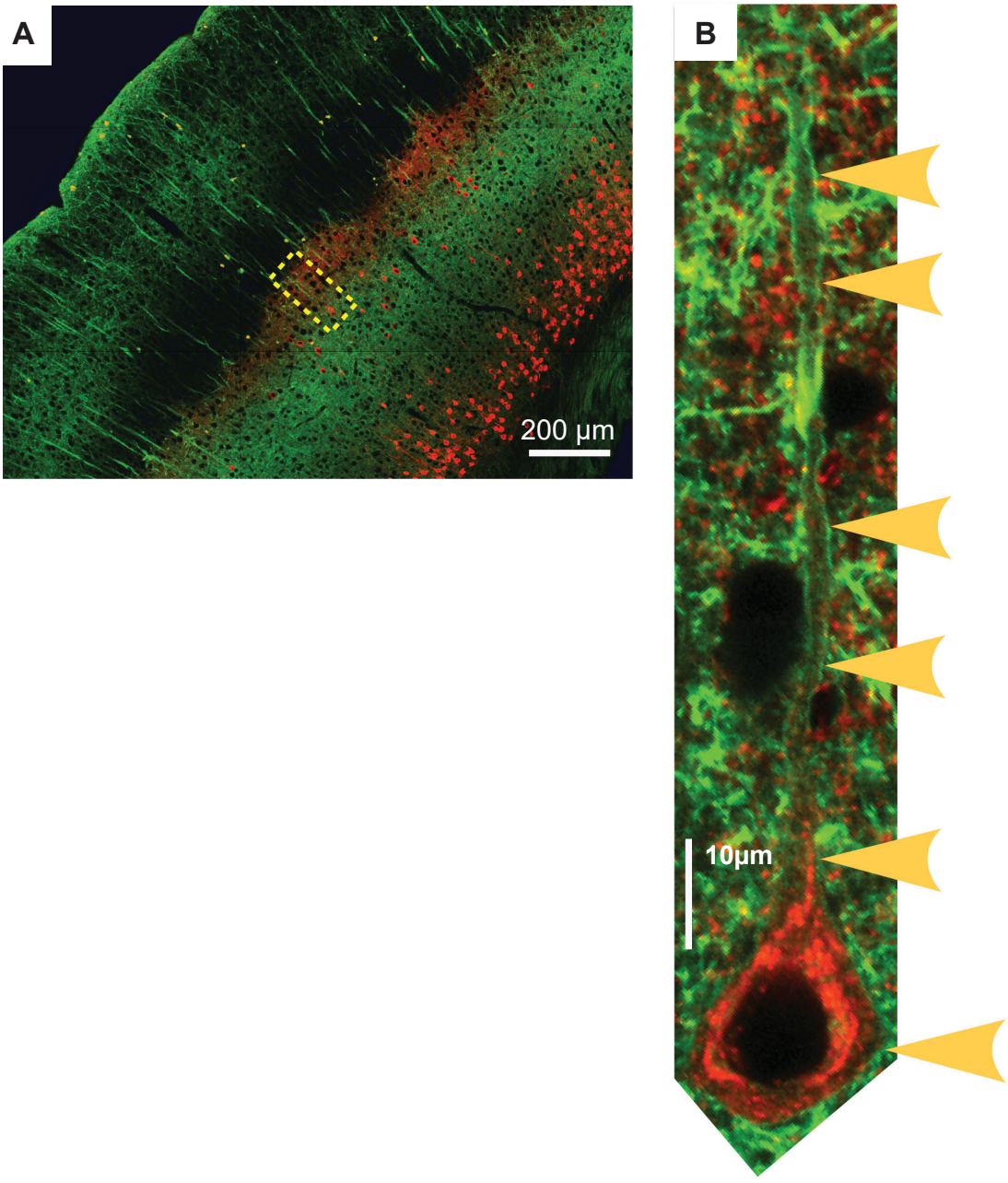

Figure S2. Retrograde labeling of thy1

(A) ChR2 neurons in L5B project to POm. Confocal image of BC showing ChR2 expressing neurons. EYFP fluorescence marks ChR2 positive neurons in the thy1-mouse line (green from EYFP-ChR2 fusion protein, localized to plasma membranes). To reveal POm projection neurons, cholera toxin subunit B conjugated with Alexa-647 was injected into POm and retrogradely labeled cortical neurons. Retrogradely labelled neuronal somata reside in L5B and lower L6 (Bourassa et al., 1995). Yellow box depicts field of view shown in B.
(B) Field of view marked with yellow box in A at higher magnification shows one L5-ChR2-expressing neuron (green) retrogradely labelled (red) by the tracer injected into POm. EYFP (green) reporting ChR2 expression is marked with yellow arrowheads. ChR2 and retrograde tracer from POm co-localize thus demonstrating that ChR2 expressing neurons in L5 project to POm.

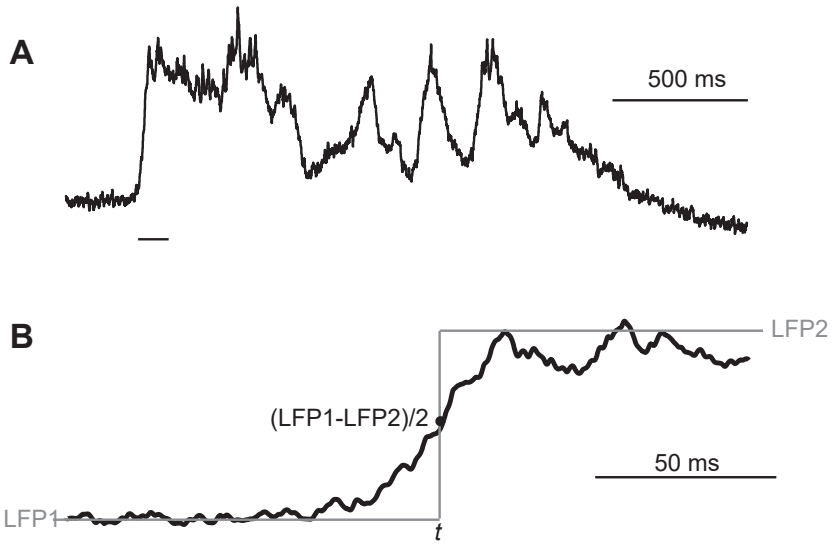

Figure S3. Transition alignment for cortical Up states.

(A) L5B LFP showing a cortical Up state. Black line indicating region shown in (B).
(B) Higher temporal resolution of Up state transition shown in A), demonstrating calculation of 50% transition from LFP1 value before Up transition and LFP2 value after the transition.

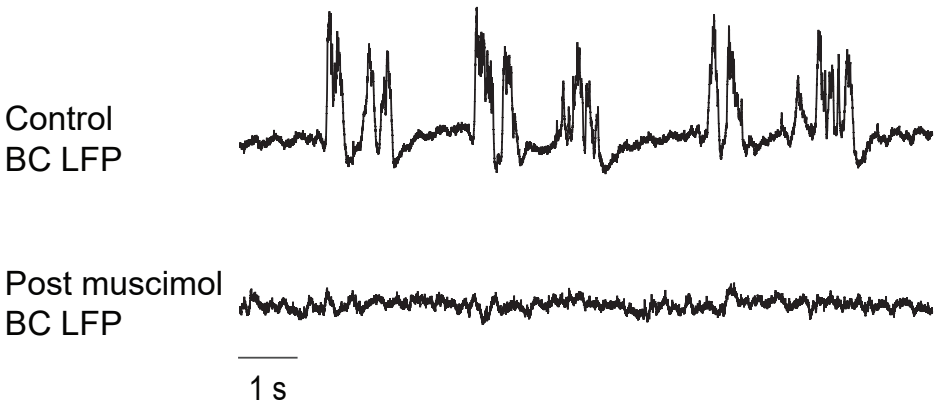

Figure S4. Muscimol abolishes cortical Up states in BC

LFP measured in BC before and approximately 10 minutes after muscimol injection into BC.

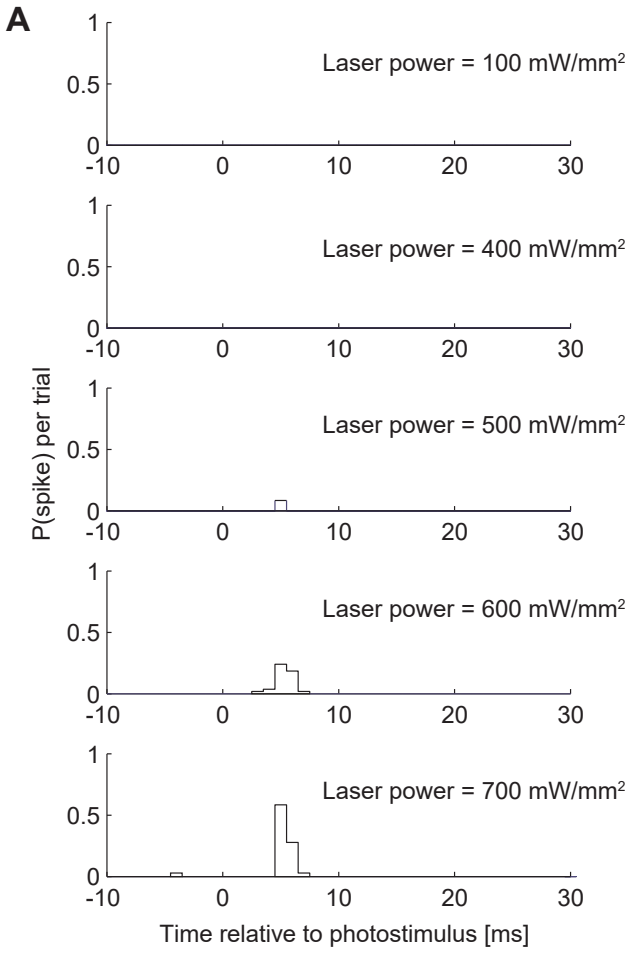

Figure S5. Responses of cortex layer 6 to photostimulation of L5B.

Juxtasomatic recordings of spike responses in L6 neurons (n=18) in thy1-Chr2 mice (n=5) to photostimuli (5 ms) of high power (100-1000 mW/mm2) delivered to the BC. The majority of L6 neurons could not be activated by photostimulation (n=8) or responded only to the maximum laser power (1000 mW/mm2, n=4). The remaining L6 neurons (n=6) had different activation thresholds with an average of 633 ± 308 mW/mm2 (For testing corticothalamic drive, L5B-ChR2 neurons were activated with maximal intensities of 32mW/mm2)

(A) PSTH for a L6 neuron stimulated with photostimuli (5 ms, onset at 0 ms) at different intensities.

(B) Scatter plot of six L6 neurons that could be activated, with varying power thresholds. The average intensity threshold for spiking for these neurons was 633 ± 308 mW/mm2. The probability of spiking (P(response)) for each photostimulation power was calculated for 100 ms windows immediately following each photostimulus (typically > 50 pulses per data point). Black dots were significantly greater than spontaneous activity (measured in a 100 ms window preceding the stimulus), grey were not (X2 test, p≤ 0.05), black line shows averaged values binned in 250 mW/mm2 increments. The laser power used to activate L5B-ChR2 neurons (blue region) was <32mW/mm2.

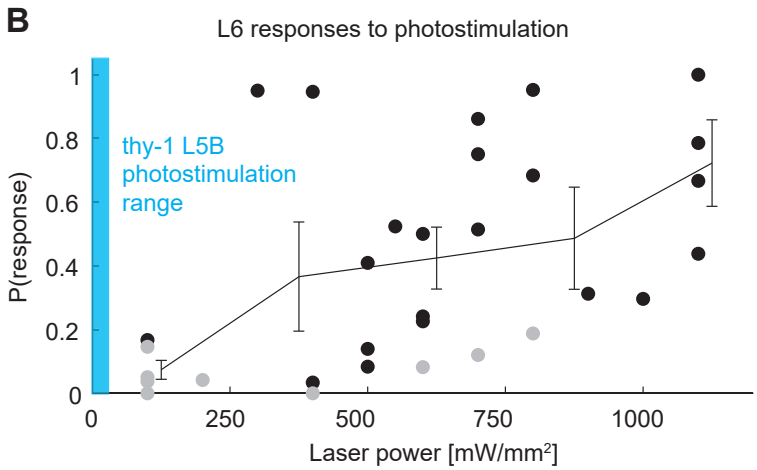

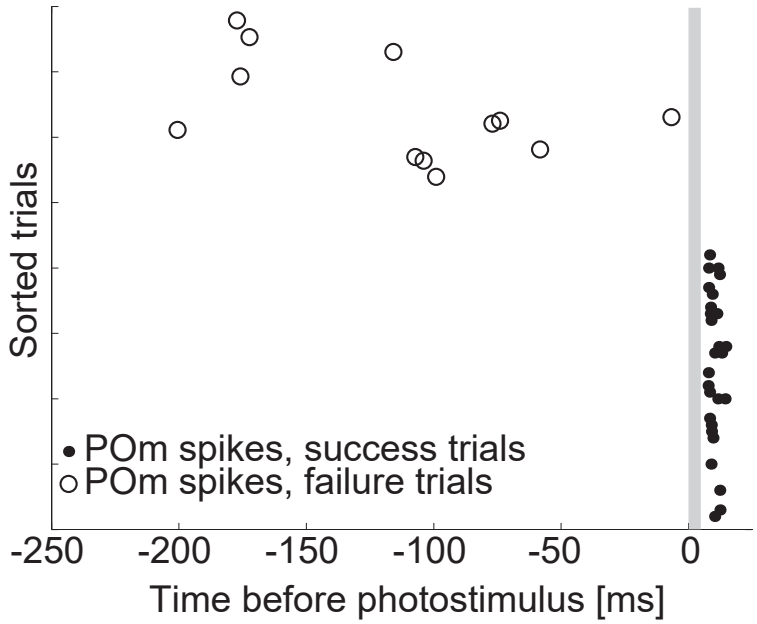

Figure S6. Interactions between evoked and spontaneous POm spikes

Example raster plot of POm spike responses elicited by L5B photostimulation and spontaneous POm spikes, sorted into failure (top, open marker) and successful (bottom, solid marker) trials. Recent spontaneous spiking had an effect on subsequent photo-evoked spiking, in that POm spiking probability in response to photostimulation decreased with the occurrence of spontaneous POm spikes preceding the photostimulus. This observation suggests that the same subthreshold input triggered spontaneous and photo-evoked POm spikes. On average (n=9, POm juxacellular recordings), failure trials were preceded by four times as many spontaneous spikes than successful trials (0.2 ± 0.05 vs. 0.05 ± 0.02 spikes) in a 100 ms window before photostimulation. These data suggest that POm spontaneous spikes are driven by the same inputs which are active during photostimulation of L5B.

Figure S7: Spontaneous EPSP quantification.

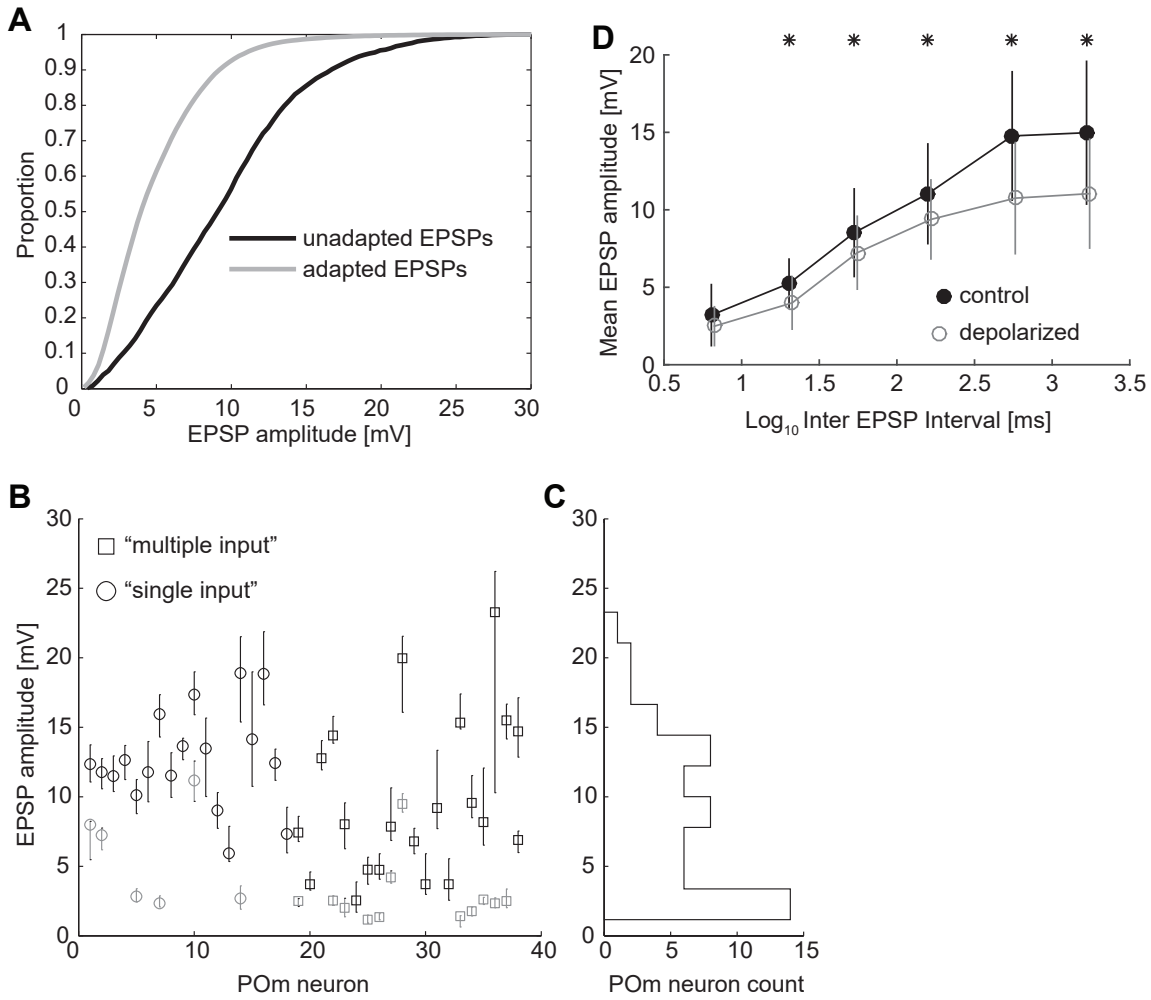

Figure S7. Spontaneous EPSP quantification.

(A) Population cumulative histogram of "unadapted" (IEI>500 ms, black, n=4572) and "adapted" (IEI<=500 ms, gray, n= 38914) EPSPs pooled from 38 POm neurons
(B) Median and interquartile ranges of "unadapted" (IEI>500 ms) EPSP amplitudes by POm neuron. "Single input" (circles) and "multiple input" (squares) were split by correlation coefficients (threshold of r=0.6). Bimodal EPSP distributions were split into two distributions, and the the median of the second peak is shown in gray. This bimodality may represent additional independent inputs, or populations of EPSPs which did and did not trigger low threshold spikes, respectively.
(C) Distribution of median EPSP amplitudes from B.
(D) Pooled (n=8 recordings) mean ± SD spontaneous POm EPSP amplitude as a function of IEI and membrane potential at EPSP onset: control (solid black markers) or depolarized (gray open markers, > approximately -60 mV). Depolarized EPSPs had significantly smaller amplitude ($p<0.05$, rank sum) than control EPSPs for IEIs > 10 ms (asterisks); this population plot recapitulates was observed in each single recording. Depolarized and control data plots are slightly offset for visual clarity. The larger depolarization-dependent decrease for long IEI EPSPs is consistent with a T-type calcium "low-threshold spike" contribution to these large, temporally isolated events.

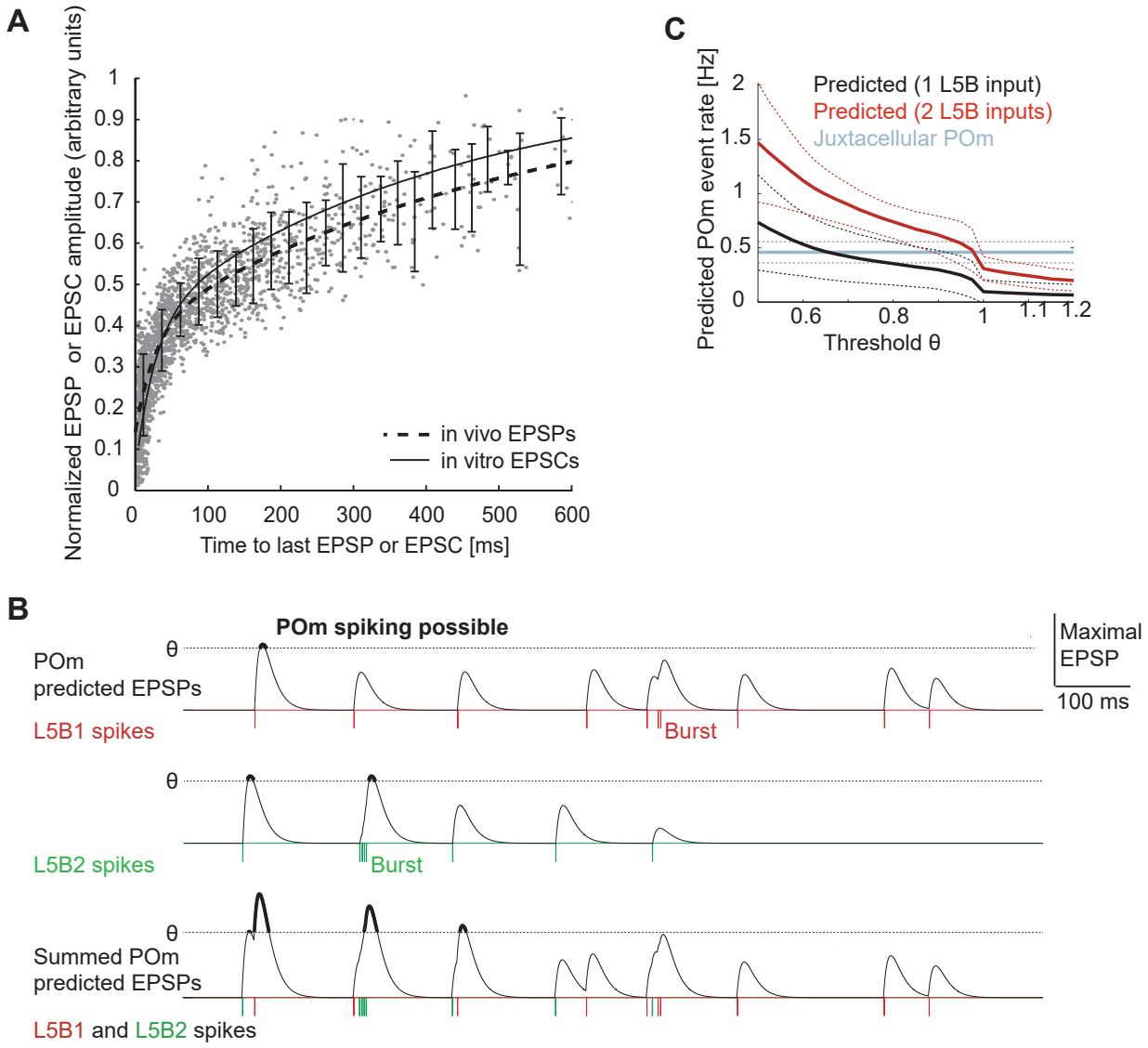

Figure S8. Predicted EPSP and spiking response to single and paired L5B spike trains

(A) Spontaneous EPSP amplitude versus inter EPSP interval (IEI) serves as an predictive curve for EPSP adaptation (Methods). Pooled data for spontaneous EPSPs from five "single input" POm neurons, EPSPs normalized by dividing individual EPSP amplitudes by the mean unadapted amplitude for each recorded neuron. Dashed line shows double exponential fit, τfast=127 ms, τslow = 550ms, as in in vitro EPSC data from (Groh et al. 2008), overplotted as solid line for comparison. The fast component was identical to that previously reported for EPSC depression; however, the slow component shows a ~25% slower recovery compared to the in vitro slow component of τ= 423 ms.
(B) Predicted EPSPs for two simultaneous juxtacellular recordings of L5B spontaneous spiking patterns (red and green show separate L5B spike trains). Threshold line indicates the degree of depolarization over which POm spiking is expected. Spikes preceded by a large interval trigger EPSP over threshold, while high-frequency L5B bursts also increase EPSP size. Lower: sum of individual predicted EPSP trains, showing enhanced POm spiking (bold black) via coincidence.
(C) Mean ± SD predicted POm event rate for single (black) and summed (red) inputs. Juxtacellularly measured POm spike rates (gray) shown for comparison.

Supplementary Methods

Cell reconstructions

After the experiments, mice were euthanized with an overdose of ketamine/xylazine and transcardially perfused with 4% PFA in phosphate buffered saline. Four hours after fixation, the brain was cut into 100 µm coronal slices and stained for cytochrome C to reveal the VPM/POm border and with DAB to reveal the soma and dendrite of the recorded neuron; both protocols are found in (Groh 2011).

Dendritic parameters were first analysed with Neurolucida (Microbrightfield Bioscience, Williston, VT, USA). Dendritic profiles along the pia to white matter axis were constructed as described in (Meyer et al. 2010), using custom software developed in the M. Helmstaedter group at the Max Planck Institute for Medical Research, Heidelberg, Germany. In brief 1) after obtaining a Neurolucida reconstruction, the Neuronregistrator3d program was used to scale dendrite measurements to the population mean pia to white matter distance; 2) Rembrandt3d was used to collapse the three-dimensional morphology into a depth-resolved (pia to white matter) histogram of summed dendritic length (50 µm bin size in all dimensions); 3) the Rothko program was used to smooth and visualize the resulting histogram. These software packages were programmed in Matlab, MathWorks, Natick, USA).

6 POm neurons and 12 Chr2-L5B neurons were recovered and all showed dendritic morphology and parameters (**Figs. 1A, S1, Supplementary Tables 1,2**) consistent with previously published descriptions of these neurons (de Kock et al. 2007; Meyer et al. 2010).

Supplementary Tables

Total apical tuft length (µm) (excluding obliques)	No. Nodes in apical tuft (excluding obliques)	Apical tuft width (µm)	Total basal length (µm)	No. nodes in basal dendrite	No. primary basal dendrites	Total oblique length (µm)	No. nodes in oblique dendrites	No. oblique dendrites
3751 ± 981	32.6 ± 6.6	464.8 ± 177.5	3126 ± 1368	19.2 ± 8.7	7.1 ± 1.9	2324 ± 846	7.9 ± 4.9	14.3 ± 4.8

Supplementary Table 1: L5B-ChR2 dendrite data, n=12. Data shown as population mean ± SD. Fluorescently labelled neurons were filled in acute slices obtained from 18- to 24-day-old mice. Biocytin was revealed by DAB stains and reconstructions were done with Neurolucida. Dendritic parameters were measured with Neuronexplorer.

Total dendritic length (µm)	No. Nodes	No. primary dendrites	Mean dendritic length (µm)	Mean No. of nodes per dendrite
9195 ± 2618	70.2 ± 15.2	10 ± 2	951 ± 330	7.3 ± 2.1

Supplementary Table 2: POm dendrite data, n=6. Data shown as population mean ± SD. Animal preparation and recordings were done with 6-8 week old thy1-ChR2. POm neurons that could be driven by photostimulation of BC were filled with biocytin, stained and reconstructed using Neurolucida. Dendritic parameters were obtained using Neuronexplorer.

Supplementary Text

The Thy1-ChR2 line contains a subset of thick-tufted L5B neurons which project to POm and express ChR2

First we determined the anatomical profile of ChR2-expressing neurons in L5 to test the consistency with the anatomy and location of thick tufted neurons in L5B, which are known to form giant synapses in POm (Hoogland et al. 1987; Bourassa et al. 1995; Killackey and Sherman 2003; Groh et al. 2010). Fluorescently-labelled neurons were filled with biocytin via whole-cell recordings in acute brain slices (Fig. S1A-D); 12 dendritic morphologies were then visualized and reconstructed. All but two dendritic morphologies indicated thick-tufted L5B neurons. Fig. S1E shows 6 of these ChR2-expressing neurons from BC. The somata of ChR2-expressing neurons were located at an average depth of 768±83 µm, n=12 (Fig. S1F), which corresponds to L5B (Groh et al. 2010). Morphological quantification further showed three dendritic compartments, typical for thick-tufted L5B neurons: (1) basal dendrites which extend mostly within L5B, (2) oblique dendrites in L5A and lower L4, and (3) extensive apical dendritic tufts (thick-tufted) in upper L2 and L1 (Fig. S1G, Supplementary Table 1). Based on this distinct dendritic morphology and soma locatio, these neurons can be classified as thick-tufted pyramidal neurons.

CT projections of L5B-ChR2 neurons were verified by depositing retrograde tracer (fluorescent cholera toxin) into POm. We found back-labelled neurons in L6 and L5B, consistent with earlier reports which showed that both layers project to POm (Hoogland et al. 1987; Bourassa et al. 1995; Killackey and Sherman 2003). L5B-ChR2 neurons were also back-labelled, demonstrating that these genetically-identified neurons form synaptic contacts in POm (Fig. S2, see also (Groh et al. 2014)). All retrogradely labeled neurons were ChR2 positive and only a fraction of ChR2 neurons were retrogradely labeled. A quantitative analysis beyond this proved difficult, mainly because retrograde labelling will not specifically label the entire POm. Therefore, the fraction of POm projecting L5B neurons in barrel cortex could not be accurately determined with this approach. Based on these limitations we can only estimate, that ChR2 neurons include a number of L5B populations with one population projecting to POm.

The target cells of L5B neurons in POm were identified by reconstructions of their soma-dendritic morphology and their location in POm after juxtasomally filling of cells that responded to photostimulation of BC. L5B photostimulation evoked spikes in 35 out of 46 POm neurons. We confirmed the location of 13 neurons in POm and reconstructed six dendritic morphologies (Fig. 1A) of POm neurons that responded with spikes to L5B photostimulation; Supplementary Table 2 summarizes dendritic parameters of our POm sample.

Supplementary References

Bourassa J, Pinault D, Deschenes M. 1995. Corticothalamic projections from the cortical barrel field to the somatosensory thalamus in rats: a single-fibre study using biocytin as an anterograde tracer. Eur J Neurosci 7:19-30.

de Kock CP, Bruno RM, Spors H, Sakmann B. 2007. Layer- and cell-type-specific suprathreshold stimulus representation in rat primary somatosensory cortex. J Physiol 581:139-154.

Groh A, Bokor H, Mease RA, Plattner VM, Hangya B, Stroh A, Deschenes M, Acsady L. 2014. Convergence of cortical and sensory driver inputs on single thalamocortical cells. Cereb Cortex 24:3167-3179.

Groh A, de Kock CP, Wimmer VC, Sakmann B, Kuner T. 2008. Driver or coincidence detector: modal switch of a corticothalamic giant synapse controlled by spontaneous activity and short-term depression. J Neurosci 28:9652-9663.

Groh A, Krieger, P. 2011. Structure–Function Analysis of Genetically Defined Neuronal Populations. In: Fritjof Helmchen, Arthur Konnerth, Yuste R, editors. Imaging in Neuroscience: A Laboratory Manual Cold Spring Harbor Cold Spring Harbor Laboratory Press.

Groh A, Meyer HS, Schmidt EF, Heintz N, Sakmann B, Krieger P. 2010. Cell-type specific properties of pyramidal neurons in neocortex underlying a layout that is modifiable depending on the cortical area. Cereb Cortex 20:826-836.

Hoogland PV, Welker E, Van der Loos H. 1987. Organization of the projections from barrel cortex to thalamus in mice studied with Phaseolus vulgaris-leucoagglutinin and HRP. Exp Brain Res 68:73-87.

Killackey HP, Sherman SM. 2003. Corticothalamic projections from the rat primary somatosensory cortex. J Neurosci 23:7381-7384.

Meyer HS, Wimmer VC, Hemberger M, Bruno RM, de Kock CP, Frick A, Sakmann B, Helmstaedter M. 2010. Cell type-specific thalamic innervation in a column of rat vibrissal cortex. Cereb Cortex 20:2287-2303.

Manuscript No 3: Cortical Dependence of Whisker Responses in Posterior Medial Thalamus in vivo

Cortical Dependence of Whisker Responses in Posterior Medial Thalamus in vivo

Rebecca A. Mease*, **Anton Sumser***, Bert Sakmann, Alexander Groh

*shared 1st authorship

Cerebral Cortex 2016

Author Contributions:

R.A.M, B.S. and A.G. designed the study, R.A.M. and A.G. performed experiments in Thy1-Chr2 animals; A.S. performed experiments in VGAT-Chr2 animals. R.A.M. and A.S. analyzed the data and generated figures; R.A.M., A.S. and A.G. jointly wrote the paper with the help of B.S.

OXFORD

Cerebral Cortex, 2016, 1–10

doi: 10.1093/cercor/bhw144
Original Article

ORIGINAL ARTICLE

Cortical Dependence of Whisker Responses in Posterior Medial Thalamus In Vivo

Rebecca A. Mease[1,2], Anton Sumser[1], Bert Sakmann[1,3] and Alexander Groh[1,2]

[1]Institute for Neuroscience of the Technische Universität München, 80802 Munich, Germany, [2]Department of Neurosurgery, Klinikum rechts der Isar, Technische Universität München, 81675 Munich, Germany and [3]Max Planck Institute for Neurobiology, 82152 Martinsried, Germany

Address correspondence to Alexander Groh. Email: alexander.groh@gmail.com

Rebecca A. Mease and Anton Sumser shared first authorship.

Abstract

Cortical layer 5B (L5B) thick-tufted pyramidal neurons have reliable responses to whisker stimulation in anesthetized rodents. These cells drive a corticothalamic pathway that evokes spikes in thalamic posterior medial nucleus (POm). While a subset of POm has been shown to integrate both cortical L5B and paralemniscal signals, the majority of POm neurons are suggested to receive driving input from L5B only. Here, we test this possibility by investigating the origin of whisker-evoked responses in POm and specifically the contribution of the L5B-POm pathway. We compare L5B spiking with POm spiking and subthreshold responses to whisker deflections in urethane anesthetized mice. We find that a subset of recorded POm neurons shows early (<50 ms) spike responses and early large EPSPs. In these neurons, the early large EPSPs matched L5B input criteria, were blocked by cortical inhibition, and also interacted with spontaneous Up state coupled large EPSPs. This result supports the view of POm subdivisions, one of which receives whisker signals predominantly via L5B neurons.

Key words: barrel cortex, cortex layer 5, corticothalamic feedback, higher order thalamus, somatosensory

Introduction

Cortical layer 5B (L5B) thick-tufted pyramidal neurons project to posterior medial thalamus (POm), forming large "giant" synapses. However, POm receives input from additional sources, and it is unclear how these different inputs contribute to spiking in POm. Three projections establish anatomically "giant" synapses with proximal POm dendrites: that from the nucleus interpolaris (SpVi) and nucleus principalis in the brainstem (Jacquin et al. 1989; Veinante and Deschenes 1999; Veinante, Jacquin, et al. 2000; Lavallee et al. 2005), and those from Layer 5 neurons in barrel cortex (BC) (Hoogland et al. 1987; Bourassa et al. 1995; Killackey and Sherman 2003; Groh et al. 2014) and secondary somatosensory cortex (Liao et al. 2010). It has been shown that in POm, giant synapses formed by L5B axons can evoke giant EPSPs and may act as drivers of POm spiking (Reichova and Sherman 2004; Groh et al. 2008, 2014).

Despite these various inputs from whisker-sensitive regions, POm has been reported to only weakly respond to whisker deflections (Diamond et al. 1992; Sosnik et al. 2001) and was recently shown to be only weakly modulated by whisker movements (Moore et al. 2015; Urbain et al. 2015). Inhibitory input to POm from zona incerta (Bartho et al. 2002) and the anterior pretectum (Bokor et al. 2005) was suggested to suppress whisker responses (Trageser and Keller 2004; Lavallee et al. 2005) via shunting inhibition. Furthermore, approximately one-third of POm neurons located in anterior POm "convergence zones" have been shown to receive both SpVi and L5B input and thus may be driven by coincident L5B and SpVi activity (Groh et al. 2014). However, the

remaining majority of POm neurons receive only cortical driving input.

Given the established effective pathway between cortical L5B and POm (Reichova and Sherman 2004; Groh et al. 2008, 2014; Seol and Kuner 2015) and the robust L5B responses to whisker deflections (de Kock et al. 2007) directly via thalamocortical activation (Constantinople and Bruno 2013), one would expect to observe large whisker-evoked POm EPSPs and spikes of L5B origin with a delay of <50 ms (here referred to as "early responses"). We find indeed that a subset of recorded POm neurons respond with small or large whisker-evoked EPSPs. These EPSPs and early spiking are suppressed by optogenetic inhibition of S1 cortex. In contrast, spiking of neurons in the ventral posterior medial nucleus (VPM) is only slightly affected, consistent with the lack of L5B afferents to VPM (Veinante, Lavallee, et al. 2000). This result, together with previous studies (Trageser and Keller 2004; Ohno et al. 2012; Groh et al. 2014), strengthens the emerging view that the input–output structure is not homogeneous throughout the POm nucleus and that the L5B-POm pathway can be the major driving input for whisker responses in a subset of POm neurons.

Methods

Ethical Approval

All experiments were done according to the guidelines of German animal welfare and were approved by the respective ethical committees.

In Vivo Electrophysiology

Animal preparation and recordings were done with 6- to 8-week-old thy1-ChR2 (line 18) or VGAT-ChR2-YFP mice anesthetized with 1% isofluorane in O_2 (SurgiVet Vaporizer) for the photostimulation experiments or urethane (1.3 µg/g body weight) for simultaneous LFP and juxtacellular recordings. Typically one or 2 experiments (simultaneous L5B/POm recordings, simultaneous L5B/L5B recordings, single L5B, or POm recordings) were done per animal. Recordings were made from a total of 56 mice: 20 animals for intracellular POm recordings, 8 animals for simultaneous POm/L5B juxtasomal recordings, 10 animals for L5B juxtasomal recordings, 10 animals for single juxtasomal POm recordings, 5 animals for VGAT juxtasomal recordings (3 for POm, 2 for VPM), and 3 animals for VGAT POm intracellular recordings.

Depth of anesthesia was continuously monitored by eyelid reflex, respiration rate, and cortical LFP, and additional urethane (10% of the initial dose) was given when necessary. Respiration rates were usually between 100 and 140 breaths per minute. In the case of isoflurane anesthesia, concentration of anesthetic was adjusted to reach steady respiration rates around 100 breaths per minute. The skull was exposed, and small craniotomies above BC and thalamus were made (dura intact). For VGAT photostimulation experiments, the skull above BC was additionally thinned to permit better light penetration into the tissue. The head was stereotaxically aligned (Wimmer et al. 2004) for precise targeting of POm. Target coordinates relative to bregma were (lateral/posterior/depth, in mm) as follows: BC L5B: 3.0/1.1/0.7; POm: 1.25/1.7/2.8–3.0; VPM: 1.7/1.5/3.0–3.2). Juxtasomal electrodes were inserted with an angle of 30° from the vertical.

In vivo juxtasomal recordings and biocytin fillings were made as described in Pinault (1996). Biocytin-labelled neurons are shown in Mease, Sumser, et al. (2016). In brief, 4.5–5.5 MΩ patch pipettes were pulled from borosilicate filamented glass (Hilgenberg, Germany) on a DMZ Universal puller (Zeitz Instruments, Germany). Pipettes were filled with (mM) 135 NaCl, 5.4 KCl, 1.8 $CaCl_2$, 1 $MgCl_2$, and 5 HEPES, pH adjusted to 7.2 with NaOH, with 20 mg/mL biocytin added. Bath solution was identical, except for biocytin. Single units were found by the increase of pipette resistance (2–2.5 times of the initial resistance) measured in voltage clamp mode. A L5B and a POm cell were recorded simultaneously with an ELC-01X amplifier (NPI Electronics, Germany) for POm and an Axoclamp 2B (Molecular Devices, USA) for L5B. Unfiltered and bandpass-filtered signals (high pass: 300 Hz, low pass: 9000 Hz) were digitized at 20 kHz with CED Micro 1401 mkII board and acquired using Spike2 software (both CED, Cambridge, UK). Typically, recordings consisted of 1 single unit that was filled at the end of the experiment with biocytin using current pulses (Pinault 1996). Whole-cell single neuron current clamp recordings in POm were done using the "blind patching" approach as described in Margrie et al. (2002). Pipette solution was (in mM) 130 K-gluconate, 10 HEPES, 10 Na-phosphocreatine, 10 Na-gluconate, 4 ATP-Mg^{2+}, 4 NaCl, 0.3 GTP, 0.1 EGTA, 2 mg biocytin, osmolarity approximately 300, and adjusted to pH 7.2 with KOH.

Cell Selection Criteria and Cell Reconstructions

For all L5B recordings, we used a combined photo- and sensory stimulation protocol to validate neurons' locations: L5B neurons were accepted for analysis if 1) photostimuli applied to the cortical surface resulted in rapid, unadapting spiking responses which persisted for the duration of a long photostimulus (3 s) (Mease, Sumser, et al. 2016) and 2) each neuron responded within 100 ms to whisker stimulation, as the majority of L5B neurons in BC respond to whisker stimulation within this time period (de Kock et al. 2007). Whisker responses were categorized as significant using a χ^2 test ($P > 0.05$) comparing matched number of trials of spike counts within 100 ms after whisker stimulation to 100 ms of spontaneous spiking before the whisker stimulus onset. This protocol ensured that each putative L5B neuron was both in L5B (photostimulation) and in BC (sensory response). In addition to these physiological parameters, L5B and POm neurons were also filled with biocytin for reconstruction of the locations and morphologies (Mease, Sumser, et al. 2016).

After the experiments, mice were euthanized with an overdose of ketamine/xylazine and transcardially perfused with 4% PFA in phosphate-buffered saline. Four hours after fixation, the brain was cut into 100-µm coronal slices and stained for cytochrome C to reveal the VPM/POm border and with DAB to reveal the soma and dendrite of the recorded neuron; both protocols are found in Groh and Krieger (2013).

In Vivo Photostimulation Setup

The stimulation of ChR2-L5B or VGAT neurons was achieved by a custom-built laser setup consisting of a solid state laser (Sapphire, Coherent, Dieburg, Germany) with a wavelength of 488 nm and a maximal output power of 20 mW. The sub-millisecond control of laser pulses was achieved by an ultrafast shutter (Uniblitz, Rochester, NY, USA). The laser beam was focused with a collimator into 1 end of a multimode fiber (Thorlabs, Grünberg, Germany; numerical aperture = 0.48, inner diameter = 125 µm). For ChR2-L5B neuron activation, the maximal output power at the end of the fiber was 1 mW, resulting in a maximal power density of approximately 32 mW/mm^2 on the brain surface. Shutter control was implemented with Spike2 software (CED, Cambridge, UK). The optical fiber was positioned at an angle of approximately 86° (from the horizontal plane) and at a distance of approximately 100 µm to the cortical surface. For each neuron, we recorded an average of 60 ± 41 photostimulation

trials. For BC VGAT photostimulation, the optical fiber was positioned at the same angle, but at a distance of approximately 2.5 mm to increase the stimulated area to a disk with a diameter of approximately 800 µm, measured on the skull above BC. For robust cortical inhibition, we used a 40 Hz series of laser pulses (12.5 ms on, 12.5 ms off) for 1 s with an approximate power density at the pia of 8.4 mW/mm^2, based on Zhao et al. (2011).

Whisker Stimulation

Whisker stimulation consisted of 50 ms (30 ms for all juxtasomal and 1 whole cell recordings in VGAT animals) air puffs (50 mbar) delivered via a plastic tube with a tube opening of approximately 1 mm. The opening was positioned 0.5–2 cm anterior of the stimulated whiskers which were deflected in caudal direction. The puff stimulus targeted the C row and deflected whiskers in at least rows B–D. The latency from command to whisker deflection was measured using 2 methods: First, the air puff was applied to a microphone positioned at the same distance as the whiskers, and the potential change was read from an oscilloscope. Secondly, a small magnetic probe (0.5 mg) was glued to a whisker, and the time of deflection was measured with a custom-built magnetic field detector. Data analysis was corrected for this delay (20 ms). For each neuron, we collected an average of 69 ± 48 and 60 ± 41 trials for intracellular and juxtasomal recordings, respectively. In experiments with simultaneous VGAT photostimulation, we acquired responses to 52 ± 30 and 189 ± 72 trials for intracellular and juxtasomal recordings, respectively.

In a minority of cases, we also used a piezo wafer to stimulate single whiskers; this procedure is described in Mease et al. (2014). In these cases, no delay correction was done. A comparison of puff and piezo responses is shown in Supplementary Figure 1.

Cortical LFP Recordings

To monitor cortical state, we acquired L5 local field potentials (LFPs) simultaneously with single neuron recordings. Depth-resolved LFPs were recorded with a 16-channel probe (Neuronexus probe model: A1X16-3mm-100-177, Neuronexus, MI, USA). The probe was inserted into BC as close as possible to the juxtacellular recording site and inserted at an angle of approximately 45° from the vertical to a tip depth of 1.5 mm from the pia. Because the location of the probe varied slightly between experiments and was not aligned with the deflected whiskers, the LFP transients triggered by whisker stimulation varied between experiments. A chlorided Teflon-coated silver wire in the bath solution above the craniotomy served as reference. Signals were amplified and filtered with an extracellular amplifier (EXT-16DX, NPI Elektronics, Tamm Germany). LFPs were bandpass filtered with 0.01 or 0.1 Hz and 500 Hz corner frequencies and amplified 1000–2000 times. All signals were digitized at 20 kHz with CED Micro 1401 mkII board and acquired using Spike2 software (both CED, Cambridge, UK). Only LFPs recorded at a depth of 750 µm, corresponding to L5B, were used for analysis.

Data Analysis

Electrophysiology data were acquired using Spike2 software and then exported for analysis in Matlab version 9 (MathWorks, Natick, USA) using custom written software. Spike times were extracted by finding local maxima in the temporal derivative of recorded voltage traces (dV/dt) above a variable threshold (typically 40–50% of maximum dV/dt). Reported values are mean ± standard deviation, unless otherwise noted. Statistical significance indicates $P < 0.05$. Unless otherwise stated, means and medians are calculated across neurons, not from pooled data.

EPSP Extraction

EPSP times and maxima were extracted by finding crossings in the first derivative of the membrane potential, and validated and/or corrected by hand.

Identification of Up States

Up states were selected by hand as large deflections in the LFP. To further standardize transition points across recordings and Up transitions with different rates of change, each individual LFP transition trace was normalized to a height of 1 and the transition point was then set to be the time at which the trace reached 50% of this maximum. For the display figures, the LFP signal was converted to a dimensionless z-score and then inverted so that positive deflections correspond to "Up states" (Hahn et al. 2006).

Results

Whisker-Evoked Spiking Responses in POm

In vitro and in vivo works (Diamond et al. 1992; Reichova and Sherman 2004; Groh et al. 2008, 2014) predict that L5B inputs to POm during whisker stimulation could generate excitatory synaptic inputs sufficient to trigger spikes. We initially measured L5B and POm spike responses to whisker stimulation on short and long time scales. Whiskers were stimulated by the application of an air puff, deflecting 2–3 whisker rows. We recorded juxtacellularly from Layer 5B neurons in BC and POm neurons in somatosensory thalamus in urethane anesthetized thy-1 ChR2 mice (Arenkiel et al. 2007). This mouse line expresses channelrhodopsin-2 in L5, including POm-projecting L5B neurons, allowing us to photostimulate the L5B-POm pathway and record from photo-responsive neurons in L5B and neurons in POm (2.9–3.0 mm from the pia).

First, L5B neuron recordings were accepted for further analysis if they showed 1) responses to whisker stimulation (within a 100 ms time period) and 2) short latency (4–6 ms, see Arenkiel et al. (2007)) responses to photostimulation of the surface of BC (Mease, Sumser, et al. 2016). These 2 criteria ensured that neurons were located both in the BC and in the L5B, respectively. POm neurons were recorded simultaneously with a L5B neuron and were accepted for analysis when 1) the paired L5B neuron responded to whisker stimulation, and 2) if the POm neuron responded with short latency (~12 ms) to photostimulation of BC. Recordings in POm were directed by stereotaxic coordinates and confirmed post hoc for a subset ($n = 6$) of POm recordings with recovered dendritic morphologies (Mease, Sumser, et al. 2016).

Examining the L5B and POm spiking responses (Fig. 1) in more detail, we found that we could categorize spike responses based on the "early" and "late" spiking components; Supplementary Figure 2 illustrates the population probability of response per trial. Figure 1A shows 2 example spike recordings from L5B neurons, 1 example with both early and late spikes (upper) and 1 example with only late spikes (lower). Figure 1B shows corresponding POm spike responses, including 1 cell that had an early response. Figure 1C shows a summary of L5B spiking relative to whisker stimulation. The majority of L5B neurons (19/31) had a bimodal whisker response with early and late components: in most neurons (16/31), the early response was sharp and within 50 ms, while the following late response (>50 ms) was gradual and

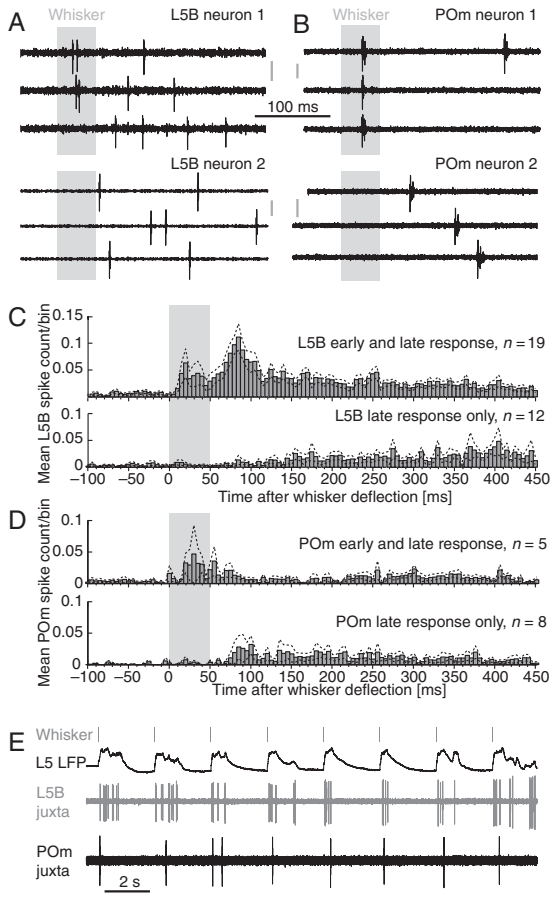

Figure 1. Two categories of L5B and POm spiking. (*A*) Two example L5B responses after whisker stimulation (3 trials, gray bar) showing a neuron with an early and late response (upper) and neuron with a late response only (lower). Voltage scale bars for upper and lower panel: 1 mV, 2 mV, respectively. (*B*) Two example POm recordings, as in *A*. Voltage scale bars for upper and lower panel: 1 mV. (*C*) Population PSTHS for L5B neurons with an early spike response (upper, $n = 19/31$) with a bin size of 5 ms. The dotted line indicates SEM of the population. Most early responders (16/19) had a response significantly greater than spontaneous activity within 50 ms of air puff onset; however, 3 neurons with a slightly delayed initial response (within 100 ms) were included in this distribution, due to a clearly bimodal response profile. The remaining neurons had only a late response ($n = 12$, lower). Significance was assessed with χ^2 test between spontaneous and evoked spike count, before and after the whisker stimulus, respectively. (*D*) Population PSTHS for POm neurons with an early spike response ($n = 4$ within 50 ms, $n = 1$ within 100 ms, upper) and only a late response ($n = 8$, lower). Plot conventions and significance assessed as in (*C*). (*E*) Simultaneous recording of cortical L5 LFP (upper), juxtacellular L5B spikes (gray, middle), and POm spikes (lower). Cortical Up states were triggered by whisker deflection (gray bars). L5B and POm spiking were correlated during cortical Up states.

less precise. We included 3 outlier neurons with slightly delayed (60–80 ms) initial early responses in this "early" group, due to clear bimodal responses with early and late components. The remaining "late" neurons showed only a late, gradual whisker response (12/31) occurring after 50 ms. In comparison, about a third of POm neurons (5/13) exhibited a comparable 2-component "early" response onset spiking response (Fig. 1*D*), and the remainder a "late" response only.

To examine the coupling of L5B and POm spikes during cortical Up and Down states evoked by whisker stimulation, in a subset of recordings we simultaneously recorded LFP in BC as well as L5B and POm spike during whisker stimulation (Fig. 1*E*). The majority of whisker stimulation trials (mean across neurons of 73 ± 15%) evoked cortical Up states within 400 ms following whisker stimulation onset. Average L5B and POm spiking rates during such evoked Up states were 2.7 ± 1.4 and 0.8 ± 0.4 Hz, respectively (L5B, $n = 19$; POm, $n = 10$; 12–181 whisker-evoked Up states per recording, mean of 60 ± 54; more details are given in Mease, Sumser, et al. (2016)). Our interpretation is that late POm spike responses are most likely a consequence of cortical Up states evoked by whisker deflections.

Block of Early POm Spiking by Cortical Inhibition via Photostimulation

To test the contribution of cortical input to whisker-evoked spike responses in POm, we inactivated S1 barrel cortex reversibly by cortical inactivation via photostimulation of channelrhodopsin-2-expressing VGAT inhibitory interneurons (Zhao et al. 2011). In cortical inactivation experiments, we recorded only from neurons with clear early whisker-evoked spike responses. Inactivation of BC robustly abolished whisker-evoked POm spiking (mean response probability reduction of 99 ± 1%; $n = 6$) (Fig. 2*A*, *C*,*E*). In contrast, inhibition of cortex had comparatively little and variable effect on the whisker-evoked spiking of ventroposteriomedial (VPM) neurons (average response probability increase of 2 ± 24%; $n = 5$) (Fig. 2*B*,*D*,*E*). This lack of a strong effect on VPM is consistent with the lack of driving cortical L5B input to VPM (Veinante, Lavallee, et al. 2000); the remaining modest effects of cortical inactivation may be due to the block of cortical L6 inputs, which modulate VPM whisker responses in a dynamic and complex fashion (Mease et al. 2014). In combination, these results confirm the earlier report (Diamond et al. 1992) that cortical inputs are necessary for whisker-evoked spikes in POm, but not in VPM.

Whole-Cell POm Recordings In Vivo Show 3 Categories of Subthreshold Whisker Responses

To investigate the subthreshold origin of the different POm spiking patterns in response to whisker stimulation, we recorded from POm neurons in whole-cell configuration ($n = 30$) while deflecting whiskers. Figure 3 shows 2 example whole-cell recordings at different time resolutions. POm membrane potentials were not riddled with IPSPs as previously described for POm neurons that receive input from SpVi and ZI (Lavallee et al. 2005). As the neurons from which we recorded receive their driving input from L5B and do not show tonic and large IPSP patterns, it is possible that nonconvergence POm neurons in general do not receive this ZI input.

As in the juxtacellular experiments (Fig. 1*E*), whisker stimulation typically led to whisker-evoked Up states in the LFP (upper traces), and concomitant POm EPSPs and action potentials (APs) (lower traces). We found EPSP response times matching the latencies of the early and late POm spike responses shown in Figure. 1*D*. About half of the recordings (18/30) showed "early" short latency (<50 ms) whisker EPSPs (Fig. 3*A*,*B*) which led to whisker-triggered APs in a minority of POm neurons (5/30). In the remaining "late" (12/30) POm whole-cell recordings, EPSP timing was locked to whisker-evoked Up states rather than the timing of the whisker stimulation (example in Fig. 3*C*,*D*).

About half (10/18) of early responder neurons had EPSPs with large amplitudes (Fig. 4*A*, median = 7.7 mV, interquartile range = 3 mV), while the remaining early responder neurons (8/18) had small EPSPs (Fig. 4*B*, median = 0.8 mV, interquartile range = 0.3 mV). The EPSPs from the late responder group had the largest

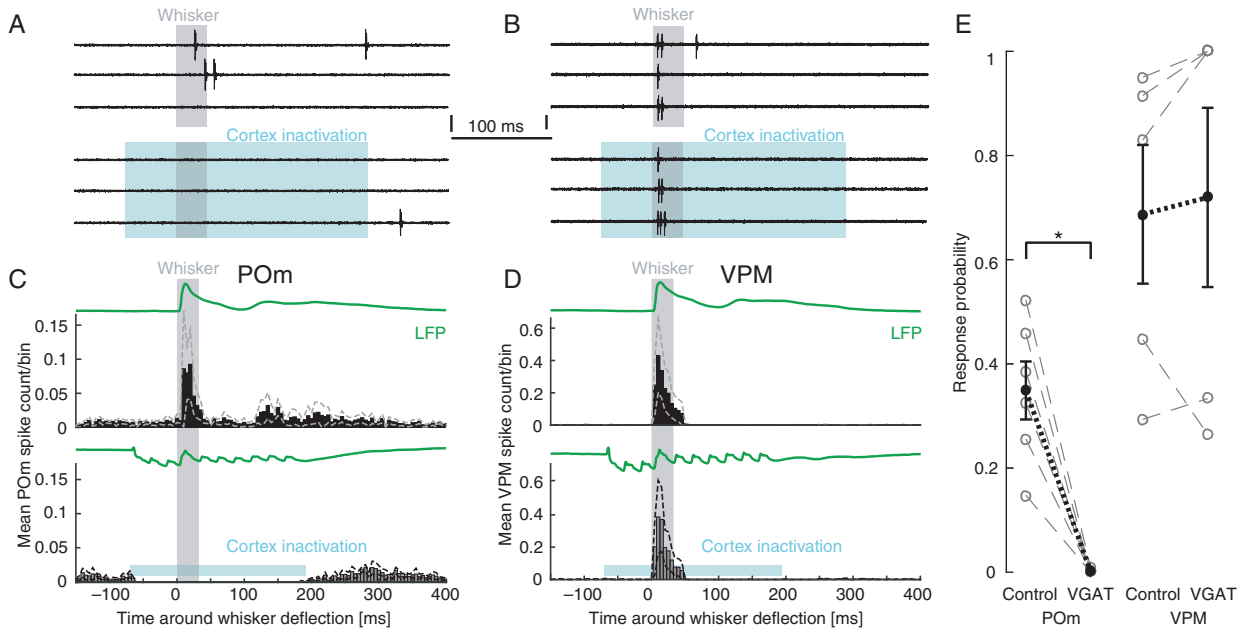

Figure 2. Elimination of early spike responses in POm but not VPM during cortical inactivation by VGAT photostimulation. (*A*) Example of a juxtasomal POm recording with an early response (upper) to whisker stimulation (gray bar, 3 trials), which is abolished during cortical inactivation (lower, light blue area). Voltage scale bar: 2 mV. (*B*) Same as *A* but for an example VPM neuron. Voltage scale bar: 2 mV. (*C*) Population PSTH of 6 POm neurons in control condition (black, upper) and during cortical inactivation (gray, lower). Dashed lines show SEM. Green line shows cortical mean LFP. (*D*) Same as in *C* but from 5 VPM neurons. (*E*) Population spike response probability in a 50 ms time window post-whisker stimulation in POm (left; $n = 6$) and VPM (right; $n = 5$). Individual neurons in gray, population mean, and SEM in black. Cortical inactivation nearly abolished POm responses in all neurons (6/6 $p < 0.05$, χ^2 test), and changed response probabilities of most VPM neurons (4/5 $p < 0.05$, χ^2 test), albeit weakly and inhomogeneously. On a population level, POm but not VPM response probability was significantly reduced by cortical inactivation ($P = 0.031$ (*) and $P = 0.625$, respectively; Wilcoxon signed rank test).

amplitudes of all 3 categories (Fig. 4C, median 10.9 mV, interquartile range = 4.6 mV), likely due to the contribution of low threshold spikes from T-type calcium channel activation (Jahnsen and Llinas 1984; Landisman and Connors 2007; Groh et al. 2008; Seol and Kuner 2015). Small early responses were additionally distinguished from both large response categories by a slower rate of rise but a slightly faster onset; see Supplementary Table 1 for a comparison of EPSP delay, rise time, and amplitude between the 3 categories. Given these slightly different parameters, these small early EPSPs may also come from trigeminal nuclei, suggesting that these neurons were in convergence zones of L5B and brainstem input.

Thus, the population of whisker-responsive POm neurons could be categorized into the following groups using the amplitude, rise time, and timing (see Supplementary Table 1) of the first post-whisker stimulus EPSP as grouping criteria: 1) early large responses followed by late large responses (10/30), 2) early small responses followed by late large responses (8/30), or 3) late large responses only (12/30). These 3 distinct categories are illustrated in Figure 4D, which shows EPSP amplitude as a function of EPSP latency for each cell.

The early large EPSPs could elicit APs in 5 out of 10 recordings (Fig. 5A), with a mean AP probability of 0.25 ± 0.19 per whisker stimulus. Successful trials were interspersed with failures that revealed hyperpolarizing potentials in 4 out of the 10 recordings (Fig. 5B). While whisker responses in these 4 recordings were nonetheless still dominated by large EPSPs (mean across neurons of 68 ± 26% of trials), IPSPs with an average amplitude of 2.8 ± 1.6 mV were observed in an average of 29 ± 27% of trials. For a quantification of whisker-evoked IPSPs, see Supplementary Table 2. In contrast to whisker-evoked IPSPs, spontaneous IPSPs at high frequencies as described by Lavallee et al. (2005) were not measurable using a 0.2 mV threshold, which is about one-tenth of the amplitude of the whisker-evoked IPSPs. Although relatively scarce, whisker-evoked IPSPs are a possible cause for smaller early EPSPs in comparison to late EPSPs in L5B-targeted POm neurons described here (Fig. 4D).

Figure 6 summarizes the average population time course of EPSP arrival after a whisker stimulus for these 3 categories, including early and late response components. Regardless of the presence of an early response, all POm neurons showed a late response, occurring during the sensory-evoked Up state. However, the origin of the observed early whisker-evoked EPSPs in POm is less clear. The majority of L5B neurons typically show short latency responses to whisker stimulation as shown before (Armstrong-James et al. 1992; de Kock et al. 2007), so in a subset of POm cells, early large whisker-evoked EPSPs may reflect L5B input from a fraction of POm-projecting L5B neurons that briskly respond to whisker deflection and project to the POm cells from which we recorded.

Interaction Between Early and Late Responses Suggests a Common Synaptic Origin for Early and Late Whisker-Evoked L5B Responses

The majority of POm has been suggested to receive driver input only from cortical L5B neurons (Groh et al. 2014). As a consequence, both spontaneous and whisker-evoked giant EPSPs should originate from the same L5B inputs in these "nonconvergence" zones, and interactions between these EPSPs are expected. In this case, the L5B whisker-evoked spikes following shortly after spontaneous Up state spiking would drive smaller EPSPs in POm due to the pathway's incomplete recovery from synaptic depression (Groh et al. 2008).

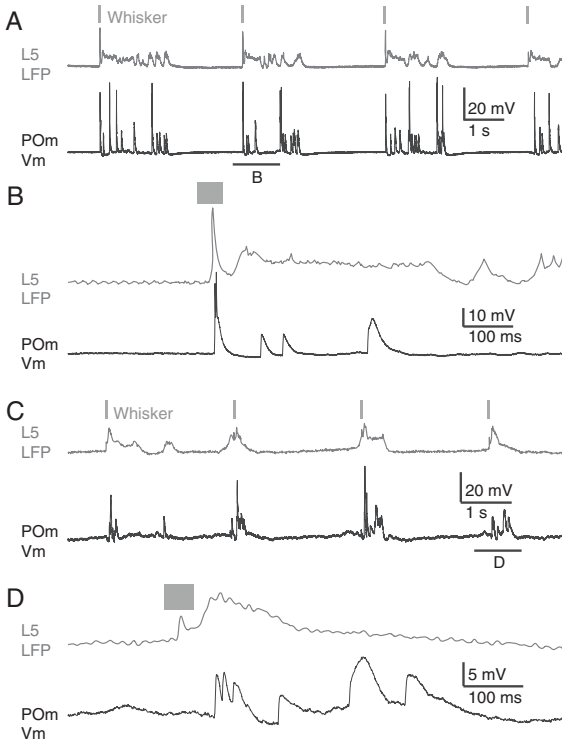

Figure 3. Example EPSPs during whisker-evoked Up states. (*A*) Example of simultaneously recorded cortical L5 LFP and POm membrane voltage during whisker deflection (gray bars), showing evoked cortical Up state and associated POm EPSPs. (*B*) Single early and late response from *A* at higher time resolution shows early large EPSP (delay ~20 ms) and late EPSPs during evoked Up state. This neuron was somewhat atypical in that the early response was sufficient to trigger APs (5 of 30 intracellular recordings had whisker-triggered APs). Resting membrane potential (RMP) = −65 mV. (*C*) As in *A* but for a POm neuron with late EPSPs only. RMP = −67 mV. (*D*) As in *C* at higher time resolution, note the lack of early POm EPSPs during the early LFP deflection.

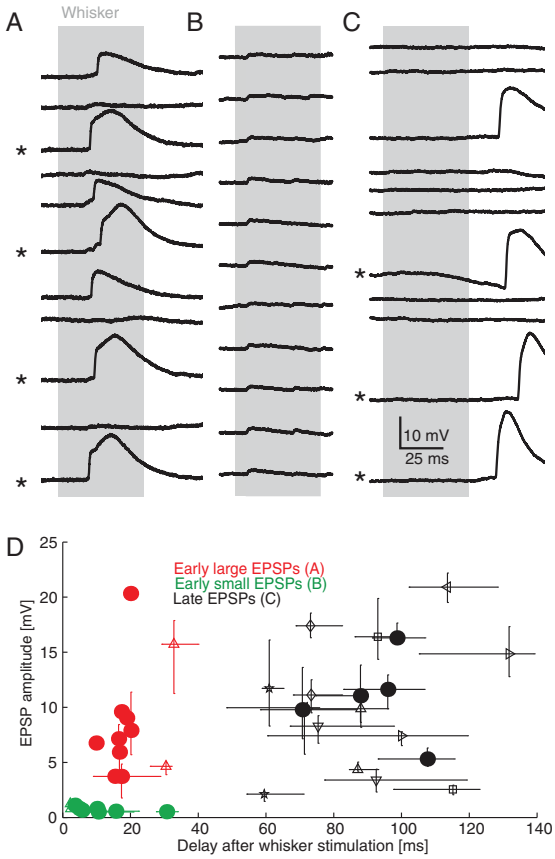

Figure 4. Early whisker-evoked EPSPs in POm. Three single neuron examples of different types of early responses to whisker stimulation (gray bar). Large EPSPs triggering low threshold spikes (*). (*A*) Large early EPSPs (10/30). RMP = −64 mV. (*B*) Small (~1.5 mV) early EPSPs (8/30). RMP = -67 mV. (*C*) Late only EPSPs (12/30). RMP = −66 mV. (*D*) Whisker-evoked EPSP amplitude versus response delay showing the 3 groupings. Values shown are median and interquartile ranges, with a different marker style for each neuron. Colors show response category: early small (green), early large (red), or late only (black). All neurons with a unimodal amplitude distribution are shown as solid circles. For some neurons (open markers), bimodal amplitude distributions were seen; individual peaks are shown using the same style marker. See Supplementary Table 1 for EPSP population amplitudes, delays, and slopes.

To test this possibility, we investigated how the early large whisker responses interacted with spontaneous EPSPs (Fig. 7). For example, in the POm recording shown in Figure 7A, whisker-evoked EPSPs that closely followed spontaneous EPSPs showed a marked (often up to 5 mV, Fig. 7B) decrease in amplitude. Similarly, EPSPs in the late response component were typically smaller in amplitude than the preceding early whisker-evoked EPSP. Overall, we found statistically significant interaction in half of the neurons (5/10): 4/10 neurons showed a significant decrease in EPSP amplitude and a significant increase was observed in 1/10 neurons (mean decrease for subsequent EPSPs, 18 ± 12% Fig. 7C). The modest average decrease in EPSP amplitudes suggests that the pathway responsible for early whisker-evoked EPSPs may be depressed by spontaneous EPSPs, consistent with a common origin of these inputs. While synaptic depression of the L5B-POm pathway is well established (Reichova and Sherman 2004; Groh et al. 2008; Seol and Kuner 2015; Mease, Sumser, et al. 2016), it should be noted that adaptation of subsequent EPSPs is also caused by postsynaptic (intrinsic) mechanisms, such as the depolarization-dependent inactivation of T-type calcium channels characteristic of thalamic neurons (Jahnsen and Llinas 1984). In Mease, Sumser, et al. (2016), we present a more in-depth analysis of spontaneous EPSPs and discuss the possible contribution of postsynaptic factors to EPSP adaptation. The amplitude reduction (Fig. 7) may reflect these postsynaptic factors to some extent, and therefore, a more direct approach was used in the following to investigate the cortical dependence of large EPSPs in POm.

Cortex Inhibition via Photostimulation Blocks Evoked Large EPSPs

To further test the cortical dependence of the early large whisker-evoked EPSPs in our sample, we recorded the membrane potential in POm neurons while reversibly inactivating BC by VGAT-Chr2 photostimulation as in Figure 2 but in whole-cell configuration. We recorded only from neurons with clear early whisker-evoked responses, and large EPSPs were included in this analysis. Figure 8A,C shows an example POm neuron with early large EPSPs evoked by whisker stimulation. Whisker stimulation during cortical inactivation failed to elicit large EPSPs in the same cell (Fig. 8B,D). We observed similar results in all ($n = 4$) whole-cell experiments with cortical inactivation (Fig. 8E, right). Spontaneous EPSPs were also abolished by cortical inactivation (Fig. 8E, left). These data suggest that both whisker-evoked and spontaneous

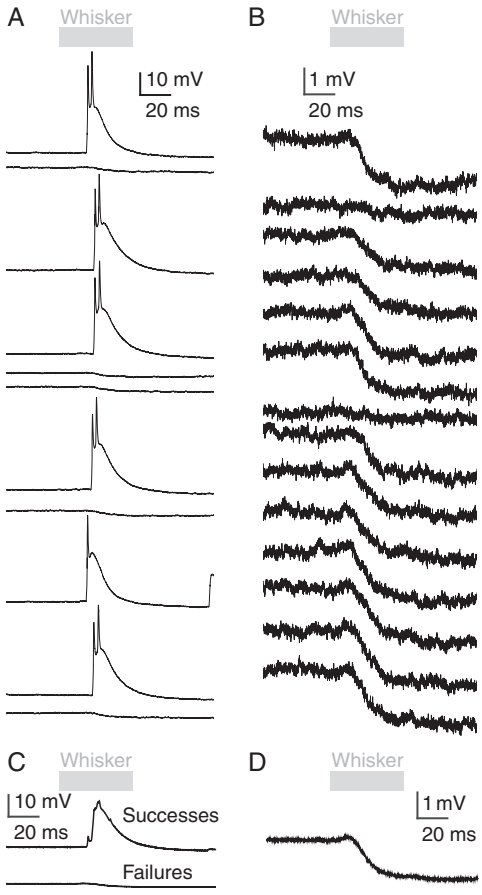

Figure 5. Early large EPSPs elicit APs in POm. An example whole-cell POm recording during whisker stimulation that evokes large early EPSPs (*A*), interspersed with failure trials showing small (1.5 ± 0.4 mV) IPSPs. RMP = −62 mV. (*B*) IPSP trials shown at greater magnification to show details of response. Mean responses for both successes and failures (*C*) and failures at higher magnification (*D*).

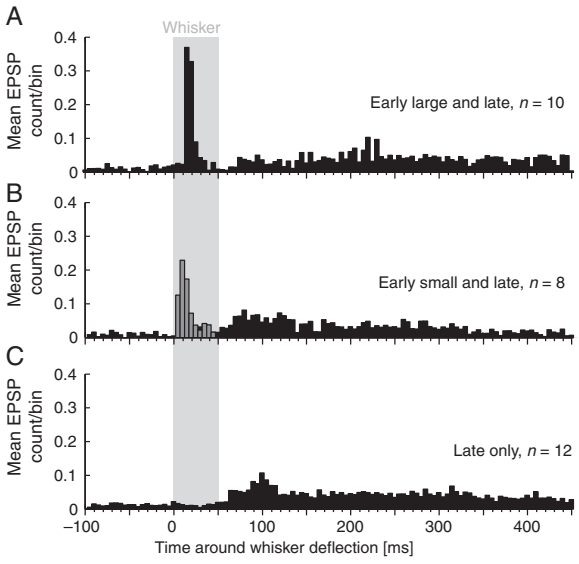

Figure 6. Population whisker-evoked EPSP times. Population means PSTHs relative to whisker deflection for (*A*) early large and late responders, (*B*) early small and late components, and (*C*) late responders bin size in *A*–*C* is 5 ms.

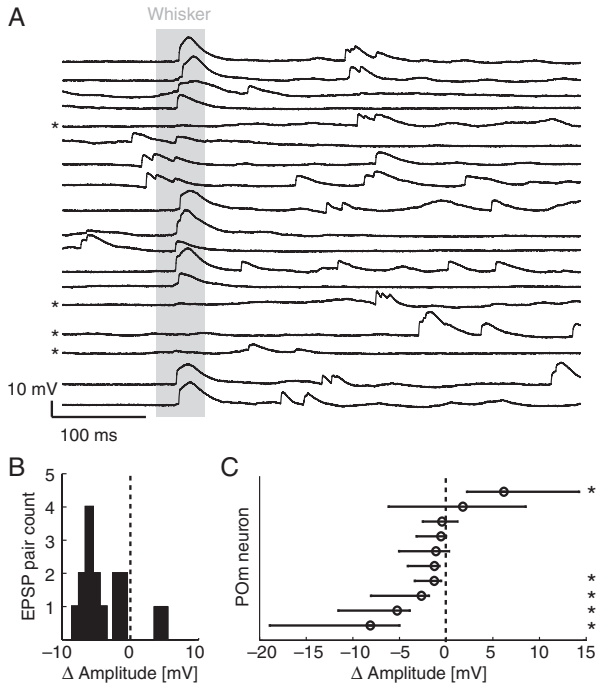

Figure 7. Interaction between early and late whisker-evoked EPSPs. (*A*) Example raw recording in which early and late whisker responses interact; note that previous spontaneous EPSPs also depress whisker-triggered EPSPs, and whisker EPSPs depress later EPSPs, suggesting a common origin of EPSPs. Evoked and spontaneous EPSP amplitudes were measured from initial inflection point to maximum voltage. RMP = −64 mV. Asterisks (*) mark failure trials in which whisker stimuli did not evoke giant EPSPs. (*B*) Summary of EPSP interaction for POm neuron shown in *A*. Histogram shows the distribution of amplitude difference (Δ) between a first EPSP (either a whisker-evoked EPSP or spontaneous EPSP preceding whisker stimulation within a 100 ms window) and a subsequent second EPSP (either spontaneous EPSP following whisker stimulation within a 250 ms window, or the whisker EPSP itself). Negative values show adaptation from EPSP 1 to EPSP 2; this neuron shows strong interaction between whisker and spontaneous EPSPs. (*C*) Population summary: median and interquartile 1st-2nd EPSP amplitude Δ for 10 POm "early large responders," sorted by median amplitude Δ value. Distributions calculated for each neuron as in *B* and only trials with a successful whisker response were included. Significance was assessed by the Wilcoxon signed rank test for zero median, $P < 0.05$. Asterisks (*) mark significant interactions. Four neurons showed significant EPSP adaptation, while 1 neuron had second EPSPs significantly larger than the first.

EPSPs were driven by L5B input and that these recordings were from POm nonconvergence zones that receive whisker input exclusively via L5B.

Discussion

Early Spike and EPSP Responses in POm

When comparing response types in juxtasomal and whole-cell recordings, we found that out of 13 POm juxtasomal recordings with late spikes, 38% (5/13) also showed early spiking. Out of 30 whole-cell recordings with large EPSPs, 33% (10/30) responded with early large EPSPS. In 5 cases, early large EPSPs were capable of evoking APs (Fig. 5). Thus, the percentage of recorded cells that show early spikes and the percentage of cells with early large EPSPs are comparable.

Early large EPSPs were somewhat smaller than late EPSPs (Fig. 4*D*), which could be the result of adaptation of the L5B-POm synapse. Because whisker deflections occasionally coincided with

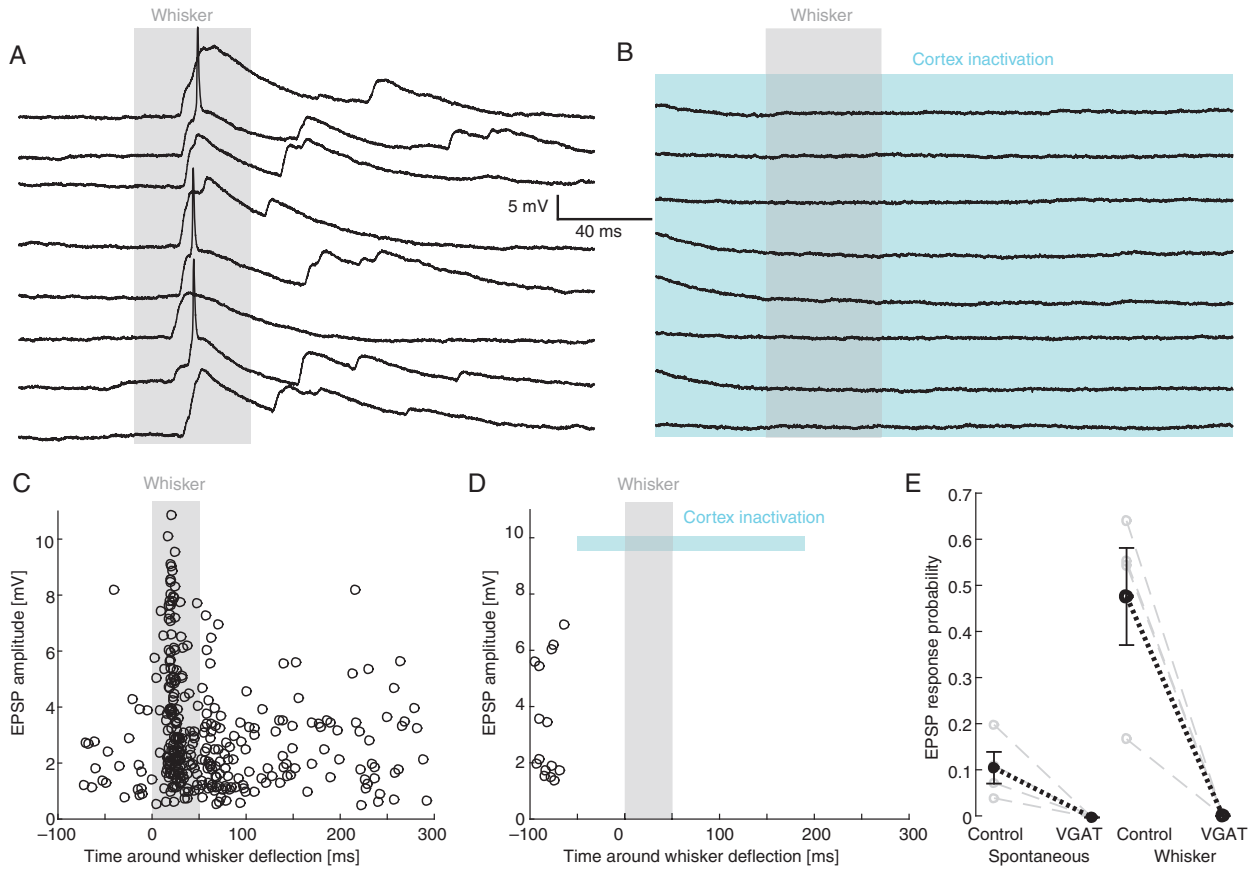

Figure 8. Elimination of early whisker EPSPs in POm during cortical inactivation by VGAT photostimulation. (*A*) Example intracellular whisker responses in POm (gray bar, 8 trials). RMP = −59 mV. (*B*) Same as in *A* but during cortical inactivation (gray bar, 8 trials). (*C*) Scatter plot of EPSP amplitudes over time after air puff, same recording as in *A* and *B*. (*D*) As in *C*, but during cortical inactivation. (*E*) Population ($n = 4$) EPSP response probability drop during cortical inactivation in spontaneous (left; 50 ms preceding whisker stimulation) and evoked conditions (right; 50 ms post-whisker stimulation). During cortical inactivation, 2 of 4 neurons receive a significantly lower EPSP probability without whisker stimulation, while all neurons have a significantly reduced EPSP probability following whisker stimulation (χ^2 test). Individual neurons are shown in gray, population mean and SEM in black.

spontaneous Up states, early EPSPs may have been partially depressed by previous activity. Alternatively, smaller early EPSPs could be due to feed-forward shunting inhibition in which whisker-evoked EPSPs are partially shunted by whisker-evoked inhibition (Trageser and Keller 2004; Lavallee et al. 2005). Whisker-evoked IPSPs in POm may arise from the L5B to zona incerta pathway (Bartho et al. 2002, 2007) or from the L6-reticular nucleus pathway (Bourassa et al. 1995; Pinault et al. 1995). Indeed, we observed whisker-evoked IPSPs in a subgroup of POm recordings (Fig. 5*B*); such IPSPs were not observed when cortex was inhibited (Fig. 8). It should be noted that the continuous "riddling" of the membrane potential by spontaneous IPSPs described for POm neurons targeted by zona incerta (Lavallee et al. 2005) was not observed in our recordings, suggesting a different inhibitory control of POm neurons in nonconvergence zones. Thus, disinhibition of the zona incerta by motor cortex stimulation (Urbain and Deschenes 2007) may not have the same sensory gating effect in POm nonconvergence zones.

Excitatory Input to POm From Different Origins

In agreement with earlier studies (Diamond et al. 1992), POm whisker-evoked responses disappeared after cortical inhibition (Figs 2 and 8), while VPM responses are only slightly modulated. Both spontaneous and evoked large EPSPs in POm were blocked by cortical inhibition, suggesting that they originate from L5B neurons in barrel cortex. The interpolar region of the spinal trigeminal nucleus (SpVi) is whisker responsive during anesthesia (Sosnik et al. 2001) and also projects to POm (Jacquin et al. 1989; Chiaia et al. 1991; Veinante and Deschenes 1999). About one-third of POm neurons receive both SpVi and L5B input (Groh et al. 2014), while the majority of POm neurons receive driver input only from cortical L5B. These nonconvergence zones—constituting two-third of POm—may receive whisker signals exclusively via cortical L5B neurons (Trageser and Keller 2004; Groh et al. 2014). The abolishment of large whisker-evoked EPSPs during our cortical inhibition experiments (Fig. 8) suggests that recorded neurons were located in nonconvergence zones. The electrophysiological signature of our sample revealed marked differences from neurons in Lavallee et al. (2005) which were continuously riddled with IPSPs. Together, these results strengthen the accumulating evidence for the subdivision model of POm (Trageser and Keller 2004; Ohno et al. 2012; Groh et al. 2014) and raise the possibility that convergence and nonconvergence zones are under different inhibitory control.

Spiking Budgets in L5B and POm Under Different Stimulation Conditions

Upon initial consideration, when it is assumed that POm early responses are predominantly evoked via the L5B-POm pathway, the

relative paucity of POm recordings with whisker-evoked early spikes and early large EPSPs stands in apparent contrast to L5B's relatively robust spike responses to single whisker deflection (Armstrong-James et al. 1992; de Kock et al. 2007), or puff stimulation involving only a fraction of all whiskers, as used here. However, taking into account anatomical data as well as differences in the time course of cortical column activation (early and late), the early spike responses in POm are expected to be much sparser.

First, only about 25% of all L5B cells project to POm (Rojas-Piloni et al. 2014); thus, a difference between early spiking in L5B and POm recordings is expected. Second, the late spike response of L5B is caused by Up state activation that travels across the entire barrel field (Wu et al. 2008; Stroh et al. 2013) and activates all columns sequentially. As a result, these travelling wave fronts may activate POm with a delay, in particular when none of the deflected whiskers are in the receptive field of the L5B neurons innervating the recorded POm neuron.

In conclusion, these considerations are in agreement with the view that in POm nonconvergence zones (Groh et al. 2014), early large EPSPs and early spike responses upon whisker deflection are due to the activation of the L5B-POm pathway in the anesthetized animal. Furthermore, the lower probability of recording early large EPSPs in relation to the later responses may be due to the experimental conditions of puff stimulation.

What is expected in the awake animal? The puzzling role of POm in the whisker system is exemplified by recent independent demonstrations that whisker self-motion is poorly encoded in POm (Moore et al. 2015; Urbain et al. 2015), although activation of POm inputs to L5 can enhance cortical whisker responses (Mease, Metz, et al. 2016). A recent study of POm sensory responses in awake rats concludes that the input/output modes of POm are state dependent, and thalamocortical transmission occurs only under the conditions of alertness (Sobolewski et al. 2015). Given the proposed function of L5B neurons in encoding passive and active whisker touch rather than whisking movement (de Kock and Sakmann 2009; Oberlaender et al. 2011, 2012), we expect that L5B cells spike only in those columns that receive input from the few whiskers that touch an object. Whether this focal activation in L5B is maintained across the L5B-POm pathway is not clear. It will strongly depend on the topography of the L5B axons projecting to POm. Projection somatotopy from BC to POm has been suggested (Alloway et al. 2003), but to answer this question conclusively, the anatomical distribution of BC L5B boutons in POm needs to be measured quantitatively.

Supplementary Material

Supplementary material can be found at: http://www.cercor.oxfordjournals.org/.

Funding

Funding was provided by the Deutsche Forschungsgemeinschaft Sachbeihilfe (GR 3757/1-1) (R.A.M.), the Max Planck Society (A.G., A.S., B.S., R.A.M.), the Institute of Advanced Studies at the TU München (A.G.), and Boehringer Ingelheim Fonds (A.S.). Funding to pay the Open Access publication charges for this article was provided by the the Max Planck Society.

Notes

We thank Arthur Konnerth for providing lab space, infrastructure, and ongoing support at the Institute for Neuroscience at the TU München, and Christiaan De Kock, Patrik Krieger, Ehud Ahissar, and Randy Bruno for comments on an earlier version of this manuscript. *Conflict of Interest*: None declared.

References

Alloway KD, Hoffer ZS, Hoover JE. 2003. Quantitative comparisons of corticothalamic topography within the ventrobasal complex and the posterior nucleus of the rodent thalamus. Brain Res. 968:54–68.

Arenkiel BR, Peca J, Davison IG, Feliciano C, Deisseroth K, Augustine GJ, Ehlers MD, Feng G. 2007. In vivo light-induced activation of neural circuitry in transgenic mice expressing channelrhodopsin-2. Neuron. 54:205–218.

Armstrong-James M, Fox K, Das-Gupta A. 1992. Flow of excitation within rat barrel cortex on striking a single vibrissa. J Neurophysiol. 68:1345–1358.

Bartho P, Freund TF, Acsady L. 2002. Selective GABAergic innervation of thalamic nuclei from zona incerta. Eur J Neurosci. 16:999–1014.

Bartho P, Slezia A, Varga V, Bokor H, Pinault D, Buzsaki G, Acsady L. 2007. Cortical control of zona incerta. J Neurosci. 27:1670–1681.

Bokor H, Frere SG, Eyre MD, Slezia A, Ulbert I, Luthi A, Acsady L. 2005. Selective GABAergic control of higher-order thalamic relays. Neuron. 45:929–940.

Bourassa J, Pinault D, Deschenes M. 1995. Corticothalamic projections from the cortical barrel field to the somatosensory thalamus in rats: a single-fibre study using biocytin as an anterograde tracer. Eur J Neurosci. 7:19–30.

Chiaia NL, Rhoades RW, Bennett-Clarke CA, Fish SE, Killackey HP. 1991. Thalamic processing of vibrissal information in the rat. I. Afferent input to the medial ventral posterior and posterior nuclei. J Comp Neurol. 314:201–216.

Constantinople CM, Bruno RM. 2013. Deep cortical layers are activated directly by thalamus. Science. 340:1591–1594.

de Kock CP, Bruno RM, Spors H, Sakmann B. 2007. Layer- and cell-type-specific suprathreshold stimulus representation in rat primary somatosensory cortex. J Physiol. 581:139–154.

de Kock CP, Sakmann B. 2009. Spiking in primary somatosensory cortex during natural whisking in awake head-restrained rats is cell-type specific. Proc Natl Acad Sci USA. 106:16446–16450.

Diamond ME, Armstrong-James M, Budway MJ, Ebner FF. 1992. Somatic sensory responses in the rostral sector of the posterior group (POm) and in the ventral posterior medial nucleus (VPM) of the rat thalamus: dependence on the barrel field cortex. J Comp Neurol. 319:66–84.

Groh A, Bokor H, Mease RA, Plattner VM, Hangya B, Stroh A, Deschenes M, Acsady L. 2014. Convergence of cortical and sensory driver inputs on single thalamocortical cells. Cereb Cortex. 24:3167–3179.

Groh A, de Kock CP, Wimmer VC, Sakmann B, Kuner T. 2008. Driver or coincidence detector: modal switch of a corticothalamic giant synapse controlled by spontaneous activity and short-term depression. J Neurosci. 28:9652–9663.

Groh A, Krieger P. 2013. Structure-function analysis of genetically defined neuronal populations.Cold Spring Harbor protocols. p. 961–969

Hahn TT, Sakmann B, Mehta MR. 2006. Phase-locking of hippocampal interneurons' membrane potential to neocortical up-down states. Nat Neurosci. 9:1359–1361.

Hoogland PV, Welker E, Van der Loos H. 1987. Organization of the projections from barrel cortex to thalamus in mice studied

with Phaseolus vulgaris-leucoagglutinin and HRP. Exp Brain Res. 68:73–87.
Jacquin MF, Barcia M, Rhoades RW. 1989. Structure-function relationships in rat brainstem subnucleus interpolaris: IV. Projection neurons. J Comp Neurol. 282:45–62.
Jahnsen H, Llinas R. 1984. Ionic basis for the electro-responsiveness and oscillatory properties of guinea-pig thalamic neurones in vitro. J Physiol. 349:227–247.
Killackey HP, Sherman SM. 2003. Corticothalamic projections from the rat primary somatosensory cortex. J Neurosci. 23:7381–7384.
Landisman CE, Connors BW. 2007. VPM and PoM nuclei of the rat somatosensory thalamus: intrinsic neuronal properties and corticothalamic feedback. Cereb Cortex. 17:2853–2865.
Lavallee P, Urbain N, Dufresne C, Bokor H, Acsady L, Deschenes M. 2005. Feedforward inhibitory control of sensory information in higher-order thalamic nuclei. J Neurosci. 25:7489–7498.
Liao CC, Chen RF, Lai WS, Lin RC, Yen CT. 2010. Distribution of large terminal inputs from the primary and secondary somatosensory cortices to the dorsal thalamus in the rodent. J Comp Neurol. 518:2592–2611.
Margrie TW, Brecht M, Sakmann B. 2002. In vivo, low-resistance, whole-cell recordings from neurons in the anaesthetized and awake mammalian brain. Pflugers Arch. 444:491–498.
Mease RA, Krieger P, Groh A. 2014. Cortical control of adaptation and sensory relay mode in the thalamus. Proc Natl Acad Sci USA. 111:6798–6803.
Mease RA, Metz M, Groh A. 2016. Cortical sensory responses are enhanced by the higher-order thalamus. Cell Reports. 14:208–215.
Mease RA, Sumser A, Sakmann B, Groh A. 2016. Corticothalamic spike transfer via the L5B-POm pathway in vivo. Cereb Cortex. doi:10.1093/cercor/bhw123.
Moore JD, Mercer Lindsay N, Deschenes M, Kleinfeld D. 2015. Vibrissa self-motion and touch are reliably encoded along the same somatosensory pathway from brainstem through thalamus. PLoS Biol. 13:e1002253.
Oberlaender M, Boudewijns ZS, Kleele T, Mansvelder HD, Sakmann B, de Kock CP. 2011. Three-dimensional axon morphologies of individual layer 5 neurons indicate cell type-specific intracortical pathways for whisker motion and touch. Proc Natl Acad Sci USA. 108:4188–4193.
Oberlaender M, de Kock CP, Bruno RM, Ramirez A, Meyer HS, Dercksen VJ, Helmstaedter M, Sakmann B. 2012. Cell type-specific three-dimensional structure of thalamocortical circuits in a column of rat vibrissal cortex. Cereb Cortex. 22:2375–2391.
Ohno S, Kuramoto E, Furuta T, Hioki H, Tanaka YR, Fujiyama F, Sonomura T, Uemura M, Sugiyama K, Kaneko T. 2012. A morphological analysis of thalamocortical axon fibers of rat posterior thalamic nuclei: a single neuron tracing study with viral vectors. Cereb Cortex. 22:2840–2857.
Pinault D. 1996. A novel single-cell staining procedure performed in vivo under electrophysiological control: morpho-functional features of juxtacellularly labeled thalamic cells and other central neurons with biocytin or Neurobiotin. J Neurosci Methods. 65:113–136.
Pinault D, Bourassa J, Deschenes M. 1995. The axonal arborization of single thalamic reticular neurons in the somatosensory thalamus of the rat. Eur J Neurosci. 7:31–40.
Reichova I, Sherman SM. 2004. Somatosensory corticothalamic projections: distinguishing drivers from modulators. J Neurophysiol. 92:2185–2197.
Rojas-Piloni G, Guest M, Johnson A, Egger R, Narayanan R, Udvary D, Sakmann B, Oberlaender M. 2014. Cell type-specific subcortical targets of layer 5 projecting neurons in the rat vibrissal cortex. Washington (DC): Society for Neuroscience Meeting.
Seol M, Kuner T. 2015. Ionotropic glutamate receptor GluA4 and T-type calcium channel Cav 3.1 subunits control key aspects of synaptic transmission at the mouse L5B-POm giant synapse. Eur J Neurosci. 42:3033–3044.
Sobolewski A, Kublik E, Swiejkowski DA, Kaminski J, Wrobel A. 2015. Alertness opens the effective flow of sensory information through rat thalamic posterior nucleus. Eur J Neurosci. 41:1321–1331.
Sosnik R, Haidarliu S, Ahissar E. 2001. Temporal frequency of whisker movement. I. Representations in brain stem and thalamus. J Neurophysiol. 86:339–353.
Stroh A, Adelsberger H, Groh A, Ruhlmann C, Fischer S, Schierloh A, Deisseroth K, Konnerth A. 2013. Making waves: initiation and propagation of corticothalamic ca(2+) waves in vivo. Neuron. 77:1136–1150.
Trageser JC, Keller A. 2004. Reducing the uncertainty: gating of peripheral inputs by zona incerta. J Neurosci. 24:8911–8915.
Urbain N, Deschenes M. 2007. Motor cortex gates vibrissal responses in a thalamocortical projection pathway. Neuron. 56:714–725.
Urbain N, Salin PA, Libourel PA, Comte JC, Gentet LJ, Petersen CC. 2015. Whisking-related changes in neuronal firing and membrane potential dynamics in the somatosensory thalamus of awake mice. Cell Rep. 13:647–656.
Veinante P, Deschenes M. 1999. Single- and multi-whisker channels in the ascending projections from the principal trigeminal nucleus in the rat. J Neurosci. 19:5085–5095.
Veinante P, Jacquin MF, Deschenes M. 2000. Thalamic projections from the whisker-sensitive regions of the spinal trigeminal complex in the rat. J Comp Neurol. 420:233–243.
Veinante P, Lavallee P, Deschenes M. 2000. Corticothalamic projections from layer 5 of the vibrissal barrel cortex in the rat. J Comp Neurol. 424:197–204.
Wimmer VC, Nevian T, Kuner T. 2004. Targeted in vivo expression of proteins in the calyx of Held. Pflugers Arch. 449:319–333.
Wu JY, Xiaoying H, Chuan Z. 2008. Propagating waves of activity in the neocortex: what they are, what they do. Neuroscientist. 14:487–502.
Zhao S, Ting JT, Atallah HE, Qiu L, Tan J, Gloss B, Augustine GJ, Deisseroth K, Luo M, Graybiel AM, et al. 2011. Cell type-specific channelrhodopsin-2 transgenic mice for optogenetic dissection of neural circuitry function. Nat Methods. 8:745–752.

Manuscript No 3: Cortical Dependence of Whisker Responses in Posterior Medial Thalamus in vivo

Cortical Dependence of Whisker Responses in Posterior Medial Thalamus in vivo

Rebecca A. Mease*, **Anton Sumser***, Bert Sakmann, Alexander Groh

Supplemental Information

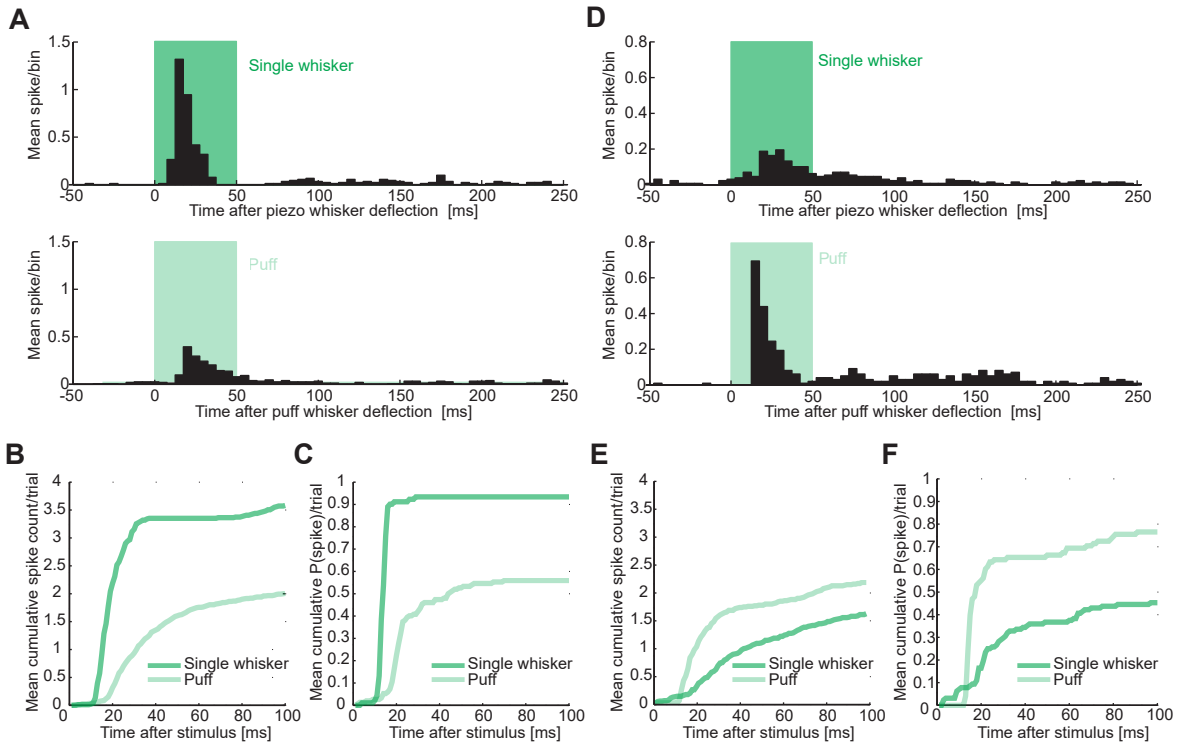

Supplementary Figure 1. L5B activation during different whisker stimulation protocols. 3/5 neurons showed greater spike output for piezo stimulation (example shown in A-C, whereas 2/5 showed greater spike output for puff stimulation (example shown in D-F), however, for these neurons, the slowly rising responses to piezo stimulation are consistent with stimulation of surround rather than principal whiskers.
(A,D) Example L5B spiking responses recorded in juxtacellular configuration, with spike responses to piezo deflection of single whiskers (upper, dark green), or puff deflection of multiple whiskers (lower, light green).
(B,E) Cumulative spike counts as a function of time post whisker stimulation.
(C,F) Cumulative response probability for the same neuron.

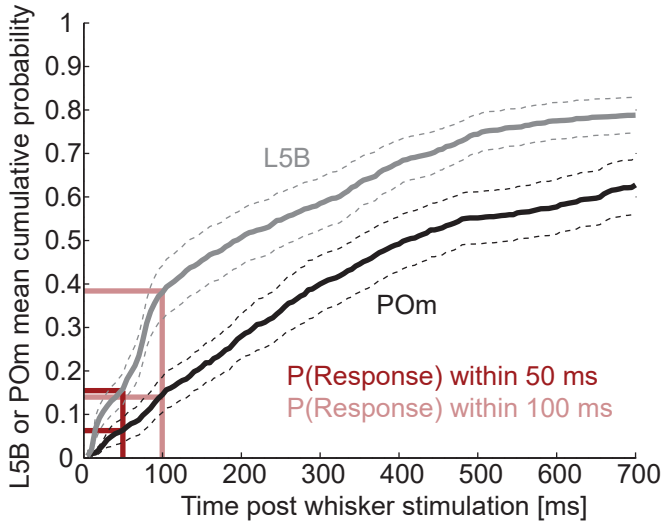

Supplementary Figure 2. Whisker responses in POm are sparser than those in L5B. Population cumulative histograms for juxtacellular recorded L5B (n=31) and POm (n=12). Responses within 50 ms and 100 ms shown in dark and light red, respectively.

Supplementary Table

Whisker response	Amplitude [mV]	Latency [ms]	Slope [mV/ms]
Early large (n=10)	6.3 7.7 9.3	16.1 17.8 20.2	2.3 3.0 6.3
Early small (n=8)	0.7 0.8 1.0	5.3 8.4 15.8	0.3 0.4 0.7
Late (n=12)	8.6 10.9 13.2	80.7 93.4 100.4	3.3 4.9 7.5

Supplemental Table 1: Three classes of fast whisker responses in POm, population whisker-evoked EPSP characteristics. Values shown are first quartile, median, and third quartile. All three categories were significantly different based on delay; small early had significantly smaller slope and amplitude than late large or early large ($p<0.05$, Wilcoxon rank sum). Reported values are based on an average ± SD of 69±48 trials per neuron, excluding failure trials.

Cell	Prob-ability IPSP	Prob-ability EPSP	Latency IPSP [ms]	Latency EPSP [ms]	Rise time IPSP [ms]	Rise time EPSP [ms]	Amplitude IPSP [mV]	Amplitude EPSP [mV]
1	0.15	0.73	17.5 ± 1.6	18.7 ± 1.7	21.4±8.5	2.0 ± 0.8	3.6 ± 1.7	9.4 ± 1.7
2 (Fig. 5)	0.68	0.31	17.5 ± 2.1	20.3 ± 2.9	16.9 ± 6.7	1.9± 0.8	1.5 ± 0.4	20.3 ± 0.7
3	0.24	0.76	15.7 ± 1.5	16.9 ± 1.5	9.3 ± 6.7	1.0 ± 0.2	4.7 ± 2.7	9.3 ± 1.5
4	0.08	0.91	5.9 ± 1.5	16.3 ± 1.7	21.3 ± 3.6	1.9 ± 1.2	1.5 ± 0.6	7.4 ± 1.3
N=4 Mean + SD	0.29 ± 0.27	0.68 ± 0.26	**14.2 ± 5.6**	**18.0 ± 0.5**	**17.2 ± 5.7**	**1.7 ± 0.5**	**2.8 ± 1.6**	**11.6 ± 5.9**

Supplemental Table 2: Quantification of PSP characteristics for the four POm intracellular recordings with whisker-evoked IPSPs (example shown in Fig. 5, main text). Values are mean ± standard deviation. Probability of EPSPs and IPSPs was measured during 50 ms after whisker deflection, as the number of successful trials with an observed PSP divided by the number of total trials.

Discussion

The posterior group nuclei and POm lateral in particular are in a central hub position of whisker processing. Its function however is unclear and contradictory theories are abundant. While PO receive input from many sources in brainstem, midbrain and cortex, we show in the presented manuscripts that the major input (at least to POm lateral) originates from barrel cortex L5B neurons over giant boutons [Manuscript (MS) 1], both during spontaneous slow oscillations [MS2] and whisker stimulation [MS3]. Cortical drive of higher-order thalamic nuclei is a common pattern in many sensory systems, therefore the obtained results may be applicable to other modalities (Sherman 2016). We also demonstrate that L5B neurons target 4 separate regions in PO with specific projection parameters, supporting the division of PO into functionally different nuclei [MS1]. Sparse and powerful synapses drive POm lateral neurons, however the transmission strength is under strong dynamic control due to paired pulse depression (adaptation) [MS2]. We show that L5B neurons have only few (~40 [MS1]) synapses in a somatotopic map organization in POm lateral [MS1]. This sparse and mapped innervation leads to an estimate of only 1-3 [MS2] functional L5B neurons contacting an individual L5B neuron making the pathway very parallelized, with low divergence. Consequently, POm lateral neurons would broadcast a low-pass filtered signal from a few L5B neurons back to BC and to many other areas.

Structure of PO relating to corticothalamic projections

The posterior group nuclei span a large area in the mouse brain (approximately 1x1x1 mm) and it is unclear if it is one large nucleus, or if it actually comprises multiple distinct nuclei. The most straightforward definition of a nucleus would be that it is, first, structurally homogenous and, second, its neurons have identical input and output regions. In MS1, using anterograde tract tracing and full reconstructions of thalamic bouton locations, we show that L5B projections in dorsal thalamus have four separate foci: an anterior, medial, lateral and posterior region, together forming a ring in the horizontal plane. Histological markers (Nissl and Cytochrome C Oxidase) suggest that at least three of these areas belong to PO, therefore we call them POa, POm medial, POm lateral. However, some authors suggest that the anterior region is actually the ventral lateral nucleus, which is associated with motor functions and basal ganglia (Zakiewicz et al. 2014, 2015). The medial region is sometimes referred to as angular nucleus (Bourassa et al. 1995; Lévesque et al. 1996; Deschênes et al. 1998; Zliang and Deschênes 1998), however to my knowledge no functional studies have been published in this area. The lateral area of PO, next to the border to VPM is the best studied and is commonly referred to as POm. Here cortical input dominates thalamic activity [MS2,3; (Groh et al. 2008)]. As sometimes the whole PO area is termed POm, it is not always clear if different laboratories

targeted the same lateral region. If the posterior area still belongs to PO or constitutes a separate posterior triangular nucleus (PoT,(Franklin and Paxinos 2008)) is inconclusive. We decided to retain the published nomenclature, calling the posterior region getting L5B afferents PoT.

Each area has specific projection input parameters. POm lateral for example receives twice as many boutons as the other three PO areas respectively [MS1]. In contrast, bouton clouds in PoT are spread over larger volumes than POm medial, lateral and POa. Consequently, bouton density is highest in POm lateral, low in PoT and POm medial and POa range in between. Interestingly, even though dual injections always were non-overlapping, bouton clouds in PO did overlap to different degrees. Both POm medial and POm lateral have low target area overlap (<25%) from dual injections, while the overlap in POa and PoT was variable and on average higher (>40%). Considering that L5B neurons have wide receptive fields including multiple whiskers, column-specific somatotopic precision would be surprising. PoT has been associated with nociceptive processing (Gauriau 2004) and the detection of noxious stimuli conceptually does not need high spatial resolution, fitting to higher overlap in this area. Interestingly, concerning whisker map organization, the four areas together generate a complete picture with a particular organization: The projections from columns in the same row were stacked on top of each other in all areas, with arc 1 on top of arc 2. Projections from columns in the same arc, however were oriented inwards, so row A projections were lateral of row B in POm lateral and opposite in POm medial.

I reviewed literature to check if the different areas receive different inputs or project to different areas and thereby constitute different nuclei according to the nucleus definition. Hereby it becomes evident that most areas targeting dorsal thalamus innervate only parts of the PO volume. However it is not always clear if that is a result of only partial labeling of the afferents or indeed (sub) nucleus specific innervation. BC L6 projects mostly to POm lateral (Bourassa et al. 1995; Zliang and Deschênes 1998), which is also visible in MS1. All four PO regions project to BC in approximately equal measures, PoT however less strongly (Fabri and Burton 1991; Gauriau 2004). Reciprocal connectivity to motor cortex seems to be established mostly with POm medial and lateral and less with POa and PoT (Cicirata et al. 1986; Urbain and Deschênes 2007b). S2 targets all of PO (Bokor et al. 2008) but seems to be slightly biased to posterior PoT (Lévesque et al. 1996), which is reported to only project to S2 and not BC (Gauriau 2004). PoT, POm medial and POm lateral project to the dorsolateral striatum (DLS), in contrast to POa (Smith et al. 2012). Axons from thalamic reticular nucleus (Rt) seem to be restricted to the POm lateral area (Lam and Sherman 2007). The zona incerta has been reported to innervate the majority of PO, however with bouton densities lowest in PoT and highest in POm lateral (Barthó et al. 2002). The anterior pretectum inhibits mostly anterior and lateral PO (Bokor et al. 2005). Brainstem SpVi afferents are only present in a third of PO, however the pattern

does not colocalize with the areas reported here (Groh et al. 2014). SpVo afferents however are exclusively found in PoT. Multi-whisker responsive cells in PrV project mostly to POm lateral (Veinante and Deschênes 1999).

Connectivity in respect to PO subnuclei	POa	POm lateral	POm medial	PoT
Barrel Cortex L5B afferents	+	+++	++	+
Barrel Cortex L6 afferents	+	+++	+/-	+
Barrel Cortex efferents	++	+++	+++	+
Motor Cortex reciprocal	+/-	++	++	+/-
Secondary Somatosensory Cortex reciprocal	+	++	++	+++
Dorsolateral Striatum efferents	-	++	++	++
Thalamic Reticular Nucleus afferents	-	+++	-	-
Zona Incerta afferents	++	+++	++	+
Anterior Pretectum afferents	++	+++	+/-	+/-
Trigeminal PrV afferents	+	++	+	-
Trigeminal SpVo afferents	-	-	-	+
Trigeminal SpVi afferents	++	++	++	++

Table 1: Estimated connection strengths to the four areas in PO, synthesized from published literature and MS1

The number of (+) symbols indicates estimated connection strengths between putative subnuclei; (+/-) indicates inconclusive results; (-) shows lack of connection.

Next to overall connectivity, PO regions can also be different in finer details of axonal morphologies. Thalamocortical projection neurons can be classified into two not sharply segregated types: one mostly projecting to a single cortical area with focal axon arborizations in mainly L5A; The other projecting to two or more cortical areas, with more widespread axonal arbors, predominantly in L1 (Clascá et al. 2012). Using these criteria, one review summarizes that focally projecting type neurons are located in the lateral PO and multi-area projecting type neurons in medial PO (Clascá et al. 2012). Another study reports a division in the anterior-posterior direction, showing focal projecting neurons predominantly in a region comprising POa ad POm lateral and medial, multi-area projection neurons however predominantly in posterior PO (Ohno et al. 2012). Table 1 illustrates estimated connectivity differences between the regions in PO. In summary, only a few connections discriminate sharply between putative subnuclei, but most are biased to parts of PO. PoT stands out, having the most

differing projection patterns compared to the others. Consequently, it can be hypothesized that the different input-output organizations lead to functional differences. Functional studies so far concentrated on POm lateral. Therefore it is currently unknown if the other areas show deviating functional characteristics. Consequently, when discussing PO physiology I will retain established nomenclature and refer to just POm, even so most laboratories apparently target their recordings to POm lateral.

Properties and importance of L5B corticothalamic projections to POm in vivo

Most cortical neurons innervate their postsynaptic partners by numerous but individually small and weak synapses (Sherman 2016). Subcortical projections from L5B in primary sensory cortices are unique in that they instead contact their target neurons with sparse, huge and strong synapses, best understood in the BC L5B to POm (lateral) innervation (Hoogland et al. 1991; Bourassa et al. 1995; Groh et al. 2008). The huge size of these synaptic boutons (Hoogland et al. 1991) allowed for electrical stimulation of individual boutons and measuring their physiological impact on POm neurons in vitro (Groh et al. 2008). There it became evident, that although a single synapse in principle can elicit postsynaptic action potentials on its own, it is also strongly adapting and would be mostly depressed during typical firing rates of L5B neurons under anesthesia (Groh et al. 2008). It was therefore unclear, if the strength of the L5B to POm synapse is diminished in vivo. We approached this by using dual juxtasomal recordings in BC L5B and POm as well as whole-cell intracellular recordings in POm during spontaneous slow oscillatory activity of anesthetized mice [MS2]. We observed that L5B neurons fired throughout phases of elevated cortical activity (‘up states’), POm neurons in contrast spiked predominately at the transitions from down to up-state. Through whole-cell recordings it was possible to isolate individual EPSPs during such transitions, showing that EPSP amplitude decreased over the duration of up states, fitting to similar adaptation principles as reported in vitro. We show that barrel cortical activity is necessary for POm sub- and suprathreshold activity, evidenced by a near complete lack of major membrane voltage fluctuations during pharmacological or optogenetic inactivation of BC. Furthermore, by optogenetically stimulating L5B neurons in BC we demonstrate that L5B spiking monosynaptically causes giant EPSPs and spikes in POm and therefore are sufficient for driving POm in vivo. Necessity and sufficiency of functional L5B inputs to elicit responses in POm are strong arguments that L5B drives POm in anesthetized animals.

However, as expected from in vitro (Groh et al. 2008), the corticothalamic drive is under strong dynamic control. While L5B neurons can follow optogenetic stimulations up to 50 Hz, the transmission gain to POm diminishes strongly at rates over 5 Hz. The dynamic attenuation of the

spike transmission gain is likely caused by smaller EPSP amplitudes at short presynaptic inter-spike-intervals. Interestingly, a simple threshold model that uses L5B activity and the measured adaptation function of the L5B to POm synapse can reconstruct most of the up state triggered activation shape in POm. In summary, L5B neurons drive POm neurons in spontaneous slow oscillations following periods of relative inactivity in anesthetized animals in vivo. Through adaptation, transmission gain decreases during sustained cortical activity. Consequently POm neurons send a high pass filtered version of L5B activity, e.g. the onset of up states, to its respective targets. Other inputs to POm seem not to play a decisive role in this condition.

L5B corticothalamic innervation in sensory processing

So far it remained unclear, if similar principles hold during sensory stimulation. A part of PO receives direct innervation from SpVi in the brainstem (Erzurumlu et al. 1980; Veinante, Jacquin, et al. 2000; Groh et al. 2014) and therefore POm is considered to be part of the ascending paralemniscal pathway to cortex (Bosman et al. 2011). However, whisker deflection responses in POm have been demonstrated to be quite late (peak response latency approximately 25 ms) and unreliable (spike responses in less than 50% of stimulation trials) (Diamond, Armstrong-James, and Ebner 1992). The poor excitability of POm by whisker deflections can be partly explained by possible state dependent continuous inhibition or stimulus related feedforward inhibition via zona incerta or anterior pretectum (Trageser and Keller 2004; Bokor et al. 2005; Lavallée et al. 2005; Trageser et al. 2006; Urbain and Deschênes 2007a). However, already nearly 20 years ago, it has been demonstrated that POm whisker responses depend on a functional cortex (Diamond, Armstrong-James, Budway, et al. 1992) and activation of POm via cortex fits to the reported latencies. Furthermore, whisker stimulation, paired with optogenetic L5B activation has been shown to supralinearly boost POm responses (Groh et al. 2014).

We investigated the origin of whisker stimulus related POm (lateral) activation, by recording in a similar setup as before [MS2], but additionally applied whisker deflections by brief air puffs targeting 2-3 whisker rows [MS3]. We observed that out of the recorded population approximately two thirds of L5B neurons and one third of POm neurons responded to whisker stimulation with ‘early’ (<50 ms) spike responses. Responses in only a subset of neurons, following stimulation of a subset of whiskers fits to the model of somatotopic innervation in POm [MS1]. Whisker stimulation typically resulted in an evoked up state, consequently all recorded neurons in both L5B and POm showed (additional) gradual and late activation following the stimulus. We further demonstrated that optogenetic cortical inactivation all but abolishes spike responses to whisker stimulation in POm, further supporting a cortical origin of evoked responses. In confirmation that VPM, the primary whisker-related thalamic nucleus, is largely independent of cortex we show that VPM spike responses to

whisker stimulation are largely unaffected by optogenetic cortical inactivation. At the subthreshold level, a subset of approximately 1/3 of the recorded neurons responded with early and large EPSPs to whisker stimulation, nearly half of the neurons had only late large EPSPs. Interestingly, in a subset of neurons, whisker stimulation trials that did not succeed in evoking a large EPSP revealed small whisker evoked inhibitory potentials (IPSPs). However, we did not observe continuous barrages of IPSPs, that could gate POm responses as was suggested before (Lavallée et al. 2005). In a similar approach as in MS2, we investigated if the early large whisker evoked EPSPs have cortical origin. We, first, observed that whisker evoked early EPSP amplitude often interacted with spontaneously occurring previous EPSPs as well as with late EPSPs (presumably related to evoked up states). If whisker stimulation was preceded by a spontaneous EPSP, the evoked early EPSP amplitude was smaller than in cases of previous inactivity. In parallel whisker evoked late EPSPs were typically smaller than early EPSPs. The monotonous rule of adaptation suggests a common origin. Secondly, optogenetic cortical inactivation during whisker stimulation abolished any detectable EPSPs in neurons that normally respond with early EPSPs.

Together, these results strongly suggest that whisker evoked activity in POm (lateral) comes from L5B in cortex and not from trigeminal brainstem, at least in anesthesia. The whisker-evoked L5B innervation might be influenced by stimulus related feedforward inhibition. The dynamic properties of the L5B to POm synapse further suggest that whisker signal transmission to POm and onwards depends on cortical state. Already high cortical activity could for example reduce the transmission efficacy of whisker related signals to POm.

Corticothalamic divergence and convergence

Using the anatomical and physiological data presented here, we can make first estimates about corticothalamic convergence (i.e. how many L5B neurons innervate a single POm neuron) and divergence (i.e. how many POm neurons are innervated by a single L5B neuron) on a neuron and bouton basis. Such calculations are not directly possible by counting neurons in the respective areas, because PO/POm borders are not well defined and because it is dependent on axonal arborizations. But using the number of labeled L5B neurons, the number of boutons in the target area, as well as bouton cloud volume and soma density we can approximate corticothalamic convergence. We found that on average a single L5B neuron sends approximately 40 boutons into POm lateral [MS1], fitting to previous single neuron reconstructions (Veinante, Lavallee, et al. 2000) and equaling the theoretical maximum of POm lateral neurons a single L5B neuron could innervate on average. Dividing the bouton density by soma density results in the number of boutons an average target neuron has available, approximately 9 in POm lateral. Depending on the number of contacts between individual neurons, the average number of L5B neurons innervating a single POm lateral neuron can

be maximally 9. As a caveat, we did not label the whole barrel cortex and densities typically decreased towards the edges of the bouton clouds, therefore the real average of innervated POm lateral neurons is probably slightly larger. Taken together, the average number of contacted POm lateral neurons by a single L5B neuron should be larger than 4.4 (40 boutons per L5B divided by 9 per target). The exact values of these estimations depend on the number of contacts between individual neurons and the axonal spread of L5B neurons. We can however further approximate the convergence factor by using parameters inferred from physiological measures.

Remarkably, in nearly half of the recordings of MS2, EPSP amplitude was strongly correlated to inter-EPSP-interval (IEI, equivalent to the inter-spike-interval of all functional inputs). This can be the case if multiple inputs to the recorded neuron fire exactly synchronously (which is highly unlikely) or the recorded cells get only a single functional input with a simple adaptation rule during spontaneous up states. This result already suggested low functional convergence of the pathway. However, taking this a step further, we predicted the correlation of IEI and EPSP amplitude depending on the number of functional inputs. We used modeled EPSPs out of spike trains from up to 5 independent converging functional inputs. Spike trains for up to 2 functional inputs were measured from simultaneous recordings in L5B, 3-5 inputs were simulated by shuffling spike patterns. Matching the resulting predicted correlation values to measured correlations, we concluded that the median of functional L5B inputs in POm is between 2 and 3. Independently, by comparing average L5B spike rates and average POm EPSP rates, we arrived at a similar value of on average 2.5 L5B neurons innervating one POm neuron.

Taking anatomical and physiological results together, we can therefore conclude that on average 9 giant boutons from 2.5 L5B neurons innervate one POm lateral neuron. Consequently one L5B neuron contacts one POm lateral neuron with approximately 3.5 (9/2.5) boutons. Finally, an average L5B bouton sends 40 boutons to POm lateral. So if of those 40 boutons on average 3.5 contact one POm neuron, a L5B neuron on average innervates 11 POm lateral neurons. Even though the multiplicative error margins in these calculations are large and a certain variance in the projection is to be expected, this is the first estimate of corticothalamic divergence and convergence to my knowledge and serves as a starting point for more precise analyses.

Corticothalamic interactions with inhibitory nuclei

Next to PO, barrel cortex L5B neurons also contact inhibitory nuclei in ventral thalamus (zona incerta) and anterior midbrain (anterior pretectum). As evidenced in MS1, both nuclei receive substantial L5B innervation that varied across experiments. While APT is innervated by dense and compact bouton clouds, ZI innervation from L5B is broader and less dense. Due to lower density of somata in ZI

however, both nuclei have similar numbers of L5B boutons available per neuron (5-9). Somatotopic precision of the projections is low in ZI (~60% overlap) and higher in APT (~35%).

The zona incerta is connected to nearly all regions in the brain (Mitrofanis 2005). Its functions are uncertain, true to its name, and have been associated with visceral activity, arousal, attention, posture and locomotion. Notably ZI predominantly targets higher-order thalamic nuclei like POm, and the visual pulvinar (Mitrofanis 2005). It has been implied that ventral ZI tonically inhibits POm, evidenced by high frequency IPSPs and enhanced responses in POm during ZI lesions (Lavallée et al. 2005). This inhibitory blockade of POm activity might also be relieved (gated) during motor cortex or cholinergic input to locally inhibiting ZI neurons, thereby disinhibiting POm (Trageser and Keller 2004; Trageser et al. 2006; Barthó et al. 2007; Urbain and Deschênes 2007a). If barrel cortex L5B input has a net elevating or suppressing effect on ZI inhibitory output is as of yet unresolved. However we find L5B boutons predominantly in dorsal ZI [MS1] while POm projecting ZI neurons are located in ventral ZI (Barthó et al. 2002), speaking against a directly inhibiting effect of barrel cortex L5B on POm [MS1]. If barrel cortex L5B is involved in the proposed state dependent gating process, somatotopic precision is probably not important, fitting to L5B innervation that is relatively map unspecific.

Similar to ZI, APT also innervates higher-order thalamic nuclei, i.e. POm, but not primary nuclei (Bokor et al. 2005). Additionally APT innervates ZI neurons, in particular those neurons in turn innervating POm (Giber et al. 2008). However ZI projections and POm projections do not come from the same neurons but reflect two different APT populations, one with an inhibitory effect on POm, the other disinhibitory (Giber et al. 2008). Through intense local connectivity between these neuronal cell types differential inputs to those cell types can regulate the net effect on POm. Lesioning APT however elevates POm rates. Stimulating APT has anti-nociceptive (pain relief) effects and lesioning APT increases pain related behavior (Rees and Roberts 1993). It was therefore concluded that POm activity correlates with noxious signals (Murray et al. 2010; Whitt et al. 2013), a result awaiting causal evidence. From our dataset we cannot conclude if L5B neurons target specific subpopulations of APT neurons. The relatively precise map organization of the cortical projections however speaks for a spatially specific function of APT [MS1].

In summary, BC L5B innervates ZI and APT, both GABAergic nuclei that inhibit POm. Nevertheless, the net effect of cortical innervation of those nuclei on POm is unclear. Through local connectivity, functionally different cell types and connections between APT and ZI, cortex can have either a disinhibitory or inhibitory effect. However, in the experiments for MS2 and MS3 we could not reproduce the previous finding that POm receives continuous “riddles” of IPSPs (Lavallée et al. 2005). However we did detect small yet robust whisker evoked IPSPs in a subset of recordings [MS3]. In additional unpublished experiments, using small positive current injections in whole cell POm

recordings I demonstrated reliable whisker deflection evoked IPSPs but spontaneously occurring IPSP frequencies below 0.2 Hz. Consequently, the POm population targeted in our experiments did receive whisker deflection triggered feed-forward inhibition but not substantial continuous inhibition. Recently published recordings of ZIv activity in head-fixed rats demonstrated no significant modulation during whisking behavior, but very precise responses to whisker air puffs (Moore et al. 2015), indicating a more specific feedforward inhibitory function of the ZI to POm projection.

POm as a transthalamic relay

In the manuscripts of this thesis I present that the corticothalamic driver pathway to POm is topographic [MS1], the near exclusive input to POm during spontaneous [MS2] and sensory stimulated situations [MS3] under anesthesia and dynamically regulated [MS2]. What do these findings mean for the function of POm?

We find giant synapses, large EPSPs, driving capability and paired-pulse depression in the BC L5B to POm projections, which perfectly matches characteristics of transthalamic driver pathways described by the Sherman group (Sherman 2016). The basic idea is that while primary thalamic nuclei relay information from the periphery to primary sensory cortex, higher-order thalamic nuclei relay information from primary sensory cortical areas to higher sensory cortical areas (Theyel et al. 2010). The transthalamic driver pathway would then additionally be supplemented by weaker modulatory direct connections between the cortical areas (Chen et al. 2013). It was expected that the transthalamic signal is influenced by other inputs into POm, especially since S2 and SpVi input to POm also has driver properties (Liao and Yen 2008; Liao et al. 2010; Groh et al. 2014). However, in our recording conditions sub- and suprathreshold activity in POm was nearly completely absent during cortical inactivation [MS2, 3], suggesting that the recorded population of neurons had no other functional inputs. In light of the high interconnectivity of BC and POm over a few synapses (Bosman et al. 2011) it cannot be ruled out that cortical inactivation had effects on other POm input structures. We deem it unlikely however, that other putative POm input areas are completely contingent on cortical activity, in that no trace of their input remains during cortical inactivation. Therefore we can assume that in anesthesia BC L5B comprises the only relevant input to POm. Consequently POm neurons transmit a filtered L5B signal to their respective targets.

We find that corticothalamic spike transmission is under dynamic control [MS2, (Groh et al. 2008)], in that transmission efficacy starts to drop above 3 Hz and dramatically so between 5 and 10 Hz stimulation frequency. In parallel, repetitive whisker stimulation up to 10 Hz results in decreasing POm responses (Ahissar et al. 2000; Masri et al. 2008b). Spontaneous activity has been reported to be high in L5B neurons, up to 6 Hz in anesthesia (de Kock et al. 2007) and 3-10 Hz during wakefulness

(de Kock and Sakmann 2009). From average rates we cannot deduce however that the synapse is in a constantly depressed state, because L5B firing is strongly patterned: In anaesthetized animals, during down states L5B neurons do not fire at all for seconds and awake animals undergo state changes from idle, to engaged and behaving, which are paralleled by profound changes in spontaneous activity (Poulet et al. 2012). Consequently, small changes in the physiological range of L5B rates result in large changes of spike transmission efficacy. As a result POm spiking is biased to the start of cortical activity after longer pauses, i.e. at the beginning of up states [MS2], acting as a high-pass filter for cortical activity. Additionally, sensory signal transmission is affected by cortical state, evidenced by smaller whisker evoked EPSPs following spontaneous activity [MS3]. Another level of complexity is added when we consider the regular occurrence of L5B high-frequency action potential bursts (Chagnacamital et al. 1990). Bursts can be transmitted to POm even over the depressed synapse, bypassing the adaptation rule [MS2]. As of yet it is unclear, however, if L5B bursts occur during specific sensory situations.

We found that the BC L5B projection is somatotopic [MS1]. Topographic projections are well established in L6 modulatory corticothalamic projections, but less clear in driver pathways (Sherman 2016). Together with low signal convergence (2-3 L5B neurons give input to one POm neuron [MS2]), it follows that POm transmits a possibly column specific L5B signal. A certain degree of overlap in the corticothalamic projections mirrors the relatively wide receptive fields of L5B neurons (de Kock et al. 2007; Ramirez et al. 2014). However, it should be considered that receptive field measurements in spontaneously active neurons are problematic and that the response magnitude is highest for the principle whisker, diminishing rapidly for surrounding whiskers. Interestingly, L5B dendrites and cortical axons are restricted to the home barrel column (Oberlaender et al. 2011), the multi-whisker innervation presumably results from a population of horizontally projecting L6 neurons (Narayanan et al. 2015). The wide receptive fields of L5B and POm neurons, together with the pronounced synaptic depression opens the possibility for interactions between signals from different whiskers. In a situation, where two whiskers in the receptive field of a L5B neuron are deflected consecutively, the first deflection would deplete the synapse, attenuating the response to the second deflection of the other whisker. Additionally, horizontal L6 projections and L5B receptive fields are often asymmetric to one side (de Kock et al. 2007; Narayanan et al. 2015). Consequently, stimulation strokes over multiple whiskers could elicit different responses, depending on the direction of the apparent (global) stimulation direction and thereby the order of subsequently deflected whiskers. In consequence, POm neuronal responses could be depending on the shape of the touched object. The concept of global motion direction selectivity has been indicated to be a factor in VPM responses (Ego-Stengel et al. 2012), but might be more pronounced in POm.

A spike in POm has ambiguous meanings: It can, first, indicate a change of cortical state from low to high activity. Secondly, it can be a response to deflections of a number of whiskers. And finally it could also indicate L5B burst spiking. POm neurons are active spontaneously (up to 1 Hz during up states in anesthesia [MS2]; up to 20 Hz in awake animals (Moore et al. 2015; Urbain et al. 2015)); it is therefore likely that POm employs a rate or spike timing code, rather than an all-or-nothing signal. A POm spike rate increase predominately indicates a change in cortical activity either of sensory or non-sensory origin. It has been suggested that large portions of brain activity reflect internal states and is only modulated by sensory input (Llinas and Pare 1991). Barrel cortex to POm signaling fits into this picture.

POm function in sensorimotor signaling

One of the most heatedly debated putative functions of POm is its role in whisker motion coding (Ahissar et al. 2000, 2008; Yu et al. 2006; Masri et al. 2008a, 2008b; Moore et al. 2015). For reliable discrimination of object location, it is crucial for the animal to know the position of its moveable whiskers at the moment of a touch. Whisker movement muscles, however, lack substantial innervation from proprioceptive sensors (Moore et al. 2015), but barrel cortical neurons are modulated by whisking phase (Curtis and Kleinfeld 2009). Consequently, the information of whisker position is probably transmitted through channels containing mixed re-afferent (i.e. sensory signals resulting from whisker bending by movement inertia) and ex-afferent (i.e. signals caused by whisker contacts) signals. To separate these signals, the brain could either employ selective filters on the signal structure or efference copy signals (also corollary discharge, i.e. an internal copy of motor commands to sensory centers (Poulet and Hedwig 2007)).

Anatomically, POm is at a junction of sensory and motor signals, as it is next to its sensory affiliation connected to motor cortex and striatum and was therefore hypothesized to play a role in whisker motion coding. It has been repeatedly shown that POm neurons reliably encode whisker position during “artificial whisking” (Ahissar et al. 2000; Yu et al. 2006). Hereby, the lightly anesthetized animal exhibits whisker movements caused by electric rhythmic stimulations of the facial nerve and that resemble voluntary whisking. POm activity during artificial whisking in air and artificial whisking against an object is indiscernible, supporting the motion coding concept (Yu et al. 2006). However, in awake head-fixed animals, POm activity correlates poorly to whisker motion parameters, in contrast to a subset of VPM neurons that are significantly modulated both during whisking in air (“re-afference”) and active touch (“ex-afference”) (Masri et al. 2008b; Moore et al. 2015; Urbain et al. 2015). In preliminary recordings in awake head-fixed mice I could confirm the same finding (not shown). Two possible explanations could reconcile these seemingly contradicting results: First, the group of Ehud Ahissar consistently might record in a different subnucleus of PO [MS1] than the other

groups. Demonstrated anatomical reconstructions of recording locations however show lateral positions in PO (Yu et al. 2006), similar to other published data. The second, more likely possibility is that during voluntary whisker movements, motion signals are subtracted from afferent signals using a central mechanism. As artificial whisking are naturally not paired to putative efference copy signals, the subtrahend is lacking and the resulting signals include re-afferent signals. The subtraction of efference copy from mixed re- and ex-afferent signals could happen in barrel cortex. The major cortical input from L5B to POm [MS1-3] would then contain only ex-afferent signals, separated from re-afferent self-motion signals. If that is the case, L5B activity should not be locked to whisker motion. Publications on firing patterns of identified L5B neurons during awake whisking behavior are surprisingly scarce; one study however reports weak modulation (de Kock and Sakmann 2009). Alternatively, efference copy subtraction could happen in POm itself. POm excitatory input then would be mixed ex- and re-afference signals, while inhibitory input would be the negative efference copy, canceling re-afferent signals out. Inhibitory input to POm comes from the reticular nucleus, zona incerta and anterior pretectum (Crabtree et al. 1998; Bokor et al. 2005; Urbain and Deschênes 2007a). The reticular nucleus however is not associated with motor centers, inhibits VPM in parallel and is therefore an unlikely candidate (Guillery et al. 1998). This leaves ZI and APT, both receiving input from motor and premotor areas as well as the somatosensory brainstem SpVi nucleus (Bosman et al. 2011). Recently it has been shown however, that ZI neuron spiking does not lock to whisker motion, but instead precisely respond to air puff whisker deflections (ex-afferent signals) in awake rats (Moore et al. 2015). ZI hosts a very diverse population of neurons and is not clear if the recorded neurons project to POm. APT physiology in awake animals has not been reported to my knowledge. Independent of the origin of inhibition, efference copy correction in POm is only possible if POm receives whisking phase-locked IPSPs. Conceptually, the combination of inhibition, large driver input and T-type Ca channels could generate a very sensitive error detection mechanism: while exactly coincident inhibitory and excitatory inputs would nullify each other, if the IPSP arrives slightly earlier than the large EPSP, hyperpolarization could de-inactivate T-type Ca channels. The large EPSP then could trigger a low-threshold Ca spike and actually boost POm output.

In our recordings in anaesthesia, we could not detect residual synaptic inputs in POm neurons of neither excitatory nor inhibitory nature during cortex inactivation [MS2, 3], or spontaneously occurring IPSPs during current injection (not shown). The phase locked efference copy inhibition however is expected to be silent during anesthesia. In preliminary whole-cell recordings in POm of awake head-fixed mice we see a massive increase in EPSP input and firing rate during whisking in air (Figure 8A). Magnifying membrane voltage during whisking (Figure 8B) makes the variable size of EPSPs visible (up to ~12 mV). Furthermore putative IPSPs are visible. EPSPs, IPSPs and spikes are not evidently phase-locked to whisker movements however. Interestingly, cortex inactivation almost

completely abolishes inputs and action potentials, indicating that also in awake animals, inputs to POm are dependent on cortex. These preliminary results await quantification and repetition.

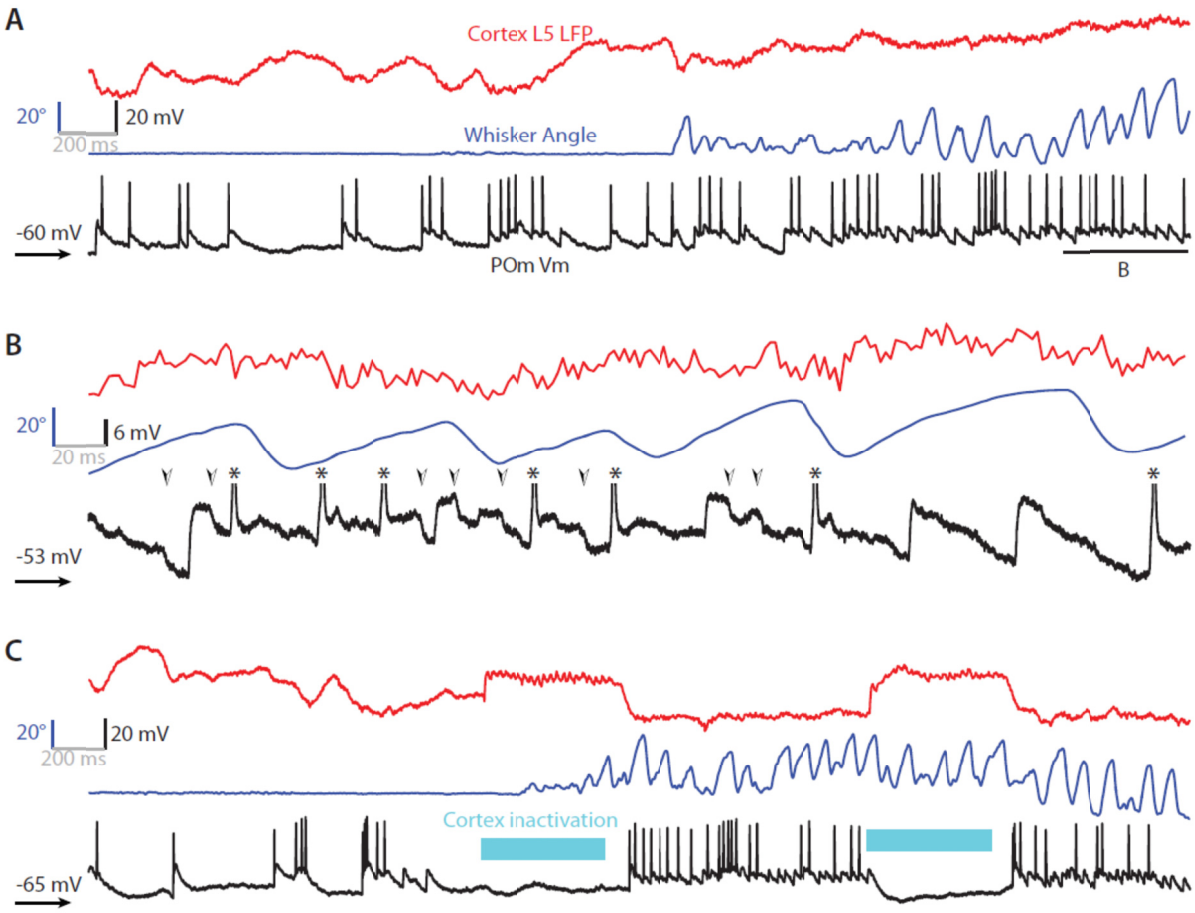

Figure 8: POm membrane voltage in head-fixed awake behaving mice

A: Cortical local field potential (LFP, red, top), whisker angle (blue, middle) and POm membrane voltage (black, bottom) during spontaneously occurring whisking behavior. Note a massive increase of EPSP and spike rates during whisking and LFP state change. EPSP amplitude in contrast diminishes. Resting membrane potential at -60 mV. B: Magnification of the area shown in A. Same conventions, action potentials clipped and indicated with asterisks (*). Putative IPSPs visible (arrowheads). C: Same neuron and conventions as in A, but with optogenetic inactivation of barrel cortex. Note that inputs and output appear completely silent during cortex inactivation.

Conclusions and outlook

The functions of higher order thalamic nuclei are a controversial subject, resulting from their extensive connectivity and ambiguous response patterns. In the manuscripts of this thesis we were able to directly confirm that the somatosensory higher-order thalamus, POm, is probably subdivided into four different areas. We further show topographic corticothalamic projections from barrel cortex layer 5 neurons and narrow convergence and divergence, demonstrating a high degree of parallelization, especially, because thalamic relay neurons are not interconnected (Sherman 2016). In anesthetized animals, cortical input dominates signaling below and above threshold. Signal transmission however is under tight dynamic control introducing interesting functional hypotheses. From this point onwards, a number of feasible follow-up projects could further advance our understanding of this mysterious nucleus: Systematic functional studies of responses in the different subnuclei of POm to sensory and cortical signals could clarify if the structural differences have functional correlates. As these nuclei are all located in the same horizontal plane, even simultaneous recordings, using multi-electrode array electrophysiology or Ca imaging with endoscopic lenses should be possible. Secondly, corticothalamic signal convergence could be quantified in more detail using transynaptic tracer techniques, e.g. employing modified pseudorabies (Callaway 2008). Due to the receptive field structure of L5B neurons and the dynamic properties of the L5B to POm synapse, responses to serial deflections of multiple whiskers in specific directions might be enhanced by POm neurons. Construction of a whisker stimulator to that effect and recording in POm is an obvious next step. Due to connectivity to motor control areas and interesting theories on efference copy processing in POm, a conclusive picture of POm functions will only emerge when based on recordings in awake behaving animals. There, it should be reevaluated if cortical dominance is still the rule or if other inputs come into play. Additionally, using intracellular recordings we could confirm or rule out efference copy processing, by testing the existence or absence of whisker motion locked inputs.

References

Ahissar E, Golomb D, Haidarliu S, Sosnik R, Yu C. 2008. Latency Coding in POm: Importance of Parametric Regimes. J Neurophysiol. 100:1152–1154.

Ahissar E, Sosnik R, Haidarliu S. 2000. Transformation from temporal to rate coding in a somatosensory thalamocortical pathway. Nature. 406:302–306.

Alitto HJ, Usrey WM. 2003. Corticothalamic feedback and sensory processing. Curr Opin Neurobiol. 13:440–445.

Alloway KD, Hoffer ZS, Hoover JE. 2003. Quantitative comparisons of corticothalamic topography within the ventrobasal complex and the posterior nucleus of the rodent thalamus. Brain Res. 968:54–68.

Alloway KD, Olson ML, Smith JB. 2008. Contralateral corticothalamic projections from MI whisker cortex: Potential route for modulating hemispheric interactions. J Comp Neurol. 510:100–116.

Alloway KD, Smith JB, Watson GDR. 2014. Thalamostriatal projections from the medial posterior and parafascicular nuclei have distinct topographic and physiologic properties. J Neurophysiol. 111:36–50.

Arabzadeh E, Zorzin E, Diamond ME. 2005. Neuronal encoding of texture in the whisker sensory pathway. PLoS Biol. 3.

Aronoff R, Matyas F, Mateo C, Ciron C, Schneider B, Petersen CCH. 2010. Long-range connectivity of mouse primary somatosensory barrel cortex. Eur J Neurosci. 31:2221–2233.

Azevedo FAC, Carvalho LRB, Grinberg LT, Farfel JM, Ferretti REL, Leite REP, Filho WJ, Lent R, Herculano-Houzel S. 2009. Equal numbers of neuronal and nonneuronal cells make the human brain an isometrically scaled-up primate brain. J Comp Neurol. 513:532–541.

Barthó P, Freund TF, Acsády L. 2002. Selective GABAergic innervation of thalamic nuclei from zona incerta. Eur J Neurosci. 16:999–1014.

Barthó P, Slézia A, Varga V, Bokor H, Pinault D, Buzsáki G, Acsády L. 2007. Cortical control of zona incerta. J Neurosci. 27:1670–1681.

Bertram EH. 2010. Exploring the Thalamus and Its Role in Cortical Function, 2nd Edition. J Neuro-Ophthalmology.

Bokor H, Acsády L, Deschênes M. 2008. Vibrissal Responses of Thalamic Cells That Project to the Septal Columns of the Barrel Cortex and to the Second Somatosensory Area. J Neurosci. 28:5169–5177.

Bokor H, Frère SG a, Eyre MD, Slézia A, Ulbert I, Lüthi A, Acsády L. 2005. Selective GABAergic control of higher-order thalamic relays. Neuron. 45:929–940.

Bosman LWJ, Houweling AR, Owens CB, Tanke N, Shevchouk OT, Rahmati N, Teunissen WHT, Ju C, Gong W, Koekkoek SKE, De Zeeuw CI. 2011. Anatomical Pathways Involved in Generating and Sensing Rhythmic Whisker Movements. Front Integr Neurosci. 5:53.

Bourassa J, Pinault D, Deschênes M. 1995. Corticothalamic projections from the cortical barrel field to the somatosensory thalamus in rats: A single-fibre study using biocytin as an anterograde tracer. Eur J Neurosci. 7:19–30.

Brand A, Behrend O, Marquardt T, McAlpine D, Grothe B. 2002. Precise inhibition is essential for microsecond interaural time difference coding. Nature. 417:543–547.

Brecht M, Naumann R, Anjum F, Wolfe J, Munz M, Mende C, Roth-Alpermann C. 2011. The neurobiology of Etruscan shrew active touch. Philos Trans R Soc B Biol Sci. 366:3026–3036.

Brecht M, Preilowski B, Merzenich MM. 1997. Functional architecture of the mystacial vibrissae. Behav Brain Res. 84:81–97.

Brecht M, Sakmann B. 2002. Dynamic representation of whisker deflection by synaptic potentials in spiny stellate and pyramidal cells in the barrels and septa of layer 4 rat somatosensory cortex. J Physiol. 543:49–70.

Cadusseau J, Roger M. 1991. Cortical and subcortical connections of the pars compacta of the anterior pretectal nucleus in the rat. Neurosci Res. 12:83–100.

Callaway EM. 2008. Transneuronal circuit tracing with neurotropic viruses. Curr Opin Neurobiol. 18:617–623.

Carvell GE, Simons DJ. 1987. Thalamic and corticocortical connections of the second somatic sensory area of the mouse. J Comp Neurol. 265:409–427.

Carvell GE, Simons DJ. 1990. Biometric analyses of vibrissal tactile discrimination in the rat. J Neurosci. 10:2638–2648.

Castro-Alamancos M a. 2002. Different temporal processing of sensory inputs in the rat thalamus during quiescent and information processing states in vivo. J Physiol. 539:567–578.

Cauller L. 1995. Layer I of primary sensory neocortex: where top-down converges upon bottom-up. Behav Brain

Res. 71:163–170.
Chagnacamital Y, Luhmann HJ, Prince D a. 1990. Burst Generating and Regular Spiking Layer-5 Pyramidal Neurons of Rat Neocortex Have Different Morphological Features. J Comp Neurol. 296:598–613.
Chen JL, Carta S, Soldado-Magraner J, Schneider BL, Helmchen F. 2013. Behaviour-dependent recruitment of long-range projection neurons in somatosensory cortex. Nature. 499:336–340.
Chmielowska J, Carvell GE, Simons DJ. 1989. Spatial organization of thalamocortical and corticothalamic projection systems in the rat SmI barrel cortex. J Comp Neurol. 285:325–338.
Cicirata F, Angaut P, Cioni M, Serapide MF, Papale a. 1986. Functional organization of thalamic projections to the motor cortex. An anatomical and electrophysiological study in the rat. Neuroscience. 19:81–99.
Clascá F, Rubio-Garrido P, Jabaudon D. 2012. Unveiling the diversity of thalamocortical neuron subtypes. Eur J Neurosci. 35:1524–1532.
Cohen JD, Castro-alamancos MA. 2010. Behavioral state dependency of neural activity and sensory (whisker) responses in superior colliculus. J Neurophysiol. 104:1661–1672.
Constantinople CM, Bruno RM. 2013. Deep Cortical Layers Are Activated Directly by Thalamus. Science (80-). 340:1591–1594.
Crabtree JW, Collingridge GL, Isaac JT. 1998. A new intrathalamic pathway linking modality-related nuclei in the dorsal thalamus. Nat Neurosci. 1:389–394.
Curtis JC, Kleinfeld D. 2009. Phase-to-rate transformations encode touch in cortical neurons of a scanning sensorimotor system. Nat Neurosci. 12:492–501.
de Kock CPJ, Bruno RM, Spors H, Sakmann B. 2007. Layer- and cell-type-specific suprathreshold stimulus representation in rat primary somatosensory cortex. J Physiol. 581:139–154.
de Kock CPJ, Sakmann B. 2009. Spiking in primary somatosensory cortex during natural whisking in awake head-restrained rats is cell-type specific. Proc Natl Acad Sci U S A. 106:16446–16450.
Deschênes M, Veinante P, Zhang ZW. 1998. The organization of corticothalamic projections: Reciprocity versus parity. Brain Res Rev. 28:286–308.
Desîlets-Roy B, Varga C, Lavallée P, Deschênes M. 2002. Substrate for cross-talk inhibition between thalamic barreloids. J Neurosci. 22:218–222.
Destexhe A, Neubig M, Ulrich D, Huguenard J. 1998. Dendritic low-threshold calcium currents in thalamic relay cells. J Neurosci. 18:3574–3588.
Diamond ME. 1995. Somatosensory Thalamus of the Rat. In: Cerebral Cortex, Vol. 11. Springer US. p. 189–219.
Diamond ME, Armstrong-James M, Budway MJ, Ebner FF. 1992. Somatic sensory responses in the rostral sector of the posterior group (POm) and in the ventral posterior medial nucleus (VPM) of the rat thalamus: dependence on the barrel field cortex. J Comp Neurol. 319:66–84.
Diamond ME, Armstrong-James M, Ebner FF. 1992. Somatic sensory responses in the rostral sector of the posterior group (POm) and in the ventral posterior medial nucleus (VPM) of the rat thalamus. J Comp Neurol. 318:462–476.
Diamond ME, von Heimendahl M, Knutsen PM, Kleinfeld D, Ahissar E. 2008. “Where” and “what” in the whisker sensorimotor system. Nat Rev Neurosci. 9:601–612.
Ego-Stengel V, Cam J Le, Shulz DE. 2012. Coding of apparent motion in the thalamic nucleus of the rat vibrissal somatosensory system. J Neurosci. 32.
Erişir A, Van Horn SC, Sherman SM. 1997. Relative numbers of cortical and brainstem inputs to the lateral geniculate nucleus. Proc Natl Acad Sci U S A. 94:1517–1520.
Erzurumlu RS, Bates CA, Killackey HP. 1980. Differential organization of thalamic projection cells in the brain stem trigeminal complex of the rat. Brain Res. 198:427–433.
Fabri M, Burton H. 1991. Topography of connections between primary somatosensory cortex and posterior complex in rat: A multiple fluorescent tracer study. Brain Res. 538:351–357.
Fanselow EE, Sameshima K, Baccala LA, Nicolelis M. 2001. Thalamic bursting in rats during different awake behavioral states. Proc Natl Acad Sci. 98:15330–15335.
Feldmeyer D. 2012. Excitatory neuronal connectivity in the barrel cortex. Front Neuroanat. 6:1–22.
Foster GA, Sizer AR, Rees H, Roberts MHT. 1989. Afferent projections to the rostral anterior pretectal nucleus of the rat: a possible role in the processing of noxious stimuli. Neuroscience. 29:685–694.
Franklin KBJ, Paxinos G. 2008. Paxinos and Franklin’s The mouse brain in stereotaxic coordinates.
Furuta T, Timofeeva E, Nakamura K, Okamoto-Furuta K, Togo M, Kaneko T, Deschênes M. 2008. Inhibitory Gating of Vibrissal Inputs in the Brainstem. J Neurosci. 28:1789–1797.
Gambino F, Pagès S, Kehayas V, Baptista D, Tatti R, Carleton A, Holtmaat A. 2014. Sensory-evoked LTP driven by dendritic plateau potentials in vivo. Nature. 515:116–119.
Gauriau C. 2004. Posterior Triangular Thalamic Neurons Convey Nociceptive Messages to the Secondary Somatosensory and Insular Cortices in the Rat. J Neurosci. 24:752–761.

Giber K, Slézia A, Bokor H, Bodor AL, Ludányi A, Katona I, Acsády L. 2008. Heterogeneous output pathways link the anterior pretectal nucleus with the zona incerta and the thalamus in rat. J Comp Neurol. 506:122–140.

Gibson JM, Welker WI. 1983a. Quantitative Studies of Stimulus Coding in 1st-Order Vibrissa Afferents of Rats .2. Adaptation and Coding of Stimulus Parameters. Somatosens Res. 1:95–117.

Gibson JM, Welker WI. 1983b. Quantitative studies of stimulus coding in first-order vibrissa afferents of rats. 1. Receptive field properties and threshold distributions. Somat Res. 1:51–67.

Groh A, Bokor H, Mease RA, Plattner VM, Hangya B, Stroh A, Deschênes M, Acsády L. 2014. Convergence of cortical and sensory driver inputs on single thalamocortical cells. Cereb Cortex. 24:3167–3179.

Groh A, de Kock CPJ, Wimmer VC, Sakmann B, Kuner T. 2008. Driver or Coincidence Detector: Modal Switch of a Corticothalamic Giant Synapse Controlled by Spontaneous Activity and Short-Term Depression. J Neurosci. 28:9652–9663.

Groh A, Meyer HS, Schmidt EF, Heintz N, Sakmann B, Krieger P. 2010. Cell-Type Specific Properties of Pyramidal Neurons in Neocortex Underlying a Layout that Is Modifiable Depending on the Cortical Area. Cereb Cortex. 20:826–836.

Guillery RW. 1969. A quantitative study of synaptic interconnections in the dorsal lateral geniculate nucleus of the cat. Zeitschrift für Zellforsch und Mikroskopische Anat. 96:39–48.

Guillery RW, Feig SL, Lozsádi D a., Lozsadi DA. 1998. Paying attention to the thalamic reticular nucleus. Trends Neurosci. 21:28–32.

Haidarliu S, Ahissar E. 2001. Size gradients of barreloids in the rat thalamus. J Comp Neurol. 429:372–387.

Hayashi H. 1980. Distributions of vibrissae afferent fiber collaterals in the trigeminal nuclei as revealed by intra-axonal injection of horseradish peroxidase. Brain Res. 183:442–446.

Hires SA ndrew, Pammer L, Svoboda K, Golomb D. 2013. Tapered whiskers are required for active tactile sensation. Elife. 2:e01350.

Hoogland P V, Welker E, van der Loos H. 1987. Organization of the projections from barrel cortex to thalamus in mice studied with Phaseolus vulgaris-leucoagglutinin and HRP. Exp brain Res. 68:73–87.

Hoogland P V, Wouterlood FG, Welker E, van der Loos H. 1991. Ultrastructure of giant and small thalamic terminals of cortical origin: a study of the projections from the barrel cortex in mice using Phaseolus vulgaris leuco-agglutinin (PHA-L). Exp brain Res. 87:159–172.

Ibrahim L, Wright EA. 1975. The growth of rats and mice vibrissae under normal and some abnormal conditions. J Embryol Exp Morphol. 33:831–844.

Ito M. 1988. Response properties and topography of vibrissa-sensitive VPM neurons in the rat. J Neurophysiol. 60:1181–1197.

Jacquin MF, Mooney RD, Rhoades RW. 1986. Morphology, response properties, and collateral projections of trigeminothalamic neurons in brainstem subnucleus interpolaris of rat. Exp brain Res. 61:457–468.

Kandel ER, Schwartz JH, Jessell TM. 2013. Principles of Neural Science, Neurology.

Kerr JND, de Kock CPJ, Greenberg DS, Bruno RM, Sakmann B, Helmchen F. 2007. Spatial Organization of Neuronal Population Responses in Layer 2/3 of Rat Barrel Cortex. J Neurosci. 27:13316–13328.

Khatri V, Bermejo R, Brumberg JC, Zeigler HP. 2010. Whisking in air: Encoding of kinematics by VPM neurons in awake rats. Somatosens Mot Res. 27:111–120.

Knutsen PM, Ahissar E. 2009. Orthogonal coding of object location. Trends Neurosci. 32:101–109.

Knutsen PM, Pietr M, Ahissar E. 2006. Haptic Object Localization in the Vibrissal System: Behavior and Performance. J Neurosci. 26:8451–8464.

Lam Y-W, Sherman SM. 2007. Different Topography of the Reticulothalmic Inputs to First- and Higher-Order Somatosensory Thalamic Relays Revealed Using Photostimulation. J Neurophysiol. 98:2903–2909.

Lavallée P, Urbain N, Dufresne C, Bokor H, Acsády L, Deschênes M. 2005. Feedforward inhibitory control of sensory information in higher-order thalamic nuclei. J Neurosci. 25:7489–7498.

Lee CC, Sherman SM. 2008. Synaptic Properties of Thalamic and Intracortical Inputs to Layer 4 of the First- and Higher-Order Cortical Areas in the Auditory and Somatosensory Systems. J Neurophysiol. 100:317–326.

Lee S, Kruglikov I, Huang ZJ, Fishell G, Rudy B. 2013. A disinhibitory circuit mediates motor integration in the somatosensory cortex. Nat Neurosci. 16:1662–1670.

Leergaard TB, Alloway KD, Mutic JJ, Bjaalie JG. 2000. Three-dimensional topography of corticopontine projections from rat barrel cortex: correlations with corticostriatal organization. J Neurosci. 20:8474–8484.

Leergaard TB, Bjaalie JG. 2007. Topography of the complete corticopontine projection: from experiments to principal Maps. Front Neurosci. 1:211–223.

Leiser SC, Moxon KA. 2007. Responses of Trigeminal Ganglion Neurons during Natural Whisking Behaviors in the Awake Rat. Neuron. 53:117–133.

Lévesque M, Gagnon S, Parent A, Deschênes M. 1996. Axonal arborizations of corticostriatal and corticothalamic fibers arising from the second somatosensory area in the rat. Cereb Cortex. 6:759–770.

Liao C-C, Chen R-F, Lai W-S, Lin RCS, Yen C-T. 2010. Distribution of large terminal inputs from the primary and secondary somatosensory cortices to the dorsal thalamus in the rodent. J Comp Neurol. 518:2592–2611.

Liao C-C, Yen C-T. 2008. Functional connectivity of the secondary somatosensory cortex of the rat. Anat Rec (Hoboken). 291:960–973.

Lichtenstein SH, Carvell GE, Simons DJ. 1990. Responses of rat trigeminal ganglion neurons to movements of vibrissae in different directions. Somat Mot Res.

Llinas RR, Pare D. 1991. Of dreaming and wakefulness. Neuroscience. 44:521–535.

Ma PM. 1991. The barrelettes--architectonic vibrissal representations in the brainstem trigeminal complex of the mouse. I. Normal structural organization. J Comp Neurol. 309:161–199.

Manita S, Suzuki T, Homma C, Matsumoto T, Odagawa M, Yamada K, Ota K, Matsubara C, Inutsuka A, Sato M, Ohkura M, Yamanaka A, Yanagawa Y, Nakai J, Hayashi Y, Larkum ME, Murayama M. 2015. A Top-Down Cortical Circuit for Accurate Sensory Perception. Neuron. 86:1–6.

Manns ID, Sakmann B, Brecht M. 2004. Sub- and suprathreshold receptive field properties of pyramidal neurones in layers 5A and 5B of rat somatosensory barrel cortex. J Physiol. 556:601–622.

Maravall M, Diamond ME. 2014. Algorithms of whisker-mediated touch perception. Curr Opin Neurobiol. 25:176–186.

Masri R, Bezdudnaya T, Trageser JC, Keller A. 2008a. Reply to Ahissar et al. J Neurophysiol. 100:1155–1157.

Masri R, Bezdudnaya T, Trageser JC, Keller A. 2008b. Encoding of stimulus frequency and sensor motion in the posterior medial thalamic nucleus. J Neurophysiol. 100:681–689.

Masri R, Trageser JC, Bezdudnaya T, Li Y, Keller A. 2006. Cholinergic regulation of the posterior medial thalamic nucleus. J Neurophysiol. 96:2265–2273.

Matthews DW, Deschênes M, Furuta T, Moore JD, Wang F, Karten HJ, Kleinfeld D. 2015. Feedback in the brainstem: An excitatory disynaptic pathway for control of whisking. J Comp Neurol. 523:921–942.

Matyas F, Sreenivasan V, Marbach F, Wacongne C, Barsy B, Mateo C, Aronoff R, Petersen CCH. 2010. Motor Control by Sensory Cortex. Science (80-). 330:1240–1243.

McCormick DA, von Krosigk M. 1992. Corticothalamic activation modulates thalamic firing through glutamate “metabotropic” receptors. Proc Natl Acad Sci U S A. 89:2774–2778.

Mease RA, Krieger P, Groh A. 2014. Cortical control of adaptation and sensory relay mode in the thalamus. Proc Natl Acad Sci. 111:6798–6803.

Mease RA, Metz M, Groh A. 2015. Cortical Sensory Responses Are Enhanced by the Higher-Order Thalamus. Cell Rep. 14:208–215.

Meyer HS, Wimmer VC, Hemberger M, Bruno RM, de Kock CPJ, Frick A, Sakmann B, Helmstaedter M. 2010. Cell Type-Specific Thalamic Innervation in a Column of Rat Vibrissal Cortex. Cereb Cortex. 20:2287–2303.

Meyer HS, Wimmer VC, Oberlaender M, de Kock CPJ, Sakmann B, Helmstaedter M. 2010. Number and Laminar Distribution of Neurons in a Thalamocortical Projection Column of Rat Vibrissal Cortex. Cereb Cortex. 20:2277–2286.

Mitrofanis J. 2005. Some certainty for the “zone of uncertainty”? Exploring the function of the zona incerta. Neuroscience. 130:1–15.

Mitrofanis J, Mikuletic L. 1999. Organisation of the cortical projection to the zona incerta of the thalamus. J Comp Neurol. 412:173–185.

Moore JD, Mercer Lindsay N, Deschênes M, Kleinfeld D. 2015. Vibrissa Self-Motion and Touch Are Reliably Encoded along the Same Somatosensory Pathway from Brainstem through Thalamus. PLoS Biol. 13:e1002253.

Mountcastle VB. 1997. The columnar organization of the neocortex. Brain. 120:701–722.

Murray PD, Masri R, Keller A. 2010. Abnormal anterior pretectal nucleus activity contributes to central pain syndrome. J Neurophysiol. 103:3044–3053.

Naito J, Kawamura K. 1982. Thalamocortical neurons projecting to the areas surrounding the anterior and middle suprasylvian sulci in the cat. Exp Brain Res. 45–45:59–70.

Narayanan RT, Egger R, Johnson AS, Mansvelder HD, Sakmann B, de Kock CPJ, Oberlaender M. 2015. Beyond Columnar Organization: Cell Type- and Target Layer-Specific Principles of Horizontal Axon Projection Patterns in Rat Vibrissal Cortex. Cereb Cortex. bhv053-.

Oberlaender M, Boudewijns ZSRM, Kleele T, Mansvelder HD, Sakmann B, de Kock CPJ. 2011. Three-dimensional axon morphologies of individual layer 5 neurons indicate cell type-specific intracortical pathways for whisker motion and touch. Proc Natl Acad Sci. 108:4188–4193.

Ohno S, Kuramoto E, Furuta T, Hioki H, Tanaka YR, Fujiyama F, Sonomura T, Uemura M, Sugiyama K, Kaneko T. 2012. A morphological analysis of thalamocortical axon fibers of rat posterior thalamic nuclei: A single

neuron tracing study with viral vectors. Cereb Cortex. 22:2840–2857.
Petersen RS, Brambilla M, Bale MR, Alenda A, Panzeri S, Montemurro MA, Maravall M. 2008. Diverse and temporally precise kinetic feature selectivity in the VPm thalamic nucleus. Neuron. 60:890–903.
Pierret T, Lavallee P, Deschênes M. 2000. Parallel streams for the relay of vibrissal information through thalamic barreloids. J Neurosci. 20:7455–7462.
Poulet JFA, Fernandez LMJ, Crochet S, Petersen CCH. 2012. Thalamic control of cortical states. Nat Neurosci. 15:370–372.
Poulet JFA, Hedwig B. 2007. New insights into corollary discharges mediated by identified neural pathways. Trends Neurosci. 30:14–21.
Ramaswamy S, Markram H. 2015. Anatomy and physiology of the thick-tufted layer 5 pyramidal neuron. Front Cell Neurosci. 9:1–29.
Ramirez A, Pnevmatikakis EA, Merel J, Paninski L, Miller KD, Bruno RM. 2014. Spatiotemporal receptive fields of barrel cortex revealed by reverse correlation of synaptic input. Nat Neurosci. 17:866–875.
Rees H, Roberts MHT. 1993. The anterior pretectal nucleus: a proposed role in sensory processing. Pain. 53:121–135.
Reichova I, Sherman SM. 2004. Somatosensory corticothalamic projections: distinguishing drivers from modulators. J Neurophysiol. 92:2185–2197.
Rice FL, Mance A, Munger BL. 1986. A comparative light microscopic analysis of the sensory innervation of the mystacial pad. I. Innervation of vibrissal follicle-sinus complexes. J Comp Neurol. 252:154–174.
Sachdev RNS, Sato T, Ebner FF. 2002. Divergent movement of adjacent whiskers. J Neurophysiol. 87:1440–1448.
Senft SL, Woolsey T a. 1991. Mouse barrel cortex viewed as Dirichlet domains. Cereb Cortex. 1:348–363.
Sherman SM. 2001. Tonic and burst firing: dual modes of thalamocortical relay. Trends Neurosci. 24:122–126.
Sherman SM. 2005. Thalamic relays and cortical functioning. Prog Brain Res. 149:107–126.
Sherman SM. 2016. Thalamus plays a central role in ongoing cortical functioning. Nat Neurosci. 16:533–541.
Shosaku a, Kayama Y, Sumitomo I. 1984. Somatotopic organization in the rat thalamic reticular nucleus. Brain Res. 311:57–63.
Slézia A, Hangya B, Ulbert I, Acsády L. 2011. Phase Advancement and Nucleus-Specific Timing of Thalamocortical Activity during Slow Cortical Oscillation. J Neurosci. 31:607–617.
Smith JB, Mowery TM, Alloway KD. 2012. Thalamic POm projections to the dorsolateral striatum of rats: potential pathway for mediating stimulus-response associations for sensorimotor habits. J Neurophysiol. 108:160–174.
Smith JB, Watson GDR, Alloway KD, Schwarz C, Chakrabarti S. 2015. Corticofugal projection patterns of whisker sensorimotor cortex to the sensory trigeminal nuclei. Front Neural Circuits. 9.
Steriade M, Nuñez A, Amzica F. 1993. A novel slow (< 1 Hz) oscillation of neocortical neurons in vivo: depolarizing and hyperpolarizing components. J Neurosci. 13:3252–3265.
Stroh A, Adelsberger H, Groh A, Rühlmann C, Fischer S, Schierloh A, Deisseroth K, Konnerth A. 2013. Making Waves: Initiation and Propagation of Corticothalamic Ca2+ Waves In Vivo. Neuron. 77:1136–1150.
Theyel BB, Llano DA, Sherman SM. 2010. The corticothalamocortical circuit drives higher-order cortex in the mouse. Nat Neurosci. 13:84–88.
Timofeeva E. 2004. Synthesis of Multiwhisker-Receptive Fields in Subcortical Stations of the Vibrissa System. J Neurophysiol. 91:1510–1515.
Timofeeva E, Mérette C, Emond C, Lavallee P, Deschênes M. 2003. A map of angular tuning preference in thalamic barreloids. J Neurosci. 23:10717–10723.
Trageser JC, Burke KA, Masri R, Li Y, Sellers L, Keller A. 2006. State-dependent gating of sensory inputs by zona incerta. J Neurophysiol. 96:1456–1463.
Trageser JC, Keller A. 2004. Reducing the uncertainty: gating of peripheral inputs by zona incerta. J Neurosci. 24:8911–8915.
Urbain N, Deschênes M. 2007a. Motor Cortex Gates Vibrissal Responses in a Thalamocortical Projection Pathway. Neuron. 56:714–725.
Urbain N, Deschênes M. 2007b. A New Thalamic Pathway of Vibrissal Information Modulated by the Motor Cortex. J Neurosci. 27:12407–12412.
Urbain N, Salin PA, Libourel P, Petersen CCH, Urbain N, Salin PA, Libourel P, Comte J, Gentet LJ, Petersen CCH. 2015. Whisking-Related Changes in Neuronal Firing and Membrane Potential Dynamics in the Somatosensory Thalamus of Awake Mice Report Whisking-Related Changes in Neuronal Firing and Membrane Potential Dynamics in the Somatosensory Thalamus of Awake Mice. CellReports. 1–10.
Van Der Loos H. 1976. Barreloids in mouse somatosensory thalamus. Neurosci Lett. 2:1–6.
Veinante P, Deschênes M. 1999. Single- and multi-whisker channels in the ascending projections from the

principal trigeminal nucleus in the rat. J Neurosci. 19:5085–5095.
Veinante P, Jacquin MF, Deschênes M. 2000. Thalamic projections from the whisker-sensitive regions of the spinal trigeminal complex in the rat. J Comp Neurol. 420:233–243.
Veinante P, Lavallee P, Deschênes M. 2000. Corticothalamic projections from layer 5 of the vibrissal barrel cortex in the rat. J Comp Neurol. 424:197–204.
Welker C. 1971. Microelectrode delineation of fine grain somatotopic organization of (SmI) cerebral neocortex in albino rat. Brain Res. 26:259–275.
Whitt JL, Masri R, Pulimood NS, Keller A. 2013. Pathological activity in mediodorsal thalamus of rats with spinal cord injury pain. J Neurosci. 33:3915–3926.
Wise SP, Jones EG. 1977a. Somatotopic and columnar organization in the corticotectal projection of the rat somatic sensory cortex. Brain Res. 133:223–235.
Wise SP, Jones EG. 1977b. Cells of origin and terminal distribution of descending projections of the rat somatic sensory cortex. J Comp Neurol. 175:129–157.
Wise SP, Murray EA, Coulter JD. 1979. Somatotopic organization of corticospinal and corticotrigeminal neurons in the rat. Neuroscience. 4:65–78.
Woolsey TA, van der Loos H. 1970. The structural organization of layer IV in the somatosensory region (SI) of mouse cerebral cortex. The description of a cortical field composed of discrete cytoarchitectonic units. Brain Res. 17:205–242.
Woolsey TA, Welker C, Schwartz RH. 1975. Comparative anatomical studies of the SmL face cortex with special reference to the occurrence of “barrels” in layer IV. J Comp Neurol. 164:79–94.
Yamashita T, Pala A, Pedrido L, Kremer Y, Welker E, Petersen CCH. 2013. Membrane Potential Dynamics of Neocortical Projection Neurons Driving Target-Specific Signals. Neuron. 80:1477–1490.
Yu C, Derdikman D, Haidarliu S, Ahissar E. 2006. Parallel Thalamic Pathways for Whisking and Touch Signals in the Rat. PLoS Biol. 4:e124.
Yu C, Horev G, Rubin N, Derdikman D, Haidarliu S, Ahissar E. 2015. Coding of Object Location in the Vibrissal Thalamocortical System. Cereb Cortex. 25:563–577.
Zacksenhouse M, Ahissar E. 2006. Temporal decoding by phase-locked loops: unique features of circuit-level implementations and their significance for vibrissal information processing. Neural Comput. 18:1611–1636.
Zakiewicz IM, Bjaalie JG, Leergaard TB. 2014. Brain-wide map of efferent projections from rat barrel cortex. Front Neuroinform. 8:5.
Zakiewicz IM, Majka P, Wójcik DK, Bjaalie JG, Leergaard TB. 2015. Three-Dimensional Histology Volume Reconstruction of Axonal Tract Tracing Data : Exploring Topographical Organization in Subcortical Projections from Rat Barrel Cortex. PLoS One. 10:1–16.
Zhang ZW, Deschênes M. 1997. Intracortical axonal projections of lamina VI cells of the primary somatosensory cortex in the rat: a single-cell labeling study. J Neurosci. 17:6365–6379.
Zliang ZW, Deschênes M. 1998. Projections to layer VI of the posteromedial barrel field in the rat: A reappraisal of the role of corticothalamic pathways. Cereb Cortex. 8:428–436.

List of Figures and Tables

Affidavit

Hiermit versichere ich an Eides statt, dass ich die vorliegende Dissertation „*Structure and Dynamics of the Corticothalamic Driver Pathway in the Mouse Whisker System*“ selbstständig angefertigt habe, mich außer der angegebenen keiner weiteren Hilfsmittel bedient und alle Erkenntnisse, die aus dem Schrifttum ganz oder annähernd übernommen sind, als solche kenntlich gemacht und nach ihrer Herkunft unter Bezeichnung der Fundstelle einzeln nachgewiesen habe.

I hereby confirm that the dissertation “*Structure and Dynamics of the Corticothalamic Driver Pathway in the Mouse Whisker System*” is the result of my own work and that I have only used sources or materials listed and specified in the dissertation.

München, den 20.06.2016

_____

Anton Sumser

List of Publications and Manuscripts

Author Contributions

1. Sumser A, Sakmann B and Groh A. Organization and somatotopy of corticothalamic projections from barrel cortex layer 5B. Manuscript in preparation.
   A.S. designed the study together with A.G. and B.S.; A.S. performed all injections, post-processing and imaging, developed analysis programs and analyzed the data including figure generation; A.S. wrote the manuscript with help of all authors.
2. Mease RA, Sumser A, Sakmann B, Groh A. Corticothalamic Spike Transfer via the L5B-POm Pathway in vivo. Cereb Cortex. Online Advance Access: 2016 May 12.
   R.A.M, B.S. and A.G. designed the study, R.A.M. and A.G. performed experiments in Thy1-Chr2 animals; A.S. performed experiments in VGAT-Chr2 animals. R.A.M. and A.S. analyzed the data and generated figures; R.A.M. and A.G. jointly wrote the paper with the help of all authors.
3. Mease RA*, Sumser A*, Sakmann B, Groh A. Cortical Dependence of Whisker Responses in Posterior Medial Thalamus In Vivo. Cereb Cortex. Online Advance Access: 2016 May 26.
   R.A.M, B.S. and A.G. designed the study, R.A.M. and A.G. performed experiments in Thy1-Chr2 animals; A.S. performed experiments in VGAT-Chr2 animals. R.A.M. and A.S. analyzed the data and generated figures; R.A.M., A.S. and A.G. jointly wrote the paper with the help of B.S.
   * shared first authorship

_____	_____	_____
Anton Sumser	Prof. Bert Sakmann Supervisor	Dr. Rebecca Mease Shared 1st author